reactions

MDPI

Review

Synthesis, Photocatalytic and Bio Activity of ZnO-TiO_2 Nanocomposites: A Review Study

Fulvia Pinzari

Istituto di Scienze del Patrimonio Culturale—CNR (ISPC—CNR), Via Salaria, km 29.300, Monterotondo Scalo, 00015 Rome, Italy; fulvia.pinzari@cnr.it

Abstract: Zinc oxide and titanium dioxide are materials with strong photocatalytic and antimicrobial activity. This activity is greater when the material is in nanocrystalline form. It has been seen that these properties are also present in the ZnO-TiO_2 nanocomposite material, and the extent depends on multiple factors, such as crystallinity, structural composition, crystallite size, and morphology. These structural properties can be varied by acting on the synthesis of the material, obtaining a wide variety of composites: random nanoparticles, nanorods, nanowires, nanotubes, nanofibers, tetrapods, core–shell, hollow spheres, inverse opal structures (IOSs), hierarchical structures, and films. When an interface between nanocrystallites of the two oxides is created, the composite system manages to have photocatalytic activity greater than that of the two separate oxides, and in certain circumstances, even greater than P25. The antimicrobial activity results also improved for the composite system compared to the two separate oxides. These two aspects make these materials interesting in various fields, such as wastewater and air treatment, energy devices, solar filters, and pharmaceutical products and in the context of the restoration of monumental cultural assets, in which their use has a preventive purpose in the formation of biofilms. In this review we analyse the synthesis techniques of ZnO-TiO_2 nanocomposites, correlating them to the shape obtained, as well as the photocatalytic and antimicrobial activity. It is also illustrated how ZnO-TiO_2 nanocomposites can have a less negative impact on toxicity for humans and the environment compared to the more toxic ZnO nanoparticles or ZnO.

Keywords: composite materials; ZnO-TiO_2; photocatalyst; antimicrobial

Citation: Pinzari, F. Synthesis, Photocatalytic and Bio Activity of ZnO-TiO_2 Nanocomposites: A Review Study. *Reactions* **2024**, *5*, 680–739. https://doi.org/10.3390/reactions5040035

Academic Editors: Annalisa Volpe, Caterina Gaudiuso and Maria Chiara Sportelli

Received: 3 July 2024
Revised: 24 September 2024
Accepted: 26 September 2024
Published: 2 October 2024

1. Introduction

Both ZnO and TiO_2 have received great attention for their unique properties, which make them suitable for a lot of application. The most common and well/known allotropic phase of ZnO is the hexagonal wurtzite, which is the stable phase at ambient conditions. ZnO presents two other cubic allotropic phases: rocksalt and zinc blende [1]. TiO_2 has four natural allotropic phases: rutile, the most stable one, anatase, brookite and TiO_2 (B), and two synthetic high-pressure phases: TiO_2 (II) and TiO_2 (H) [2]; anatase and brookite transform into rutile if heated above 750 °C [3].

ZnO and TiO_2 are semiconductors with a wide band gap energy, they have thermal stability, antibacterial and photocatalytic properties. They are transparent in the visible range of the electromagnetic spectrum and absorb in the UV region. Moreover, ZnO is a piezoelectric material and TiO_2 is biocompatible [1–4].

Titanium dioxide in the anatase phase shows reversible wetting behavior when exposed alternately to the dark or to UV irradiation. It is hydrophobic after dark exposition and hydrophilic after UV exposition. This allows us to create transparent antifogging coatings [5].

All these excellent properties make them suitable for applications in many fields ranging from biomedical to environmental remediation, photovoltaics, photo catalysis, photonic devices, and protective and/or antibacterial coatings.

ZnO-TiO_2 nanocomposites (ZTNCs) have been proposed in most applications already tested for pure ZnO nanoparticles (ZNPs) and TiO_2 nanoparticles (TNPs), in order to improve performances of the pristine oxides. ZTNCs may present very differentiated structure and properties because of the combination of different allotropic phases of both oxides and the coexistence of different allotropic phases of the same oxide. Synthesis methodologies and strategies have been explored to give rise to a large variety of shape, structure and composition. The availability of different chemical, physical and hybrid synthesis methodologies, combined with the possibility of modifying numerous process variables, make it possible to obtain materials with different structural characteristics, such as crystalline structure, morphology, particle size, energy gap, and surface area, which give very diversified properties, and therefore possibilities of applications for the material itself. All synthesis methods usually use high temperature as a final treatment, and this can potentially lead to the formation of titanium–zinc mixed oxide: cubic spinel zinc orthotitanate (Zn_2TiO_4) [6,7], zinc metatitanate ($ZnTiO_3$) [6] as the hexagonal ilmenite [7] or cubic perovskite [8,9] and the cubic $Zn_2Ti_3O_8$ [7]. Moreover, Zn may migrate into the TiO_2 crystal lattice and, vice versa, and Ti can migrate into the ZnO crystal lattice. This last aspect is specifically faced only in certain studies in the calculation of the lattice parameters, but most of time it is neglected.

This review collects papers about the synthesis, properties, photocatalytic and bio activity of ZTNCs; this review does not consider those papers in which $Zn_xT_yO_z$ formation is relevant. Solid solutions of zinc in titania or of titanium in zinc oxide are, indeed, considered here, in virtue of the fact that this aspect is not always faced in many papers and mutual solubility of one oxide in the other may be always present, and probably is, even when both phases are identified by XRD [10]. This review consists of three parts. The first one refers to describing synthesis methodology and strategies, and the structural properties of the ZTNCs, such as structure, crystallite size, surface area, and energy band gap, which determine synergistic effects between two oxides and influence the final photocatalytic properties, as described in the second part. Finally, since the use and potential applications of nanoparticles (NPs) have been increasing in recent years, possible toxic effects on human and environmental health are taken into consideration in the third part. ZTNCs have been synthesized in a wide variety of shapes and structures, and in this review we have chosen to deal with the synthesis methodologies as a function of the shape of the final composite, considering as a separate section the solid solutions of zinc oxide in titanium dioxide and titanium dioxide in zinc oxide. The section concerning the photocatalytic reactions has been addressed by classifying the reactions based on their purpose and, possibly, the target molecule. Finally, the section about the bio-activity of the ZTNCs will analyze factors influencing antimicrobial and toxic activity of ZTNCs compared to those of ZNPs and TNPs. Scheme 1 shows the shapes of the synthesized ZTNCs.

The synthesis could be obtained by a single-step reaction only for the simpler shapes, such as Zn-doped TiO_2 and Ti-doped ZnO, ZnO-TiO_2 random nanoparticles, hollow spheres, French fries, and nanofibers; moreover, some of these shapes have been synthesized with alternative methodologies. In Scheme 2, the synthesis method used to prepare these simpler shapes is shown.

Appropriate synthesis strategies for more complex shapes, such as core–shell nanostructures, hierarchical structures, hierarchical films on substrate, and composites on titanium dioxide nanotubes, include two or more stages. Furthermore, these shapes often include several sub-shapes, and a simple schematization of the methodologies used is not possible. Scheme 3 shows some of the sub-forms included in the more complex shapes already listed, while the description of the methodologies used is faced in the Synthesis Section.

Scheme 1. Different ZnO-TiO_2 composite shapes synthetized.

Ti-doped ZnO and Zn-doped TiO_2	•sol-gel method •precipitation •hydrothermal synthesis •magnetron sputtering •atomic layer deposition •solid state reaction
ZnO-TiO_2 random nanoparticles (ZT/r/NPs)	•Mixing in suspension •Solid state reaction •Impregnation •Precipitation •Hydrothermal method •Sol-gel method •Green synthesis •Glycerol nitrate combustion •pulsed laser ablation in liquid •Plasma discharge in water medium
Hollow spheres and Yolk shell microsphere	•Spray pyrolysis •Solvothermal synthesis
French fries	•Furfural alcohol derived polymerization-oxidation reaction
ZnO-TiO_2 Nanofibers	•Electrospinning

Scheme 2. Alternative synthesis methodologies used for the simpler ZTNC shapes.

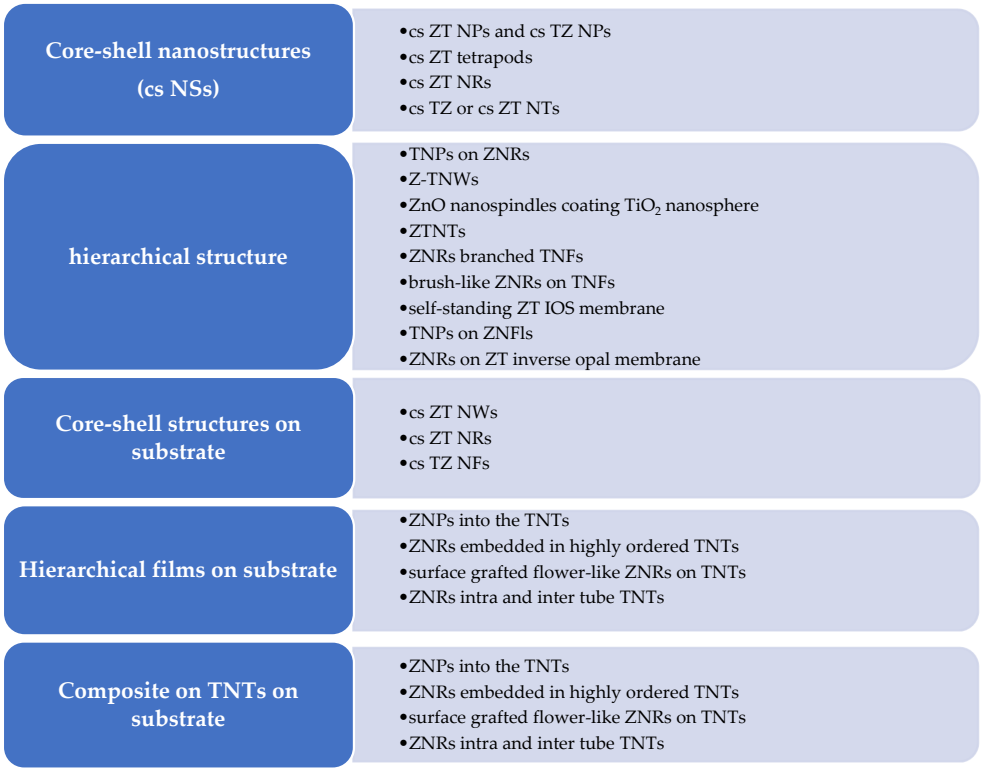

Scheme 3. Sub-shapes of the more complex shapes.

The section concerning the photocatalytic reactions has been addressed by classifying the reactions based on their purpose: dye degradation, environmental contaminant degradation and energy-generation reaction; additionally, the dye-degradation reactions were further classified according to the dye itself. In this section it is shown that most of the time ZTNCs are more photoactive than ZnO and TiO_2 NPs, and, sometimes, more than P25 TiO_2, which is considered a standard in photocatalysis. Factors enhancing the photoactivity of ZnO-TiO_2 nanocomposite are considered, such as energy gap, electron–hole recombination, oxygen vacancies creation, crystallinity, surface area, zero-point charge, catalyst acidity, and working photocatalysis parameters (catalyst loading, initial dye concentration and pH solution), as highlighted in Scheme 4.

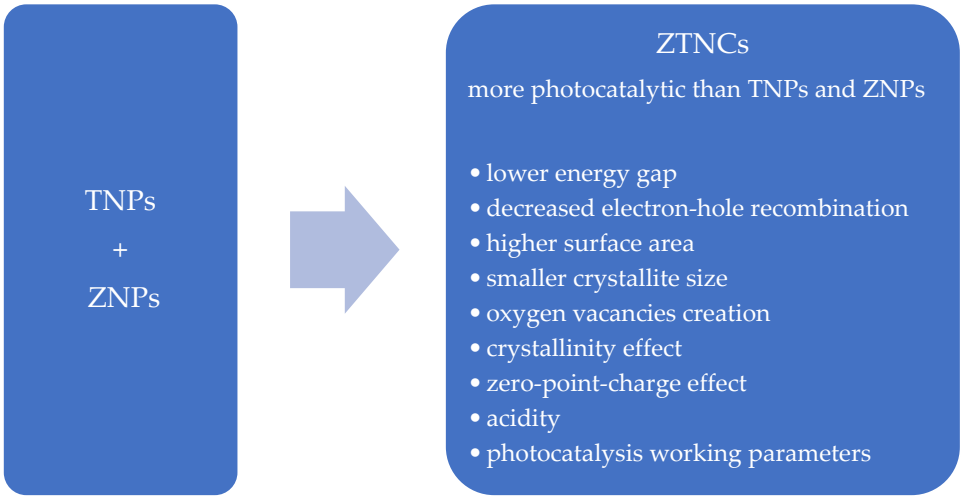

Scheme 4. Factors influencing the increased photocatalytic effect of ZTNCs compared to TNPs and ZNPs.

The bioactivity section shows how the antimicrobial activity of ZTNCs against bacteria and fungi also increases compared to TNPs and ZNPs, and, at the same time, reduced cytotoxicity is found and the factors that influence the different activity are analyzed.

2. Synthesis

This section outlines the preparation methodologies for ZTNCs, categorized by shape. It considers the main synthesis parameters and characteristics of the final products. While these synthesis parameters can vary depending on the method, they typically include the starting materials, synthesis technique, heat treatments, and product composition. The properties of ZTNCs here examined are those that, as discussed in the photocatalysis section, significantly affect the material performance in term of photocatalysis and bio activity. These include crystalline structure, crystallite and particle size, surface area, and energy gap. Not all materials here presented have been effectively used in photocatalytic or antimicrobial activities, but we aim to include these as suggestions for future research.

The first paragraph focuses on Zn-doped TiO_2 and Ti-doped ZnO. Although these materials are not typically regarded for their photocatalytic and antimicrobial properties, they are particularly interesting because there is likely mutual solubility between the two oxides in all ZTNCs. Therefore, the text analyzes the solubility limits observed in certain synthesis, though there are few detailed studies on this topic. It also describes how material properties relevant to photocatalytic performance, such as crystallite size, surface area, and energy gap, are changed when solubilization occurs.

2.1. Zn-Doped TiO_2 and Ti-Doped ZnO

ZnO and TiO_2 have different crystal structure and present a misfit in ionic radius, which is 0.61 Å for Ti^{4+} and 0.74 Å for Zn^{2+} [11]. Nevertheless, they can show a moderate mutual solubility, with relevant results in the context of semiconductor and photocatalysis. Although the mutual solubility limits of the two oxides are thermodynamic data, the experimental values found can vary, based on the synthesis conditions.

Zn concentration higher than 0.1 at.% in nanocrystalline anatase gave rise to ZnO segregation on samples obtained by solid-state reaction between pristine oxides at a temperature of 300 °C; a slightly higher solubility (0.1–0.5%) was allowed with a calcination temperature of 600 °C [12].

Zinc was dissolved into anatase lattice up to 10% (at.%) using a sol–gel synthesis method followed by a drying in supercritical conditions and a calcination treatment at 500 °C for 10 h [11]. Increasing the amount of dissolved zinc in the anatase lattice caused it to distort, which prevented particle growth, and thus a decrease in crystallite size, from 17 nm (pure anatase) to 13 nm (anatase with 10% zinc) and an increase in surface area from 77 to 94 $m^2\ g^{-1}$ were found. The increasing amount of dissolved zinc was also associated with an increase in the energy gap from 2.96 eV to 3.02 eV.

An increase in surface area from 19 to 53 $m^2\ g^{-1}$ with increasing zinc concentration from 0% to 1% (Zn/Ti at. ratio) was also found in anatase microsphere synthetized by precipitation method and calcinated at 450 °C, together with a decrease in crystallite size [13].

Zn-doped anatase NPs synthesized by the hydrothermal method showed an increase in d101 spacing compared to pristine anatase, together with an expansion in the <001> direction and no evidence of ZnO either in XRD or STEM, revealing a homogeneous dispersion of zinc in the anatase lattice for Zn-doped anatase up to 3% [14].

Zn-doped nanocrystalline porous anatase synthesized using agarose gel with a calcination temperature of 450 °C allowed a maximum solubility of zinc in the anatase structure of 2%; also, in this case, the Zn doping caused a distortion in the anatase lattice and prevented the growth of the crystallite size [15].

Zn-doped anatase nanotubes (NTs) grown by atomic layer deposition (ALD) using a polycarbonate (Millipore) as a template and followed by annealing at 450 °C, showed

a Zn solubility of up to 8 at.%, but a surface enrichment of zinc up to 16% with local amorphization of TiO_2 was present [16].

Zn-doped anatase NPs prepared by the polymeric precursor method and calcined at 500 °C, showed surface segregation of ZnO on TiO_2. ZnO was detected only by XPS, and not by XRD. In this case, the surface-segregated ZnO was lixiviated by HNO_3 and a maximum residual bulk solubility of zinc oxide in anatase lattice was limited to 0.39% mol, with an initial composition of 8.5% [17].

Zn-doped TiO_2 properties and synthesis conditions are reported in Table 1.

Table 1. Zn-doped TiO_2 properties and synthesis conditions.

Shape and Particle Size (PS)	Synthesis Method	Starting Materials	Composition	Thermal Treatments	Crystal Phases (CP) and Crystallite Size (CS)	Surface Area (SA) and E Gap	Ref.
Nanosized mesoporous NPs	Sol–gel method	TTIP, EtOH DW, ZN, HNO_3	Zn mol.% = 0, 0.1, 0.2, 0.3, 0.5, 1, 2, 5, 10%	Drying: supercritical conditions: T_c = 235.1 °C, P_c = 47.6 bar, ρ_c = 0.273 gcm^{-3}; calcination: 500 °C. 10 h, air	CP: anatase. CS: 17–13 nm, decreases with increasing Zn content. c dimension decreases (9.509–9.493 Å) with increasing Zn content	SA = 77–94 m^2 g^{-1}, increases with increasing Zn content. E gap: 2.96–3.02 eV, increases with increasing Zn content	[11]
Microspheres. PS: decreases with increasing Zn content	precipitation method	ZN, EG, TTIP, acetone, DW	Zn/Ti at. ratio = 0, 0.25, 0.5, 1%	Annealing: 450 °C, 2 h	CP: anatase. CS: 15–25 nm decreases with increasing Zn content	SA = 19–53 m^2 g^{-1} increases with increasing Zn content	[13]
<001> elongated NPs	hydrothermal method	TBT, ZAc, TEA, DW	Zn/Ti at. ratio = 0, 3.5, 8, 13.5	Autoclave: 180 °C, 16 h	CP: anatase and wurtzite (W only in ZnO mol% = 13.5%)	SA = 43 m^2 g^{-1}	[14]
Mesoporous nanosized NPs	Hydrolysis condensation in agarose gel template	ZAc, TTIP, DW, MeOH, agarose gel	Zn at.% = 0, 0.5, 1, 2, 4, 6, 8	Drying: 60 °C, 5 h; calcination: 450 °C, 10 h	CP: anatase. CS: 15–11 nm, decreases with increasing Zn content up to 2% then remains constant. c dimension: 9.490–9.465 Å decreases for Zn(%at.) 0–2, then remains constant	SA = 60–70 m^2 g^{-1}	[15]
TNTs inner $\varnothing_{TNTs}$ ~100 nm, wall thickness ~50–100 nm, length$_{NTs}$ = 10–15 µm	ALD (400 cycles) on polycarbonate (Millipore) template	$TiCl_4$, $ZnEt_2$, DW, N_2	Zn at.% = 1, 2, 3, 8%	450 °C, 2 h	CP: anatase CS: 20–15 nm, decreases with increasing Zn content		[16]

Table 1. *Cont.*

Shape and Particle Size (PS)	Synthesis Method	Starting Materials	Composition	Thermal Treatments	Crystal Phases (CP) and Crystallite Size (CS)	Surface Area (SA) and E Gap	Ref.
Agglomerated NPs	Polymeric precursor method (sol–gel Pechini)	TTIP, EG, CitrA (citric acid), ZN, DW	Zn mol.% = 0, 0.39, 0.85, 4.25, 8.55%	Calcination: 450 °C, 5 h + 500 °C, 15′	CP: anatase. CS: 25–10 nm, decreases with increasing Zn content	SA = 27–46 m^2 g^{-1}, increases with Zn content from 0 up to 5% and then decreases	[17]

Ti-doped ZNPs synthesized by the Pechini sol–gel method and calcined at 500 °C showed only the wurtzite phase; moreover, the increasing TiO_2 content up to 5% (wt.%) caused distortions in the lattice and a decrease in the crystallite size from 24 to 16 nm [18]. Ti-doped wurtzite films grown by simultaneous RF and DC magnetron sputtering showed the wurtzite structure with a preferential (002) orientation with a surface elemental content ratio Zn/O/Ti = 89.3/9.6/1.1, and amorphization occurred with a higher Ti content [19]. Similar results were found for films grown by RF magnetron sputtering with a post-annealing treatment at 700 °C; higher crystallinity allowed lower resistivity [20].

Films deposited by ALD showed a wurtzite structure with a Ti/Zn atomic ratio up to 1/5; moreover, films had a preferential orientation depending on Ti content. The lower Ti/Zn atomic ratio (1/20) gave rise to the (002) preferential orientation and lower resistivity [21].

ZnO tetrapods obtained by thermal evaporation were doped with titanium by solid-state reaction at 550 °C, and the titanium dioxide content was 10 wt.%. The effective titanium doping was confirmed by the shift in the E2 and A1 Raman signals to lower and higher wavenumbers, respectively [22].

Ti-doped ZnO properties and synthesis conditions are listed in Table 2.

Table 2. Ti-doped ZnO properties and synthesis conditions. The numbering in the synthesis-method column and starting-material column indicates the succession of steps in the synthesis.

Shape and Particle Size	Synthesis Method	Starting Materials	Composition	Thermal Treatments	Crystal Phases (CP) and Crystallite Size (CS)	SA and E Gap	Ref.
Agglomerated spherical NPs PS = 100 nm	Pechini sol–gel	ZAc, TBT, EG, CitrA, NH_4OH	Ti wt.% = 0, 1, 3, 5%	Drying: 120 °C; calcination: 300 °C, 3 h, 500 °C, 4 h	CP: Wurtzite. CS: 25–15 nm, decreases with increasing Ti content		[18]
Film on glass	Simultaneous RF (ZnO) and DC (Ti doping) magnetron sputtering	ZnO, Ti	Zn/O/Ti at. ratio = 89.3/9.6/1.1, 88.3/10.0/1.7, 86.6/10.6/2.8, 81.9/14.1/4.0		CP: amorphous (Ti at.% > 2%), (002) oriented wurtzite (Ti at.% =< 2%);	E gap = 3.39–3.92 eV	[19]
Film on corning glass	Magnetron sputtering	sintered (1000–1300 °C) targets from ZnO and TiO_2 powder	Ti/Zn/O at. Ratio = 0.7/46.2/531, 1.4/44.5/54.1, 2.0/43.7/54.3, 2.8/42.5/54.7, 3.4/41.0/55.6	Annealing: 700 °C, in Ar	CP: amorphous (Ti at.% > 2%), (002) oriented wurtzite (Ti at.% < 2%);	E-gap = 3.33–4.33 eV, increases with increasing Ti content	[20]

Table 2. *Cont.*

Shape and Particle Size	Synthesis Method	Starting Materials	Composition	Thermal Treatments	Crystal Phases (CP) and Crystallite Size (CS)	SA and E Gap	Ref.
film on quartz glass, film thickness = 100 nm	ALD	TTIP, $ZnEt_2$, DW	Zn/Ti at. ratio = 20, 10, 5, 2, 1		CP: amorphous (Zn/Ti = 1, 2); wurtzite (Zn/Ti $\geq$ 5),	E gap = 3.26–3.99 eV, increases with increasing Ti content	[21]
Ti-doped ZnO nanotetrapods with hexagonal branches. branch Ø = 200–300 nm	(1) ZnO tetrapods by direct thermal evaporation; (2) Ti doping by solid-state reaction	(1) Zn, O_2, Ar; (2) ZnO tetrapods, TiO_2	TiO_2 wt.% = 10%		CP: anatase (traces), wurtzite		[22]

2.2. *ZnO-TiO_2 Random Nanoparticles (ZT/r/NPs)*

In this section, the methodologies used for the synthesis of ZTNCs which do not have a specific shape, and therefore here called random, are presented. These methodologies are both physical and chemical, and are introduced in order of increasing complexity.

The mixing of two materials followed by a heat treatment, whether involving or not a solid-state reaction, is one of the simplest methodologies that can be used in the synthesis of composite materials. ZT/r/NPs were synthetized by dispersion of ZnO and TiO_2 in water [23] or methanol [24], followed by a simple drying [24] and or calcination at 400–600 °C [23,25]. TiO_2 was usually present as the anatase phase, with irregular [24] or spherical agglomerated [25] particles, while ZnO in the wurtzite phase showed rod-like particles [24,25]. Surface areas were limited to the range 5–60 $m^2\ g^{-1}$ [24–26], depending on the starting material feature and composition and on the calcination temperature. ZT/r/NPs were also obtained by a direct solid-state reaction between $TiO_2 \cdot xH_2O$and zinc carbonate, performed in a platinum crucible at 600 °C [27].

ZT/r/NPs were synthetized by titania impregnation with a water solution containing a zinc salt, such as nitrate [28,29], acetate [28] or sulphate [30], followed by calcination at 400 °C [28–30]. The use of zinc nitrate gave rise to a greater crystallinity of the wurtzite phase compared to zinc acetate [28]. Surface areas were limited to 50–60 $m^2\ g^{-1}$ if anatase was used as support [28–30] and to 10 $m^2\ g^{-1}$ if rutile was used [28]; moreover, surface area values decreased with increasing zinc content [28,29]. ZnO was not detectable by XRD up to 10% (mol.%) and prevented anatase-to-rutile thermal transformation [30].

ZT/r/NPs were obtained by the hydrolysis/precipitation method in alkaline [31–35] or acid [36] solution, usually followed by calcination in the temperature range 300–600 °C. The precipitation process could be assisted by ultrasound [31] or microwave [33] treatment. Surface areas of ZT/r/NPs synthetized by precipitation/hydrolysis could exceed 100 $m^2\ g^{-1}$ [31,36], and decreased with increasing zinc content [36]. Typical crystallite sizes were in the range 6–20 nm for anatase, [32,34,36,37] with decreasing values for increasing zinc content, and at least 40–65 nm for wurtzite [34,36]

ZT/r/NPs synthetized by the hydrothermal method in autoclave used final thermal treatment lower than 200 °C. The use of lower final-decomposition temperatures helped to obtain ZT/r/NPs with larger surface area and smaller wurtzite-crystallite size. [38]. Surface area could reach a value well over 200 $m^2\ g^{-1}$ [38–41], and wurtzite crystallite size could decrease by up to 10 nm [39]. With the increase in the autoclave-treatment temperature value, the surface area decreased [39], while by increasing the autoclave treatment time, the surface area could increase or decrease, depending on the composition of the composite

and the treatment duration itself. The highest value of surface area obtained for ZT/r/NPs by the hydrothermal method in autoclave was 375 m^2 g^{-1} [41]. The pH of the solution could affect the final structure and surface area, and the highest surface area value was of 360 m^2 g^{-1}, which was associated with the co-existence of anatase and amorphous TiO_2 phases and was obtained with alkaline solution during the synthesis [40]. Full spheres were synthesized by an autoclave treatment of TBT, ZAc and EtOH at 150 °C for 24 h, followed by calcination at 500 °C. Spheres were made of anatase and wurtzite, had a surface area below 10 m^2 g^{-1}, and the crystallite size was 5–9 nm [42].

ZT/r/NPs synthetized by sol–gel contained anatase and wurtzite phases, and sometimes rutile phase [10,43–45], and showed a large variety of morphology such as spherical, agglomeration, hexagonal, pyramidal and rod-like shape. Morphology control could be obtained by changing the surfactant and/or calcination temperature [44]. The catalyst obtained with sodium dodecyl benzene sulfonate (DBS) and calcinated at 600 °C had a spherical shape, while using sodium dodecyl sulfonate (SDS) and calcinating at 700 °C meant the morphology changed from cubic to hexagonal nanorods and nanobelts, by decreasing the zinc oxide content [44]. The calcination temperature was usually set at 500–600 °C, while at higher temperatures other phases were formed: $ZnTiO_3$ [10,46], and Zn_2TiO_4 [46]. Sol–gel ZT/r/NPs have been synthetized also by limiting the calcination temperature to 200–220 °C [46,47], and in this, the resulting case particle size was smaller. By increasing calcination temperature from 220 °C to 620 °C, the wurtzite crystallinity increased and anatase peak intensity decreased because TiO_2 partially dissolved into the wurtzite structure [46]. Surface area of calcined materials at a typical temperature of 400–600 °C ranged from 30–50 m^2 g^{-1} [43,46] up to 130 m^2 g^{-1} [48–50]. ZT/r/NPs obtained by the sol–gel method in the presence of P123 had crystallite size not exceeding 5–10 nm and surface areas of 120 m^2 g^{-1} [51]. Drying in supercritical conditions allowed for obtaining materials with higher surface area compared to materials obtained by calcination: 140–180 m^2 g^{-1} against 126–130 m^2 g^{-1}, but also with a lower crystallinity degree [49].

ZT/r/NPs have been synthetized also by green synthesis. Using extracts of Calopogonium mucunoides leaves in water [52] as reducing and stabilizing agents, allowed for obtaining TiO_2 in the anatase phase and ZnO in wurtzite phase. The structure was preserved with a calcination temperature in the range 500–800 °C. The average crystallite size decreased in the range 20–10 nm, increasing the calcination temperature or increasing the TiO_2 content. Extracts of Allium sativum leaf in ethanol [53] have been used as capping and reducing agents and allowed for obtaining ZT/r/NPs with low Zn concentration (2.5 mol.%). Only the anatase phase with a crystallite size of 4–13 nm was detected, and the material had a surface area of 134 m^2 g^{-1}. Lignin extracted by the soda pulping process [54] had been successfully used in green synthesis of ZT/r/NPs; the calcination temperature was limited to 300 °C and ZT/r/NPs contained anatase and wurtzite phases.

Pulsed laser ablation in liquid (PLAL) resulted effective for synthesizing ZT/r/NPs by using a Nd:Yag laser at its first (λ = 1064 nm) [55] or second (λ = 532 nm) [56] harmonic, and Zn and Ti plates or TNPs and ZnO nanorods (ZNRs) in water were used as starting materials, respectively. ZT/r/NPs contained anatase and wurtzite phases, had low surface area (14 m^2 g^{-1}) [56] and a large crystallite size (average size = 86 nm) [55].

ZT/r/NPs had been synthesized by glycerol nitrate combustion [57] in the presence of glycerol syrup and urea with an ignition temperature of 250 °C and a post-thermal treatment of 450 °C. Materials were composed of rutile and wurtzite with an average crystallite size of 34 nm, had a spherical or irregular shape, and were agglomerated to form bigger particles (87 nm).

ZT/r/NPs with a very low energy gap, 1.17 eV, were synthesized by deposition of ZNPs in u.s. bath of TNPs cellulose acetate (CA) nanofibers (NFs) in DW, followed by calcination at 700 °C. TNPs CA NFs had been obtained by electrospinning using a solution of cellulose acetate (CA) in acetic acid (AcA) and acetone, containing TNPs. The final ZT/r/NPs were made of anatase and wurtzite, with a crystallite size of 21 nm [58].

ZT/r/NPs have been deposited on a viscose patch by plasma discharge in water medium. Zinc and titanium metals served as electrodes with an output voltage of up to 10 KV, and the distance between the viscose patch and the electrode was 1 cm. ZT/r/NPs contained ZnO in wurtzite phase and titania in the anatase phase [59].

ZT/r/NPs properties and synthesis conditions are reported in Table 3.

Table 3. ZT/r/NPs properties and synthesis conditions. The numbering in the synthesis-method column and starting-material column indicates the succession of steps in the synthesis. The parameter r, when present, is used to express the composition, and must refer to its own line.

Shape and Particle Size	Synthesis Method	Starting Materials	Composition	Thermal Treatments	Crystal Phases (CP) and Crystallite Size (CS)	SA and E Gap	Ref.
irregular (anatase) and rod-like (wurtzite) NPs. PS = 0.1–0.3 μm (TiO_2); $\varnothing_{ZnO}$ = 0.1–0.3 μm, $length_{ZnO}$: 0.3–1.5 μm	mixing in methanol dispersion	ZnO, TiO_2, KOH, MeOH	ZnO wt.% = 0, 1, 3, 5, 10, 15, 30, 50, 70, 90, 93, 95, 97, 99, 100	drying: 80 °C, 3 h	CP: anatase (ZnO ≤ 99%), wurtzite (ZnO > 10%)	SA = 6–15 m^2 g^{-1}, decreases with increasing Zn content	[24]
agglomerated NPs. PS = 75–100 nm (r = 4/1); 40–70 nm (r = 1/0); 50–80 nm (r = 0/1)	u.s. treatment on water-dispersed starting materials, followed by SSR	Nano-sized TiO_2, nano-sized ZnO, DW	r = TiO_2/ZnO (mol. ratio) = 1/0, 4/1, 3/2, 2/3, 1/4, 0/1	drying: 100 °C,10 h; calcination: 500 °C, 40′	CP: anatase, wurtzite. CS = 80 nm (r = 4/1); 50 nm (r = 1/0); 60 (r = 0/1)		[23]
PS = 500 nm	2 steps: (1) $TiO_2 \cdot xH_2O$ by spray drying; (2) mixing and SSR	SM: (1) H_2TiO_3, NH_4OH, (2) $TiO_2 \cdot xH_2O$ (from 1), $ZnCO_3$	r = ZnO/TiO_2 (mol. ratio) = 1, 2, 3, 4, 5	(2) calcination: 600 °C, 1 h	CP: anatase, wurtzite		[27]
rod-like shape (r = 0/1); agglomerated spherical NPs (r = 1/0); agglomerated TNPs on rod-like ZNPs (r = 1/1). PS: Ø = 470 nm (r = 0/1); 10 nm (r = 1/0)	2 steps: (1) TiO_2 and ZnO by hydrothermal method; (2) mixing and SSR	(1) ZAc, DW, NH_4OH (ZnO); TBT, EtOH, DW (TiO_2); (2) ZnO (from 1), TiO_2 (from (1)), PVA	r = TiO_2/ZnO (wt. ratio) = 1/0, 3/2, 1/1, 2/3, 0/1	(2) calcination: 500 °C, 2 h	CP: anatase, wurtzite	SA = 9 m^2 g^{-1} (r = 0/1); 141 m^2 g^{-1} (r = 1/0); 54 m^2 g^{-1} (r = 1/1) E gap = 3.31 eV (r = 0/1); 3.26 eV (r = 1/0), 3.16 eV (r = 1/1)	[25]
	mixing and SSR	ZnO, TiO_2	r = ZnO/TiO_2 (mol. ratio) = 1/3, 1/2, 1/1, 2/1, 3/1	TT: 400 °C	CP: anatase, wurtzite. CS = 18 nm (r = 1/1)	SA = : 58 m^2 g^{-1} (r = 1/1)	[26]

Table 3. *Cont.*

Shape and Particle Size	Synthesis Method	Starting Materials	Composition	Thermal Treatments	Crystal Phases (CP) and Crystallite Size (CS)	SA and E Gap	Ref.
	2 steps: (1) TiO_2 by precipitation method (2) composite by wetness impregnation method	$TiCl_3$, NH_4OH, DW: (2) ZAc or ZN, DW, TiO_2 (from 1)	ZnO mol:% = 0.1, 0.5, 2, 5, 10, 50, 60, 67	(1) drying: 100 °C, 24 h; calcination: 550 °C, 48 h, air (anatase), calcination: 800 °C 24 h air (rutile); (2) 400 °C, 24 h	Anatase (T_{calc} = 550 °C) or rutile (T_{calc} = 800 °C), wurtzite	SA <10 m^2 g^{-1} (impregnated on rutile TiO_2), 10–60 m^2 g^{-1} (impregnated on anatase TiO_2)	[28]
	Wetness impregnation method	ZS, TiO_2 (P25), DW	ZnO mol.% = 0.5, 2, 4, 10	drying: 80 °C, 12 h; calcination: 400 °C, 3 h	CP: Anatase, rutile	SA = 49–53 m^2 g^{-1}	[30]
Irregular spherical shape. PS = 200 nm	Wetness impregnation method	ZN, TiO_2, DW	Zn% (unspecified measure units): 1, 3, 5, 10%	Drying: 110 °C, 24 h; calcination: 400 °C, 5 h.	CP: anatase	SA = 8–10 m^2 g^{-1}, decreases with increasing Zn content	[29]
	u.s. assisted precipitation method	H_2TiO_3/TiO_2 (2 wt.%), ZAc, NaOH, DW	r = TiO_2/ZnO (molar ratio) = 0/1, 1/1, 2/1, 3/1, 4/1, 1/0	Drying: 80 °C, 3–4 h; calcination: 300 °C, 2 h	CP: anatase (except r = 0/1), wurtzite (r $\leq$ 3/1). CS = 44 nm (r = 1/1)	SA = 125 m^2 g^{-1} (r = 1/1)	[31]
Agglomerated spherical-like NPs. PS = 2 μm	Homogeneous hydrolysis method	TOSO, ZS, TAA, DW, H_2SO_4	Ti wt.% = 44–56; Zn wt.% = 0.5–1.4	Drying: 105 °C; annealing 600 °C, 1 h in O_2	CP: anatase; wurtzite in pristine ZnO CS = 6–15 nm (anatase), 63 nm (wurtzite)	SA = 38–110 m^2 g^{-1}, decreases with increasing Zn content; 6 m^2 g^{-1} in pristine ZnO	[36]
hexagonal shaped NPs PS = 22–23 nm	Modified ammonia evaporation-induced synthetic method	TiO_2 (P25), ZN, NH_4OH, DW	Zn% (unspecified measure units) = 7.5%	Calcination: 450 °C, 4 h	CP: anatase, rutile, wurtzite CS = 23 nm	SA = 65 m^2 g^{-1} E gap = 2.87 eV	[32]
PS < 10 nm	MW (180 W) assisted precipitation method	ZN, DW, NH_4OH, KTO	r = TiO_2/ZnO (molar ratio) = 1/1, 2/1	Drying: 70 °C, 36 h	CP: anatase, wurtzite		[33]

Table 3. *Cont.*

Shape and Particle Size	Synthesis Method	Starting Materials	Composition	Thermal Treatments	Crystal Phases (CP) and Crystallite Size (CS)	SA and E Gap	Ref.
polygonal NPs (r = 0/1); polygonal NPs (r = 1/0); fine Ps (A), polygonal and rod-like NPs (W) (r = 3/1). PS = 11 nm (r = 0/1); 65 nm (r = 1/0): 11 nm and 69 nm (r = 3/1, polygonal), 65 nm (r = 3/1, rod-like)	3 steps: (1) TiO_2 by precipitation method (hydrolysis); (2) oleic acid-coated TiO_2 by adsorption; (3) ZnO/TiO_2 by impregnation method	(1) TTIP, EtOH, DW; (2) TiO_2 NPs (from 1), DW, oleic acid, NH_4OH; (3) oleic acid-coated TiO_2 NPs (from 2), n-hexane, $ZnCl_2$, NH_4OH, DW	r = ZnO/TiO_2 (molar ratio) = 1/0, 3/1, 0/1	(1) Drying: 70 °C, 12 h; calcination: 400 °C, 2 h air; (2) drying: 70 °C, 24 h; calcination: 400 °C, 2 h, air	CP: anatase (r = 0/1); wurtzite (r = 1/0); anatase, wurtzite (r = 3/1) CS = 11 nm (r = 0/1:); 42 nm (r = 1/0:); 10.3 nm (anatase in r = 3/1), 30.2 nm (wurtzite in r = 3/1)		[34]
Rod-like NPs (r = 1/0), agglomerated NPs (r = 0/1), spherical NPs (r = 3/2, 1/1, 2/3). PS: ∅ = 44 nm; length = 1.8 μm (r = 1/0); 18 nm (r = 0/1), 32 nm (r = 3/2, 1/1, 2/3)	precipitation method	ZAc, DW, TBT, MeOEtO, NaOH	r = ZnO/TiO_2 (volume ratio) = 1/0, 3/2, 1/1, 2/3, 0/1	Drying: 100 °C, 15 h; calcination: 500 °C, 4 h	CP: wurtzite (r > 0), anatase (r = 0), rutile (r = 0), traces of $ZnTiO_3$. CS = 20–45 nm, increases with increasing Zn content	E gap = 3.1–3.3 eV, increases with increasing Zn content	[37]
	Deposition–precipitation method	TiO_2 (P25), ZN, Na_2CO_3, DW	[ZnO wt.%] = 0.5, 2, 5, 20	Drying: 60 °C, overnight; calcination: 400 °C, 3 h	CP: anatase, rutile, wurtzite (wurtzite only ZnO wt.% = 20%)	SA = 50 m^2 g^{-1}	[35]

Table 3. *Cont.*

Shape and Particle Size	Synthesis Method	Starting Materials	Composition	Thermal Treatments	Crystal Phases (CP) and Crystallite Size (CS)	SA and E Gap	Ref.
	Precipitation method: compares calcination (C) with autoclave thermal treatment (H)	ZN, $TiCl_4$, NH_4OH, DW	$TiO_{2\%}$ (unspecified units) = 5, 10, 20, 50, 70, 90, 100%	Drying: 110 °C, overnight; calcination: 500 °C, 5 h (C); autoclave: 150 °C, 10 h, drying: 110 °C, 24 h (H)	CP: anatase, wurtzite (wurtzite not in all catalysts). CS: 21 nm (calcinated catalysts), 16 nm (autoclave-treated catalysts)	SA: ZnO: close to 0 $m^2\ g^{-1}$; TiO_2: 50 $m^2\ g^{-1}$ (C), 100 (H); 225 $m^2\ g^{-1}$ (H, $TiO_{2\%}$ = 75), 60 $m^2\ g^{-1}$ ($TiO_{2\%}$ = 90, C) E gap: 2.95–3.15 eV in calcinated catalysts, lower values for intermediate composition; 3.05–3.45 eV in autoclave-treated catalysts, higher values for intermediate composition (H)	[38]
PS = 10–20 nm	Homogeneous hydrolysis method	TBT, ZAc, AcA, EG		Autoclave: 120 °C, 6 h; autoclave: 180–200 °C; drying: 60 °C, in vacuum	CP: anatase, wurtzite (TT = 190/200 °C); amorphous (TT = 180 °C) CS = 10 nm (W), 17 nm (A)	SA = 206 $m^2\ g^{-1}$ (180 °C), 97 $m^2\ g^{-1}$ (200 °C)	[39]
	Hydrothermal method	TBT, EtOH, ZAc, DW	r = TiO_2/ZnO (molar ratio) = 1/1 (pH = 12), 3/1 (pH = 12), 5/1 (pH = 12); (3/1 pH = 4, 6, 8, 10, 12)	Autoclave: 120 °C, 12 h	CP: anatase (except r = 1/1), amorphous (r = 1/1 and pH = 12, r = 3/1 and pH = 12, r = 3/1 pH = 8, 10)	SA = 120–360 $m^2\ g^{-1}$, the higher values for anatase and amorphous phase coexistence	[40]
Spherical shape PS = 900 nm; 20 (ZnO); 800 nm (TiO_2)	Hydrothermal method	TBT, ZAc, EtOH		Autoclave: 150 °C, 24 h; calcination: 500 °C, 1 h, air	CP: anatase, wurtzite CS = 5–9 nm	SA = 8–10 $m^2\ g^{-1}$	[42]

Table 3. *Cont.*

Shape and Particle Size	Synthesis Method	Starting Materials	Composition	Thermal Treatments	Crystal Phases (CP) and Crystallite Size (CS)	SA and E Gap	Ref.
	Hydrothermal method	TTIP, ZAc, NaOH, DW, IPOH	r = ZnO/TiO_2 (molar ratio) = 9/1, 7/3, 3/7, 1/9	Autoclave: 160 °C, 6 or 12 or 24 h, drying: 60 °C 6 h	CP: anatase, rutile (r = 9/1); anatase, amorphous (r = 7/3); rutile (r = 3/7, 1/9)	SA = 77–375 m^2 $g^{-}1$. Increases and then decreases with increasing Zn content. Increases and then decrease with increasing hydrothermal-time treatment. Maximum value for r = 7/3, and time = 24 h.	[41]
	Sol–gel method Post treatment: H_2SO_4 0.5M	SM: TBT, ZX, EtOH, AcA, polyglycol (PG); X = SO_4, Cl, NO_3.	r = ZnO/(TiO_2 + ZnO) (molar ratio) = 1, 2, 4, 6, 8, 10%	Gelation conditions: RT, 24 h; drying: 80 °C, 48 h; 200 °C, 1 h; Calcination: 400 °C	CP: anatase, rutile (rutile absent if r = 1%)	SA = 32 m^2 g^{-1} (r = 10%)	[43]
Irregular-shape aggregated NPs (no surfactant); spherical shape (DBS 600 °C); cubic shape to hexagonal nanorods to nanobelts with decreasing Zn/Ti content (SDS 700 °C). PS = 200–300 nm (no surfactant); 300 nm (DBS 600 °C); 0.5–1 µm (cubic), ∅ = 500 nm, length = 1.5 µm (nanorods), 500 × 50 × 8 (nm) (nanobelts) (SDS 700 °C)	Sol–gel method	TBT, ZN, EtOH, DW, HCl, DBS (or SDS)	r = ZnO/TiO_2 (molar ratio) = 0/1, 0.1/1, 0.17/1, 0.25/1, 0.5/1	Gelation conditions: 24 h RT; drying: 70 °C; calcination: 600–700 °C	CP: anatase, rutile: (DBS/600 °C/ r = 0/1, SDS); wurtzite (r > 0/1)		[44]
Granular shape	Sol–gel method	ZAc, IPOH, DEA, $TiCl_4$, HCl, H_2O		Drying: 60° C; calcination: 220 °C or 420 °C	CP: anatase, wurtzite	SA = 51 m^2 g^{-1} (T_{calc} = 220 °C), 45 m^2 g^{-1} (T_{calc} = 420 °C)	[46]

Table 3. *Cont.*

Shape and Particle Size	Synthesis Method	Starting Materials	Composition	Thermal Treatments	Crystal Phases (CP) and Crystallite Size (CS)	SA and E Gap	Ref.
Spherical shape PS = 6–14 nm	Sol–gel method	TBT, ZN, EtOH, P123, HCl, DW	ZnO wt.% = 0, 10, 30, 50, 70, 90, 100 and	Gelation conditions: RT, a few hours; drying: 80 °C, 12 h; calcination: 500 °C, 5 h, air	CP: anatase (ZnO wt.% < 100), wurtzite (ZnO wt.% = 50–100) CS = 4–10 nm (measured at low Zn content)	SA = 20–120 m^2 g^{-1}, increases and then decreases with increasing zinc content. Maximum value for ZnO wt.% = 50% E gap = 3.25–3.37 eV. Minimum value for ZnO wt.% = 70%.	[51]
	Sol–gel method	TTIP, IPOH, HNO_3, ZAc, MeOH, KOH, DW	10% ZnO (unspecified measure units)	Gelation conditions: RT, 12 h. Drying: 45 °C; calcination: 500 °C, 2 h	CP: anatase, rutile, wurtzite CS = 15.3 nm (ZTNPs), 5 nm (TNPs); 10.1 (ZNPs)	E gap = 2.91; eV (ZTNPs), 3.00 eV (TNPs), 3.1 eV (ZNPs)	[45]
agglomerated NPs (ZT NPs); irregular shape (ZNPs by sol–gel method); hexagonal shape (ZNPs by precip-itation method) PS: SG: 8–20 nm (TNPs), 30–40 nm (ZNPs), 400 nm (ZT NPs); P: 40 nm (ZnO)	Compares sol–gel method (SG) and precipitation method(P)	ZAc, NaOH, EtOH, TTIP, IPOH, DW	ZnO wt.% = 10, 20, 33, 50, 67, 80, 90, 100%	Gelation conditions: 0 °C + ageing: 3 days, RT. Drying: 100 °C, overnight; calcination: 500 °C, 3 h	CP: anatase (SG: $r \leq 10$, P: $r \leq 33$), wurtzite (SG: $r \geq 67$; P: $r \geq 80$), amorphous (SG: $20 \leq r \leq 50$, P: $0.67 \leq r \leq 0.5$)	SA = 40–120 m^2 g^{-1} (sol–gel); 110–130 m^2 g^{-1} (precipitation); decreases with increasing Zn content, 270 m^2 g^{-1} (TNPs); 8–9 m^2 g^{-1} (ZNPs) E gap: 3.5–3.26 eV (sol–gel); 3.23–347 eV (precipitation); incre-ases and then decrea-ses with increasing ZnO content. 3.32 eV (TiO_2); 3.21 eV (ZnO)	[48]
PS [nm]: 15–20 (after drying)	Sol–gel method	SM: ZN, EtOH, HNO_3, TBT	r = Zn/Ti (molar ratio) = 0.5, 1, 1.5	Gelation conditions: RT 1 day. Drying in supercritical conditions (270 °C, 10 Mpa), 2 h; calcination: 450 °C	CP: anatase, wurtzite	SA = 140–180 m^2 g^{-1} (after drying); 126–130 m^2 g^{-1} (after calcination); increases with increa-sing Zn content	[49]

Table 3. *Cont.*

Shape and Particle Size	Synthesis Method	Starting Materials	Composition	Thermal Treatments	Crystal Phases (CP) and Crystallite Size (CS)	SA and E Gap	Ref.
Rod-like shape (ZNPs); more or less evident agglomeration (ZTNPs)	Sol–gel method	TTIP, ZAc, MEA, IPOH, HNO_3, DW	r = Zn/Ti (molar ratio) = 0/1, 1/3, 1/1,2/1, 3/1, 1/0	Gelation conditions: 48 h, RT. Drying: 100 °C, 4 h; annealing: 500 °C, 4 h + 600 °C, 4 h	CP: anatase (r = 0/1), rutile (r = 0/1, 1/3), wurtzite (r > 0/1), traces of $ZnTiO_3$ (r = 1/1, 2/1). CS = 21–38 nm	SA = 95 m^2 g^{-1} (r = 1/1), 39 m^2 g^{-1} (r = 0/1), 3 m^2 g^{-1} (r = 1/0) E gap: direct 3.07–3.20 eV; indirect: 2.91–3.01 eV (Z/T = 1 the lowest value)	[10]
spherical shape (TNPs); hexagonal–pyramidal shape (ZNPs); agglomerated spherical and hexagonal–pyram-idal shape (ZT NPs)	Sol–gel method		r = Zn/Ti (molar ratio) = 0/1, 1/1, 1/0	Gelation conditions: 24 h stirring. Drying: 100 °C; calcination: 500 °C, 2.5 h	CP: anatase, wurtzite. CS = 19 nm (wurtzite, 33 in ZnO), 8 nm (anatase, 18 in TiO_2)	SA = 132 m^2 g^{-1} (ZT NPs), 32 m^2 g^{-1} (ZNPs), 98 m^2 g^{-1} (TNPs)	[50]
Spherical-like NPs. PS = 17–21 nm	Sol–gel method	SM: $ZnCl_2$, EtOH, BenzylOH, $TiCl_4$		Gelation conditions: 60 °C, 8 h. Calcination: 200 °C, 2 h	CP: anatase, wurtzite CS = 18–24 nm	E gap [eV]: 3.05 eV (ZTNPs), 3.48 (ZNPs)	[47]
	Green synthesis	Calopogonium mucunoides leaves (reducing and stabilizing agent), DW, ZAc, TiO_2, NaOH		Drying: 80 °C, 10 h; calcination: 500, 600, 700, 800 °C	CP: anatase, wurtzite. CS = 8–20 nm, decreases with increasing calcination temperature and decreasing titanium content		[52]
Agglomerated spherical shape. PS = 4–13 nm	Green synthesis	$TiCl_4$, ZN, EtOH, Allium sativum leaves (capping and reducing agent), NH_4OH	O/Ti/Zn (at. ratio) = 84.2/15.6/0.2	Drying: 3 days, annealing: 450 °C, 6 h	CP: anatase CS = 4 nm	SA = 134 m^2 g^{-1}	[53]
Agglomerated NPs	Green synthesis	$TiCl_x$, ZS, lignin (soda pulping process), NaOH, DW		300 °C, 80 min	CP: anatase, wurtzite	E gap = 2.95 eV (ZT NPs), 3.18 eV (ZNPs), 3.08 eV (TNPs)	[54]

Table 3. *Cont.*

Shape and Particle Size	Synthesis Method	Starting Materials	Composition	Thermal Treatments	Crystal Phases (CP) and Crystallite Size (CS)	SA and E Gap	Ref.
Agglomerated irregular spherical NPs. PS = 87 nm	Glycerol nitrate combustion	SM: TTIP, ZN, urea, Glycerol syrup		Ignition: 250 °C, 1 h; calcination: 450 °C, 3 h	CP: rutile, wurtzite CS = 34 nm		[57]
PS = 37 nm	2 steps: (1) TNFs by electrospinning; (2) ZnO NP deposition by u.s. treatment/mixing	(1) CA, AcA, acetone, TNPs, TBT, AcA, EtOH; (2) TNF (from 1), ZAc, DW		(2) drying: 130 °C, 1 h; calcination: 700 °C, 4 h	CP: anatase, wurtzite CS = 22 nm	E gap = 1.17 eV	[58]
PS = 100 nm	Plasma discharge in water medium	Metal Zn and Ti			Anatase, wurtzite		[59]

2.3. Hollow Spheres (or Almost), Yolk–Shell Microspheres and French Fries ZT NPs

ZT NPs synthesized by spray pyrolysis of titania and zinc nitrate exhibited a nearly complete hollow-sphere aggregation structure [60] with dimensions of nearly 500 nm [60]. These NPs contained TiO_2 in the anatase phase [60,61], rutile [60], if already present in the source material, and wurtzite [60,61]. Increasing Ti content and N_2 flow rate reduced the size of wurtzite crystallites (90–20 nm) and increased agglomeration, resulting in an increase in particle size. On the other hand, the particle size decreased by increasing the temperature reactor (500–360 nm), without affecting the crystallite size [61]. No effects of working conditions on the size of anatase crystallites were detected. Hollow spheres were successfully synthetized by solvothermal synthesis in ethanol with TBT and zinc sulphide, followed by heat treatment in an autoclave at 210 °C for 24 h. The hollow spheres measured several microns in size and were formed by the aggregation of TiO_2 nanoparticles (8.5 nm) with even smaller segregated ZnO crystals [62], and had surface area up to 150 $m^2\ g^{-1}$.

Yolk–shell microspheres were synthesized by a one-step solvothermal synthesis performed in autoclave at 200 °C for 10 h with TBT and zinc acetylacetonate (ZAcAc) as titanium and zinc precursors, respectively, in acetylacetone (Acacetone) and isopropyl alcohol. The microspheres were made of anatase and amorphous phases, and were 1–1.5 μm in diameter with a thickness of 70 nm and surface area in the range 214–290 $m^2\ g^{-1}$ [63].

Mesoporous French fries-shaped nanoparticles with high surface area (225 $m^2\ g^{-1}$) formed by anatase and a small amount of rutile were synthetized via a polymerization oxidation reaction at 95 °C for 24 h. The titanium and zinc precursors were TTIP and $ZnCl_2$, respectively, and the reaction was carried out in ethanol in the presence of HNO_3 and P123. Furfural alcohol (FA) acted as the polymerizing agent and furfural resin formed in the reaction was removed by a final oxidation performed in air at 500 °C for 9 h. French fries, 60 μm long and of 3–4 μm in diameter, were formed by nanoparticles measuring 7–11 nm [64].

Properties and synthesis conditions of hollow spheres and French fries ZT NPs are reported in Table 4.

Table 4. Properties and synthesis conditions of hollow spheres and French fries ZTNPs. The parameter r, when present, is used to express the composition, and must refer to its own line.

Shape and Particle Size	Synthesis Method	Starting Materials	Composition	Thermal Treatments	Crystal Phases (CP) and Crystallite Size (CS)	SA and E Gap	Ref.
Almost hollow spheres or aggregate of ultrafine particles (10–100 nm). PS = 360–500 nm	Spray pyrolysis	ZN, DW, TiO_2, N_2. N_2, as carrier gas, (N_2 flow rate: 8.3 × 10^{-6}–3.3 × 10^{-5} m^3s^{-1})	r = Zn/Ti (mol. ratio) = 10/10, 10/7, 10/5, 10/3, 10/0.1	$T_{reactor}$ = 700–900 °C	CP: anatase, amorphous, wurtzite. CS = 20 nm (anatase); 20–90 nm (wurtzite)		[61]
Almost hollow spheres with spherical shape, and micro porous aggregate. PS = 100–500 nm	Spray pyrolysis	TiO_2 (P25), ZN, DW, N_2. N_2, as carrier gas (N_2 flow rate: 5 l min^{-1})	Zn/(Zn + Ti) at. ratio: 0, 5, 16, 33, 66, 100 (%)	$T_{reactor}$ = 550 °C	CP: anatase, rutile, wurtzite. CS = 5–20 nm		[60]
Hollow spheres with hierarchical structure: interconnected TNPs, with smaller ZnO crystals. PS = several µm	Solvothermal synthesis	ZS, EtOH, TBT	Zn at.% = 1.1%	Autoclave: 210 °C, 24 h, drying: 80 °C	CP: anatase CS = 8.5 nm	SA 150 m^2 g^{-1}	[62]
Yolk–shell microspheres. PS = 1–1.3 µm (microsphere), 70 nm (shell thickness)	Solvothermal method	IPOH, Acacetone, TBT, ZAcAc,	r = Ti/Zn mol. Ratio = 10, 8, 5, 2	Autoclave: 200 °C, 10 h	CP: anatase (r = 1/0, 5, 8, 10), amorphous (r = 2, 5)	SA = 214–290 m^2 g^{-1}, decreases with increasing Ti content	[63]
mesoporous French fries. PS = 7–11 nm NPs agglomerated to French-fries shape, PS: Ø = 3–4 µm, length = 60 µm	FAPO (FA-derived polymerization–oxidation) reaction	TTIP, P123, $ZnCl_2$, HNO_3, EtOH, FA	Ti/Zn/O (at. ratio) = 31.2/0.7/65.1	FAPO Reaction: 95 °C, 24 h air, calcination in air 500 °C 9 h	CP: anatase, rutile. CS = 9.5 nm	SA = 225 m^2 g^{-1}	[64]

2.4. ZnO-TiO_2 Nanofibers (ZTNFs)

ZTNFs have been obtained by electrospinning of an organic solution of a polymer mixed with solutions of zinc and titanium precursors, zinc acetate, and TTIP, respectively, followed by calcination at a temperature higher than 500 °C, to remove carbon fibers. If cellulose acetate was used as a polymer, direct calcination was left to the formation of sheet particles and a hydrolyzation treatment was necessary before the calcination to ensure ZTNF formation [65]. ZTNFs were obtained with a direct electrospinning method followed by calcination when Polymethylmethacrylate (PMMA), PVP or Polyvinyl acetate (PVAc) were used as polymers [66–68]. Typical voltages applied started from 10 KV [65,66], up to

75 KV [67]. ZTNFs were made up of anatase [65–68] rutile [65–67] and wurtzite [65,67,68] and had typical diameters in the range 85–200 nm [65,66]. Synthesis conditions and properties of ZTNFs are reported in Table 5.

Table 5. ZT NF properties and synthesis conditions. The numbering in the synthesis-method column and starting-material column indicates the succession of steps in the synthesis.

Shape and Particle Size	Synthesis Method	Starting Materials	Composition	Thermal Treatments	Crystal Phases (CP) and Crystallite Size (CS)	SA and E Gap	Ref.
NFs composed of grain- like NPs. PS: Ø = 85–200 nm	2 steps: (1) electrospinning. flow rate: 10 µL min^{-1}, distance collector-needle = 12 cm, V = 10 KV; (2) hydrolyzation performed at T = RT, t = 24 h;	(1) TTIP, ZAc, CA, AcA, DMFA, acetone; (2) NaOH, DW	ZnO wt.% = 0, 12.4, 15.8, 22.1.	Drying: 50 °C, 5 h; calcination: 500 °C, 5 h, in air	Anatase, rutile, wurtzite		[65]
NFs. PS: Ø = 100 nm, length = 50 µm	Electrospinning. flow rate: = 6 µL min^{-1}, V = 10 KV	TTIP, ZAc, PMMA, DMFA, AcA	(Zn/Ti) at. Ratio = 0.17	Calcination: 500 °C, 3 h	CP: anatase, rutile		[66]
NFs composed of NPs PS: Ø = 90 nm	Me: electrospinning distance collector-needle = 19 cm, V = 75 KV, electrode rotation speed = 30 Hz	TTIP, ZAc, AcA, PVP, EtOH	ZAc content: (0–0.6 wt.%)	Compares different calcination temperatures: 550, 650, 750, 850 °C, 2 h	CP: anatase (T_{calc} = 550–750 °C), rutile ($T_{calc} \geq 650$ °C), wurtzite. CS = 10 nm (T_{calc} = 550 °C), 150 (T_{calc} = 850 °C)	SA = 42 m^2 g^{-1}. E gap = 2.97 eV (ZTNFs T_{calc} = 550 °C), 2.96 eV (ZTNFs T_{calc} = 650 °C), 2.96 eV (ZTNFs T_{calc} = 750 °C), 2.96 eV (ZTNFs T_{calc} = 850 °C), 3.13 eV (T NFs T_{calc} = 550 °C)	[67]
NFs (flower-like) PS: $Ø_{petals}$ = 80–147 nm	Electrospinning. flow rate = 1 mL h^{-1}, distance collector-needle = 10 cm, V = 15 KV	TTIP, ZAc, PVAc, DMAc, AcA, EtOH		500 °C, 4 h	CP: anatase, wurtzite		[68]

2.5. Core–Shell Nanostructures (cs NSs)

Core (TiO_2)–shell (ZnO) nanoparticles (cs TZNPs) were synthetized by covering TiO_2 (P25) NPs with a shell of ZnO by impregnation and freeze drying in liquid N_2 [69] or by u.s. hydrolysis in multi-bubble sonoluminescence conditions [70]. Particle sizes were in the range 20–30 nm and the ZnO shell thickness was in the range 0.5–20 nm.

Similarly, core (ZnO)–shell (titania) nanoparticles (cs-ZT NPs) were obtained by covering ZnO NPs with a titania shell. ZnO was acquired [71] or synthetized by precipita-

tion [72,73] or by zinc acetate thermal decomposition [74]. Titania shell was deposited by MW-assisted impregnation [71], or by sol–gel chemical growth [72,74] or by precipitation [73]. Crystallite sizes were in the range 16–35 nm, particle size did not exceed 50 nm, and the shell thickness ranged from 2 nm [72] to 18 nm [73]. Surface area values up to 180 m^2 g^{-1} could be achieved [74].

Core–shell ZnO-TiO_2 (cs ZT) tetrapods were obtained by coating zinc oxide tetrapods with a titania layer. ZnO tetrapods were obtained by direct evaporation of Zn pellets in oxygen/argon atmosphere at 900 °C and the titania layer was deposited by a vapor phase treatment using a dispersion of ZnO, TiO_2, TBT and Z-tetrapods in alcohol at 150 °C for 10 h. The Cs-ZT tetrapods had the distance between adjacent arms of approximately 30–50 µm, the arm diameter was 500 nm, and the TiO_2 layer thickness was 50 nm [75].

Cs ZT nanorods (cs ZT NRs) were obtained by a two-step route: first, the ZNRs were synthetized by hydrothermal method using zinc chloride, sodium carbonate and deionized water as starting materials, and the hydrothermal treatment was performed in autoclave at 140 °C for 2 h. Subsequently, the TiO_2 layer was deposited by ALD, with alternating pulses of TTIP at 80 °C, N_2 and H_2O. Finally, materials were calcined at 400 °C for two hours, producing anatase and wurtzite in the structure [76].

Cs ZT Nanotubes (cs ZT NTs) and cs TZ nanotubes (cs-TZ NTs) suspended over a U-shaped frame were obtained by alternately depositing ZnO and TiO_2, or vice versa, using PLD, onto PVP NFs, followed by PVP removal by calcination in air at 500 °C. PVP fibers were previously obtained by electrospinning in ethanol solution. The PLD chamber was equipped with a Nd:Yag laser. Cs ZT NTs and cs TZ NTs were made up of wurtzite and rutile phases and had a diameter of 400–500 nm. The shell thickness was 51 nm and 60 nm for cs ZT NTs and cs TZNTs, respectively [77].

Properties and synthesis conditions of cs ZT NSs and cs TZ NSs are reported in Table 6.

Table 6. Properties and synthesis conditions of cs ZT NSs and cs TZ NSs. The numbering in the synthesis-method column and starting-material column indicates the succession of steps in the synthesis. The parameter r, when present, is used to express the composition, and must refer to its own line.

Shape and Particle Size (PS)	Synthesis Method	Starting Materials	Composition	Thermal Treatments	Crystal Phases (CP) and Crystallite Size (CS)	SA and E Gap	Ref.
cs TZ NPs PS = 20 nm, shell thickness = 0.5 nm	2 steps: (1) impregnation; (2) freeze drying	(1) $ZnCl_2$, EtOH, TiO_2 (P25)		Sintering: 500 °C, 1 h	TiO_2 (starting material), ZnO (XPS)		[69]
cs TZ NPs. PS = 30 nm; uncoated TNPs = 21 nm	u.s. hydrolysis in the MBSL conditions	TiO_2 (P25), ZAc, NaOH, DW, ROH		Drying: 12 h	CP: anatase, rutile, wurtzite CS = 7–8 nm (wurtzite), 21 nm (anatase)		[70]
cs ZT NPs. PS = 30–50 nm, shell thickness = 6–10 nm	ZnO mw impregnation	ZnO (MZ500), EtOH, NH_4OH, TBT, DW		Annealing: 500 °C	CP: anatase (only with thicker TiO_2 shell), wurtzite CS = 16–22 nm (wurtzite)		[71]

Table 6. *Cont.*

Shape and Particle Size (PS)	Synthesis Method	Starting Materials	Composition	Thermal Treatments	Crystal Phases (CP) and Crystallite Size (CS)	SA and E Gap	Ref.
cs ZT NPs. PS = 40–50 nm, shell thickness = 2–6 nm	2 steps: (1) ZNPs by precipitation; (2) TiO_2 shell by chemical growth from TiO_2 sol-gel	(1) ZAc, DW, OxA; (2) TTIP, AcA, ZNPs (from 1) Compares different shell thickness		(1) drying: 80 °C, 2h, calcination: 400 °C, 2 h; (2) drying: 80 °C, 12 h, calcination: unspecified temperature, 2 h	CP: anatase (detectable only with thicker shell), wurtzite CS = 20 nm (wurtzite)		[72]
cs ZT NPs. PS = 24 nm (r = 1/15); 39 nm (r = 20); 42 nm (r = 1/25); shell thickness = 13 nm (r = 1/15); 15 nm (r = 1/20); 18 nm (r = 1/55)	2 steps: (1) precipitation; (2) precipitation	(1) ZAc, NaOH, DW, (2) TTIP, IPOH, ZnO NPs (from 1), DW, HCl	r = ZnO/TiO_2 (wt. ratio) = 1/15, 1/20, 1/25	(1) 80 °C, 24 h; 350 °C, 2 h air; (2) 90 °C, 12 h; 350 °C, 3 h air	CP: anatase CS = 25 nm (r = 1/15); 32 nm (r = 1/20); 35 nm (r = 1/25)	E gap = 3.2–3.05 eV, decreases with increasing TiO_2 thickness	[73]
cs ZT NPs in agglomerated globular shape	2 steps: (1) ZNRs by ZAc thermal de-composition; (2) TiO_2 shell by chemical growth from TiO_2 gel	(1) ZAc; (2) TTIP, IPOH, DW, ZNRs (from 1)	ZnO mol.% = 0.5–20%	(1) decomposition: 400 °C, 3 h, air; (2) drying: 70 °C, 24 h; calcination: 350 °C, 3 h, air	CP: anatase, wurtzite (wurtzite detectable only with higher ZnO content) CS = 8–18 nm, decreases with increasing ZnO content	SA = 80–180 m^2 g^{-1}, increases with increasing ZnO content. E gap = 3.13–3.25 eV	[74]
cs ZT tetrapods PS: distance between adjacent arms = 30–50 µm, $Ø_{arm}$ = 500 nm, TiO_2 thickness = 50 nm	2 steps: (1) ZnO tetrapods by direct thermal evaporation; (2) TiO_2 coating by vapor phase treatment	(1) Zn pellets; (2) Z tetrapods (from 1), ZnO, TiO_2, TBT, EtOH, DW	TiO_2 wt.% = 7%	(1) 900 °C; (2) vapor phase treatment: 150 °C, 10 h; calcination: 450 °C, 2 h	CP: anatase, wurtzite		[75]
cs ZT NRs PS: TiO_2 thickness = 4.2, 6.4, 8.5, 125 nm	2 steps: (1) hydrother-mal method; (2) ALD	(1) $ZnCl_2$, Na_2CO_3, DW; (2) TTIP, N_2, DW	(1) autoclave: 140 °C, 2 h, drying: 80 °C, overnight; calcination: 400 °C, 4 h; (2) $T_{reactor}$ = 150 °C, $T_{TTIP\ bubbler}$ = 80 °C, calcination: 400 °C 2 h	different TiO_2 thickness	CP: anatase, wurtzite		[76]

Table 6. *Cont.*

Shape and Particle Size (PS)	Synthesis Method	Starting Materials	Composition	Thermal Treatments	Crystal Phases (CP) and Crystallite Size (CS)	SA and E Gap	Ref.
cs TZ (or ZT) NTs with large area and horizontally aligned PS: $\varnothing_{NTs}$ = 400–500 nm, shell thickness 60 nm (cs TZ NTs), 51 nm (cs ZT NTs)	2 steps: (1) electrospinning; (2) PLD. (laser: Nd:Yag, λ = 1064 nm, distance $_{target-sub}$ = 70 mm, T_{sub} = 300 K, $P = 6 \cdot 10^{-3}$ Pa, laser energy = 470 mJ, f = 10 Hz, t_{dep} = 5′)	(1) PVP, EtOH; (2) TiO_2, Zn	calcination: 500 °C, 1 h air		CP: rutile, wurtzite		[77]

2.6. Hierarchical Structure

Nanocomposites consisting of anatase TNPs on wurtzite ZNRs were synthetized by direct hydrothermal reaction between $TiCl_4$ and $ZnCl_2$ and urea in ethanol solution. The mixture was treated in autoclave at 180 °C for 16 h and then calcinated at 450 °C for 2 h. Composites (Zn/Ti = 1/1 mol. ratio) had a particle size of 20 nm and surface area of 84 $m^2\ g^{-1}$. Increasing zinc content decreased surface area and increased particle size [78].

ZnO-decorated TiO_2 nanowires (NWs) were obtained by hydrothermal treatment of P25 TiO_2, followed by reflux treatment in a zinc acetate solution. The hydrothermal treatment was performed in NaOH aqueous solution in autoclave at 200 °C for 24 h and the reflux treatment in a methanol solution of zinc acetate, NaOH and DW. TNWs were made of anatase and TiO_2 (B) phases, and ZnO was in the wurtzite phase. NWs were 4 µm long and 50 nm in diameter. The ZnO NPs were 20 nm in size, and the surface area did not exceed 23 $m^2\ g^{-1}$ [79].

Urchin-like TiO_2/ZnO (UTZs) consisting of ZnO nanospindle-coated TiO_2 nanosphere were synthetized by a double-step hydrothermal route. The first step was to obtain the TiO_2 spheres, and was performed with an aqueous dispersion of P25 titania with NaOH and H_2O_2 by an autoclave treatment at 160 °C for 2 h. The TiO_2 spheres were calcinated at 450 °C for two hours and then treated for the second time in autoclave at 100 °C for 3 h in an aqueous solution of ZN and HMTA. The surface area value of UTZs was up to 187 $m^2\ g^{-1}$ and the sphere diameter was 1.5–2.5 µm. [80].

The ZNRs on TiO_2 arrays were obtained through a hydrothermal synthesis involving four steps, the first three of which were used to obtain the TiO_2 arrays and only the last one for the growth of the ZNRs. The titanium and zinc precursor were TiF_4 and ZS, respectively, and additional HCl, NaOH, NH_4F and distilled water were used. TiO_2 arrays are formed of anatase nanocrystals (20 × 70 nm) which are bounded, perpendicular to the TiO_2 array direction, a few µm in length and a few hundred nm in diameter. ZNRs were 80 nm in diameter and formed an angle of 50° with the TiO_2 array direction [81].

Composite ZnO-TiO_2 nanotubes (ZTNTs) have been obtained by a double-step hydrothermal route: in the first step, TiO_2 nanotubes (TNTs) were synthesized using titanium sulphate (TS) in EtOH, glycerine and Et_2O, with an autoclave treatment at 110 °C for 48 h; the obtained product was added to a zinc chloride and ammonium hydroxide water solution, and a further hydrothermal treatment at 95 °C for 3 h was performed. Final ZTNTs were made of anatase and wurtzite, and the nanotube (NT) diameter measured 4–5.5 µm [82].

Branched hierarchical ZNRs on TNFs were grown by a three-step route. The first step was the growth of TNFs by electrospinning on a glass substrate, using TTIP as titanium precursor and polystyrene (PS) in DMF. In the second step, the ZnO seeding was performed on TNFs by dip coating using a zinc acetate alcohol solution. Finally, ZNRs were grown by hydrothermal synthesis at 90 °C for 8 h, with an aqueous solution of zinc nitrate and hexamethylenetetramine (HMTA). TNFs were made of polycrystalline anatase and had a diameter of 150 nm; ZNRs had wurtzite structure, and grew along the [0001] direction [83].

The brush-like ZT structure formed of ZNRs on TNFs was synthetized by a double-step route. The first step was to obtain TNFs by electrospinning in a conventional way, using TBT as a titanium precursor, PVP in acetic acid and ethanol, and applying a voltage of 20 KV; the second step was a hydrothermal synthesis performed in autoclave at 100 °C for 3 h, using an aqueous solution of zinc acetate, HMTA and TNFs. Brush-like structures were made up of crystalline anatase and wurtzite and ZNRs were 100–300 nm in diameter and 1–2 μm long, while TNFs are 100 nm in diameter [84].

A self-standing ZT IOS was prepared by a double-step impregnation synthesis. The first step was performed with an ethanol solution of TTIP and DEA on PS spheres which were inserted between two glass slides; the PS spheres had a diameter of 300 nm. Then, the calcination at 500 °C gave rise to the formation to an IOS of TiO_2. The IOS was then impregnated in an ethanol/aqueous solution of zinc nitrate and annealed at 400 °C for 3 h in air. The self-standing ZT IOS membrane had a regular pore with a diameter of 205 nm and was made of the anatase and wurtzite phase. Surface area was 35 m^2 g^{-1} [85].

ZnO quantum dots (Z QDs) onto an IOS in powder have been synthesized by impregnating a layer of self-assembled PS spheres on a filter paper with a suitable Z QDs/TiO_2 gel, followed by calcination at 550°C. Z QDs, 5 nm in size, had been previously obtained by ZAc hydrolyzing and added to a mixture of TTIP, HCl, EtOH and DW to give the suitable Z QDs/TiO_2 gel. The final IOS contained an anatase phase with particle size of 5–15 nm and Z QDs with a particle size of 5–10 nm. [86].

A hierarchical structure with TNPs on ZnO nanoflakes (ZNFls) was synthesized by the hydrothermal method in autoclave at 120 °C for 8 h, using TTIP and ZN as titanium and zinc precursors, respectively, together with EtOH, NaOH and DW. Anatase and wurtzite were present, with an average crystalline size of 30–40 nm, and TNPs were 20 nm in diameter and ZNFLs were 155 nm long [87].

ZT IOS was used as substrate to grow ZNRs. TiO_2 IOS was obtained by chemical bath deposition (CBD), using an alcoholic solution of TTIP on a deposit of PS microspheres on FTO, followed by annealing at 550 °C. NRs were grown after ZnO seeding; both steps used ZAc in ethanol solution [88].

Properties and synthesis conditions of ZT hierarchical nanostructures are summarized in Table 7.

Table 7. Properties and synthesis conditions of ZT hierarchical nanostructures. The numbering in the synthesis-method column and starting-material column indicates the succession of steps in the synthesis. The parameter r, when present, is used to express the composition, and must refer to its own line.

Shape and Particle Size	Synthesis Method	Starting Materials	Composition	Thermal Treatments	Crystal Phases (CP) and Crystallite Size (CS)	SA and E Gap	Ref.
TNPs on ZNRs PS_{TNPs} = 10–20 nm (r = 0); $\varnothing_{NRs}$ = 20 nm, length $_{NRs}$ = a few 100 nm (r = 1/0)	Hydrothermal method	$ZnCl_2$, $TiCl_4$, EtOH, H_2O, urea	r = Zn/Ti (molar ratio) = 0/1, 1/2, 1/1, 2/1, 1/0	autoclave: 180 °C, 16 h; 450 °C, 2 h	CP: anatase, wurtzite	SA= 87 m^2 g^{-1} (r = 1/2); 84 m^2 g^{-1} (r = 1/1); 64 m^2 g^{-1} (r = 2/1)	[78]

Table 7. *Cont.*

Shape and Particle Size	Synthesis Method	Starting Materials	Composition	Thermal Treatments	Crystal Phases (CP) and Crystallite Size (CS)	SA and E Gap	Ref.
ZNPs TNWs (ZnO-decorated TNWs) PS: ZNPs = 20 nm,: $Ø_{TNWs}$ = 50 nm, $length_{TNWs}$ = 4 µm	2 steps: (1) TNWs by hydrothermal method; (2) ZnO by reflux method	(1) TiO_2 (P25), NaOH, DW; (2) MeOH, ZAc, TNWs (from 1), NaOH, DW	ZnO (wt.%) = 0, 10, 15, 20, 30, 50, 70%	(1) autoclave: 200 °C, 24 h; drying 80 °C, 24 h; calcination: 500 °C, 3 h; (2) reflux: 60 °C, 6 h; drying: 80 °C, 24 h	CP: anatase, TiO_2 (B), wurtzite	SA = 22–23 m^2 g^{-1} E gap = 2.99 eV (TNWs); 2.96 eV (ZNPs TNWs)	[79]
ZnO nanospindles coating TiO_2 nanosphere. PS: $∅_{nanospheres}$ = 1.5–2.5 µm	2 steps: (1) TiO_2 nanospheres by hydrothermal synthesis; (2) ZnO nanospindles on TiO_2 nanosphere by hydrothermal synthesis	(1) TiO_2 (P25), NaOH, DW, H_2O_2; (2) ZN, HMTA, DW, TiO_2 nanospheres (from 1)	(1) autoclave: 160 °C, 2 h, drying: 60 °C; calcination: 450 °C, 2 h, air; (2) autoclave: 100 °C, 3 h; drying: 60 °C		CP: anatase, wurtzite	SA = 187 m^2 g^{-1}	[80]
ZNRs on TiO_2 arrays PS: $length_{TiO2\ array}$ = a few 100 µm, $Ø_{TiO2\ array}$ = a few hundred nm; $Ø_{ZNRs}$ = 80 nm	4-step hydrothermal route	(1) TiF_4, HCl, DW, NaOH; (2) gel (from 1), TiF_4; DW; (3) product (from 2), DW; (4) product (from 3), ZS, NH_4F, DW	(1) autoclave: 180° C, 48–50 h; (2) 50 °C, 3–20 h (3) 120 °C, 21 h; (4) 60 °C, 7–15 h		CP: anatase, wurtzite		[81]
ZTNTs PS: ∅ = 4–5.5 µm	2-step hydrothermal synthesis	(1) TS, EtOH, Et_2O, glycerin, (2) $ZnCl_2$, DW, NH_4OH, TNTs (from 1)	(1) autoclave: 110 °C 48 h; drying 70 °C 12h; calcination: 450 °C 3 h; (2) autoclave: 95 °C, 3 h; drying: 40 °C, 24 h		CP: anatase, wurtzite	E gap = 3.24 eV (ZnO); 3.22 eV (TNTs); 3.12 eV (ZTNTs)	[82]

Table 7. *Cont.*

Shape and Particle Size	Synthesis Method	Starting Materials	Composition	Thermal Treatments	Crystal Phases (CP) and Crystallite Size (CS)	SA and E Gap	Ref.
ZNRs branched-TNFs PS: $Ø_{TNFs}$ = 150 nm; $Ø_{ZNRs}$ = 80 nm, $length_{ZNRs}$ = 200–400 nm	3 steps: (1) TNF growth by electro-spinning on glass slide, using V = 10 V, distance Al collector -nozzle = 15 cm; flow = 20 µL/min; t = 20 min; (2) ZnO seeding by dip coating (3) ZNR growth by hydrother-mal treatment	(1) PS, TTIP, DMFA; (2) ZAc, IPOH, TEA, TNFs (from 2); (3) ZN, HMTA, DW, seeded TNFs (from 3)	(1) 80 °C, hot-pressed; 120 °C; calcination: 500 °C, 1.5 h; (2) drying: 120 ° h, in air; (3) hydrothermal treatment; 90 °C, 8 h				[83]
brush-like ZNRs on TNFs PS: $Ø_{TNFs}$ = 100 nm; $Ø_{ZNRs}$ = 100–300 nm, $length_{ZNRs}$ = 2 µm	2 steps: (1) TNFs by elec-trospinning using V = 20 KV; (2) ZNRs by hydrother-mal synthesis	(1) TBT, AcA, EtOH, PVP; (2) TNF (from 1 after calcination), ZAc, DW, HMTA	(1) calcination: 500 °C, 2 h, air; (2) autoclave: 100 °C, 3 h; drying: 60 °C		CP: anatase, wurtzite		[84]
self-standing ZT IOS membrane PS: pore ∅ = 205 nm	(1) TiO_2 self-standing by PS sphere impregna-tion between 2 slides in a sandwich geometry; (2) Zn impregna-tion	(1) TTIP, DEA, EtOH, PSs) ZN, EtOH, DW	(1) calcination: 500 °C, 2 h; (2) annealing; 400 °C, 3 h, air.		CP: A, W	SA = 35 m^2 g^{-1}	[85]
M: IOS. PS: Z QDs 5–10 nm; TNPs = 5–15 nm	(1) Z QDs by ZAc hydrolyzing: (2) Z QDs@TiO_2 by sol–gel; (3) IOS by PS impregna-tion	(1) ZA, MeOH, KOH, TEOS, DW; (2) EtOH. HCl, TTIP, DW, Z QDs (from 1); (3) gel (from 2), self-assembled PS spheres onto filter paper	drying: 24 h; calcination: 550 °C, 12 h		CP: anatase CS = 5.5 nm (Z QDs), 8.5–11.8 nm (anatase)	SA = 33–37 m^2 g^{-1}	[86]

Table 7. *Cont.*

Shape and Particle Size	Synthesis Method	Starting Materials	Composition	Thermal Treatments	Crystal Phases (CP) and Crystallite Size (CS)	SA and E Gap	Ref.
TNPs on Z NFls PS: TNPs = 21 nm; $length_{ZNFls}$ = 155 nm	hydrothermal method	TTIP, EtOH, ZN, DW, NaOH h	r = ZnO/TiO_2 volume ratio = 1/0, 2, 4	autoclave: 120 °C, 8 h	CP: anatase, wurtzite CS = 32–40 nm, decreases with increasing Ti content		[87]
M: ZNRs on ZT inverse opal membrane	4-step route: (1) FTO immersion in ethanol dispersion of PSs followed by evaporation; (2) TiO_2 IOS by CBD; (3) ZnO seeding by CBD; (4) ZNRs by CBD	SM: (1) EtOH, PSs; (2) TTIP, EtOH, PSs on FTO (from 1); (3) ZAc, EtOH, TiO_2 on FTO (from 2); (4) ZAc, EtOH, HMTA, DW, seeded FTO (from 3)	(1) drying: 58 °C; (2) annealing: 550 °C, 2 h; (3) 450 °C, 5′; (4) CBD: 80 °C, 2 h; drying: 60 °C, 6 h, air		Anatase, wurtzite		[88]

2.7. Films

ZT films have been deposited on quartz by the sol–gel/dip coating method with an ethanol/aqueous solution of zinc acetate and TBT with HNO_3; then, drying and annealing at 400 °C for 10′ were performed, and the procedure was repeated several times, to achieve the desired film thickness. The final annealing was performed at 400 or 500 °C in N_2 atmosphere for two hours. The maximum content of Zn was 20 at.%, and only the anatase phase was detected. Particle size was 5 nm and 10 nm in films annealed at 400 and 500 °C, respectively, and the thickness was of 1.2–1.5 µm [89].

Films with numerous cracks and made of anatase were obtained by dip coating on Ti plates with an ethanol/aqueous solution of ZN, TBT, DEA and polyethylene glycol (PEG) 2000. The dipping lasted 30 s and was followed by drying at 100 °C and annealing at 520 °C for 1 h. The procedure was repeated up to five times [90].

No cracks were observed if the dip coating was performed using TTIP and $ZnCl_2$ as titanium and zinc precursors, respectively, in an isopropanol solution containing citric acid and ammonium hydroxide on a glass slide. Zn/Ti were in an atomic ratio 1/1 and an annealing treatment was performed in oxygen atmosphere at 500, 600 and 800 °C. The film was made of wurtzite and crystalline TiO_2, which was in the anatase phase and (111) rutile, if the final annealing temperature was up to 600 °C, and rutile if the final annealing temperature was higher than 600 °C [91].

ZT films were dip-coated on glass with different compositions (χ_{Ti} = 100%, 75%, 50%, 25%, and 0%), using an ethanol/aqueous solution of TBT and ZAc with AcA and DEA. The drying was performed at 100 °C for 1 h and the annealing at 500 °C for 2 h. The film was made of anatase ($\chi_{Ti} \geq$75%), wurtzite ($\chi_{Ti} \leq$ 50%.), and an amorphous phase (χ_{Ti} =25 ÷ 50%) [92].

Composite ZT films were deposited also by sol–gel spin coating [93] and by sol–gel spray–spin coating [94] on glass. Films with macropores with a diameter of 1.5–8 µm were obtained using zinc acetate and TBT, as zinc and titanium precursors, respectively, in ethanol solution in the presence of DEA and HNO_3, performing the spin-coating process at 800 rpm for 20 s and 3000 rpm for 30 s, and a final calcination at 500 °C for 30′. The film

presented only the anatase phase if the ZnO/TiO_2 molar ratio was 10 and 20%, and only the amorphous phase if the ZnO/TiO_2 molar ratio was 30 and 40% [93].

ZT composite films were grown on Si (100) and Al_2O_3 substrates by cold-wall chemical vapor deposition (CVD), using $Ti(O^iPr)_2(dpm)_2$, and $Z(hfa)_2$*TMEDA as titanium and zinc precursors, respectively, in a wet oxygen atmosphere and with nitrogen as the carrier gas [95]. Zinc oxide was deposited first with a vaporization temperature of 60 °C and setting the substrate temperature at 350 or 400 °C for 60′. Titanium dioxide was subsequently deposited at a vaporization temperature of 90 °C, a substrate temperature of 400 °C, and a deposition time of 10–30′. The ZT composite films had a columnar growth, with dispersion of guest TNPs into the host ZnO nanoplatelets. Wurtzite was formed and had the c-axis preferentially orientated in the growth direction for deposition on the Si substrate. TiO_2 in the anatase phase was detected only for the longer deposition time and higher deposition temperature on the Si substrate; otherwise, it was amorphous. Film thickness was 140 nm, and particles were rod-like shaped (10–60 nm) for the shorter deposition time of titania and spherical-like shaped (50 nm) for the longer deposition time of titania on the Si substrate.

ZT film properties and synthesis conditions are summarized in Table 8.

Table 8. ZT film properties and synthesis conditions. The parameter r, when present, is used to express the composition, and must refer to its own line.

Shape and Particle Size	Synthesis Method	Starting Materials	Composition	Thermal Treatments	Crystal Phases (CP) and Crystallite Size (CS)	SA and E Gap	Ref.
ZT films on quartz PS = 5 nm ($T_{annealing}$ = 400 °C), 10 nm ($T_{annealing}$ 500 °C). Film thickness: 1.2–1.5 μm	N cycles of sol-gel/dip coating/annealing	ZAc, TBT, EtOH, DW, HNO_3	Zn at.% = 1%, 5%, 10%, 20%.	drying: 100 °C, 20′; annealing: 400 °C, air; 500 °C, 2 h in N_2	CP: anatase	Egap = 3.25–3.43 eV ($T_{annealing}$ = 400 °C); 3.12–3.24 eV ($T_{annealing}$ = 500 °C); increases with increasing Zn content	[89]
ZT flat films on Ti plates with numerous cracks	1–5 cycles of sol–gel/dip coatings/annealing). Dip-coating by immersion for 30 s	ZN, TBT, DW, DEA, EtOH, PEG 2000	T/Zn/O at. ratio = 47.27/3.64/49.09	drying: 100 °C, 30′; annealing: 520 °C, 1 h	CP: anatase CS = 15–20 nm		[90]
ZT film on glass slide, no crack. Film thickness: 60 nm per cycle	N cycles of sol–gel/dip coating/drying/annealing. Dipping and withdrawing speed = 10 cm min^{-1}	TTIP, IPOH, CitrA; $ZnCl_2$, NH_4OH	Ti/Zn at. ratio = 1/1	Drying: 80 °C 30′; annealing: 500/600/800 °C, 1 h, O_2	CP: anatase ($T_{annealing}$ = 500 and 600 °C), rutile ((111) oriented when $T_{annealing} \leq 600$ °C); wurtzite		[91]

Table 8. *Cont.*

Shape and Particle Size	Synthesis Method	Starting Materials	Composition	Thermal Treatments	Crystal Phases (CP) and Crystallite Size (CS)	SA and E Gap	Ref.
ZT film on glass PS = 15–30 nm (χ_{Ti} = 100%); 5–15 nm (χ_{Ti} = 75%); 100–500 nm (χ_{Ti} = 25%); 20–40 m, (χ_{Ti} = 0%). Film thickness = 250 nm(χ_{Ti} = 100%)	2 cycles of sol–gel/dip coating. Dipping and withdrawing speed = 2 mm s^{-1} h	ZAc, TBT, H_2O, DEA, EtOH, AcA	χ_{Ti} = 100%, 75%, 50%, 25%, 0%	Drying 100 °C, 1 h; annealing: 500 °C, 2	CP: anatase, ($\chi_{Ti} \geq 75\%$), wurtzite ($\chi_{T\,i} \leq 50\%$.), amorphous (χ_{Ti} = 25 ÷ 50%) CS = 16 nm (χ_{Ti} = 100%); 12 nm (χ_{Ti} = 75%); 10 nm (χ_{Ti} = 50%); 27 nm (χ_{Ti} = 25, 0%)		[92]
Macroporous ZT film on glass substrate	3 cycles of sol–gel spin coating	ZAc, EtOH, DEA, TBT, acetone, HNO_3	Drying: 110 °C, 30′; calcination: 500 °C, 30′ air	r = ZnO/TiO_2 mol ratio = 10%, 20%, 30%, 40%	CP: anatase (r = 0, 10, 20%); amorphous (r = 30, 40%)		[93]
Columnar granular ZT films, TiO_2 into porous ZnO Film thickness = 140 nm	2 steps: (1) ZnO by cold-wall CVD; (2) TiO_2 by cold-wall CVD * Deposition parameter: see note at the end	(1) $Z(hfa)_2$*TMEDA, H_2O, O_2, N_2; (2) $Ti(O^iPr)_2(dpm)_2$, H_2O, O_2, N_2			CP: W (preferential orientation (002) on Si), A (on Si, longer deposition times)		[95]

* Deposition parameters: substrate: Si (100) and Al_2O_3; P = 10 mbar, T_{wall} = 110 °C; ZnO: f(N_2) = f(O_2 + H_2O) = 40 sccm, t = 60′, $T_{vaporization}$ = 60 °C, $T_{Substrate}$ = 350 and 400 °C; TiO_2: f (N_2) = 40 sccm, f (O_2 + H_2O) = 80 sccm, t = 10 and 30′, $T_{vaporization}$ = 90 °C, $T_{substrate}$ = 400 °C.

2.8. Layered Films

Layered ZnO on TiO_2 film on ITO (ZnO/TiO_2/ITO) have been grown by a double-step route: the first was the TiO_2 film deposition onto ITO by CBD [96] or by spin coating [97] and the second one was the ZnO deposition by a layer-by-layer process (LbL). The LbL process was carried out by alternating the immersion of the TiO_2 film into a zinc tetramine solution and washing it in distilled water at 90 or 95 °C various times, until obtaining the desired film thickness [96,97]. The LbL process allowed for the wurtzite formation.

Layered ZnO on TiO_2 film on FTO has been grown by TiO_2 deposition on FTO by the doctor-blade technique, followed by ZnO deposition by CVD in argon atmosphere at 500 °C. The film was composed of anatase, rutile and wurtzite [98].

Layered TiO_2 on ZnO films on quartz (TiO_2/ZnO/quartz) was grown by calcination at 500 °C of a zinc film deposited inside a quartz tube by vacuum vaporization, followed by a sol–gel dip coating with an aqueous/ethanol solution of TTIP and HNO_3 and a further calcination at 500 °C. The film was made of anatase and wurtzite, with particle size of 30 nm [99].

Layered films ZnO/TiO_2, TiO_2/ZnO [100] and ZnO/TiO_2/ZnO [101] were deposited on quartz-glass substrate by electron-beam evaporation; the wurtzite phase was detected with the c-axis preferentially oriented normally to the substrate and the crystallite size

was in the range of 15–25 nm. The TiO_2 layer improved ZnO crystallinity by increasing its particle size.

Magnetron sputtering has also been used to deposit TiO_2/ZnO film on glass substrate. ZnO and TiO_2 films were obtained by oxidation of the successively deposited Zn and Ti films and contained anatase, rutile and wurtzite when thermal oxidation was performed at a temperature not lower than 450 °C [102].

ZnO nanowires (ZNWs) have been grown by hydrothermal synthesis on TiO_2 NP film [103] or on ZNPs on TNP film [104], which had already been obtained by the screen-printing method on FTO. Hydrothermal treatment was performed with an aqueous solution of zinc nitrate and HMTA [103] and PEI, ammonium hydroxide and nitric acid at T = 88–93 °C for 10–15 h [104]. ZNWs were in the wurtzite phase and had a diameter of 50–100 nm [103]; the film thickness was 10 µm [103] or 12 µm [104].

Multilayer films of oriented (002) wurtzite ZnO and (200) rutile TiO_2 have been epitaxially grown on (006) sapphire by atomic layer epitaxy (ALE) [105]. Diethyl zinc and $TiCl_4$ have been used as zinc and titanium precursors, respectively; H_2O was used as an oxidizing agent, and the substrate temperature was 450 °C. The film was composed of 10 double layers of TiO_2/ZnO.

ZnO-TiO_2-layered film properties and synthesis conditions are summarized in Table 9.

Table 9. ZnO-TiO_2-layered film properties and synthesis conditions. The numbering in the synthesis-method column and starting-material column indicates the succession of steps in the synthesis.

Shape and Particle Size	Synthesis Method	Starting Materials	Thermal Treatments	Crystal Phases (CP) and Crystallite Size (CS)	SA and E Gap	Ref.
TiO_2 and ZnO/TiO_2 films on ITO with cone-like surface morphology. Film thickness = 1.418 µm	2 steps: (1) TiO_2 compact film on ITO by CBD; (2) ZnO crystalline film by LbL	(1) $TiCl_3$, HCl, DW, ITO, NH_4OH; (2) (a) $ZnCl_2$, NH_4OH, H_2O_2, DW, (b) H_2O 90 °C.		CP: wurtzite	E gap: 3.85 eV (TiO_2/ITO), 3.26 eV (ZnO/TiO_2/ITO)	[96]
ZnO/TiO_2 film on ITO, ZnO. Film thickness = 300 nm	2 steps: (1) TiO_2 films by spin-coating on ITO/glass: (2) ZnO film by LbL. LbL by 1–10 cycles of dipping 30 s + TT 95 °C	(1) TiO_2 (P25), Triton X-100, 2–4 pentadiene, DW, ITO/glass; (2) (a) $[(Zn(NH_3)_4]^{2+}$ solution 8 (b) 95 °C in water		CP: anatase, rutile, wurtzite		[97]
ZnO/TiO_2 film on FTO	2 steps: (1) TiO_2 film on FTO by doctor-blade technique; (2) ZnO on TiO_2 by CVD	(1) TiO_2 (P25), H_2O, acetone, PEG, polyethylene oxide (PEO); (2) Zn powder	(1) annealing: 450 °C; (2) T = 500 °C, Ar, t = 5′, 30′, 60′	CP: anatase, rutile, wurtzite		[98]
TiO_2/ZnO film inside a quartz tube PS = 30 nm	2 steps: (1) ZnO by calcination of Zn film deposited on a quartz tube by vacuum vaporization; (2) TiO_2 coating by dip coating	SM: (1) Zn Powder; (2) TTIP, EtOH, HNO_3, DW	(1) calcination: 500 °C, 1 h; (2) calcination: 500 °C, 1 h	CP: anatase, wurtzite		[99]

Table 9. *Cont.*

Shape and Particle Size	Synthesis Method	Starting Materials	Thermal Treatments	Crystal Phases (CP) and Crystallite Size (CS)	SA and E Gap	Ref.
TiO_2, ZnO, TiO_2/ZnO and ZnO/TiO_2 films on quartz glass substrate	Electron-beam evaporation using (ZnO) f (O_2) = 60 sccm, working pressure = 2.4 × 10^{-4} torr, working T = 300 °C, V = 7.11 kV, i = 78 mA, deposition rate = 5.0 Å s^{-1} (TiO_2): f (O_2) = 35 sccm, working pressure = 1 × 10^{-4} torr, working T = 200 °C, V = 7.11 kV, i = 246 mA, deposition rate = 5.0 Å s^{-1}	ZnO, TiO_2, O_2		CP: amorphous (TiO_2 film); (002) wurtzite (ZnO film); (002) wurtzite, (102) rutile (TiO_2/ZnO and ZnO/TiO_2). CS = 15 nm (W in ZnO film), 20 nm (W in TiO_2/ZnO film); 25 nm (W in ZnO/TiO_2 film).	E gap: 3.38 eV (ZnO); 3.35 eV (TiO_2/ZnO); 3.32 eV (ZnO/TiO_2); 4.0 eV (TiO_2)	[100]
ZnO, ZnO/TiO_2 and ZnO/TiO_2/ZnO film on quartz-glass substrate	electron-beam evaporation WC: TiO_2: f (O_2) = 35 sccm, p = 9 × 10^{-5} torr T = 200 °C, i = 220 mA, growth rate = 5.0 Å s^{-1} ZnO: f (O_2) = 60 sccm, p = 1 × 10^{-4} torr T = 320 °C, i = 90 mA, growth rate = 2.5 Å s^{-1}			CP: (100)- and (002)-oriented wurtzite CS: 19 nm (ZnO film); 22 nm (ZnO/TiO_2 film), 23 nm (ZnO/TiO_2/ZnO). E gap: 3.26 eV (ZnO), 3.27 eV (ZnO/TiO_2), 3.34 eV (ZnO/TiO_2/ZnO)		[101]
TiO_2/ZnO on glass substrate. film thickness = 120–130 nm	ZnO film by Zn magnetron sputtering followed by thermal oxidation; (2) TiO_2 film by Ti magnetron sputtering followed by thermal oxidation	(1) Zn metal: (2) Ti metal	400 °C, 450 °C, 500 °C, 550 °C	CP: anatase, rutile, wurtzite CS: 7–20 nm (rutile); 16–26 nm (wurtzite)		[102]
ZnO micro-rod array or ZNWs/TNPs film on FTO. PS: $Ø_{ZNWs}$ = 50–100 nm; film thickness = 10 µm	2 steps: (1) TiO_2 compact film by screen printing on FTO; (2) Z micro-rod or NWs by hydrothermal synthesis	(1) TiO_2 paste; (2) ZN, HMTA, DW	(1) 325 °C, 5′; 375 °C, 5′; 500 °C, 15′; (2) hydrothermal treatment: 88 °C, 12	CP: anatase, wurtzite		[103]

Table 9. *Cont.*

Shape and Particle Size	Synthesis Method	Starting Materials	Thermal Treatments	Crystal Phases (CP) and Crystallite Size (CS)	SA and E Gap	Ref.
ZNWs/mesoporous TZNPs film on FTO. film thickness = 12 μm	2 steps: (1) ZNPs by hydrolysis; (2) ZT mesoporous film on FTO by screen-printing method, (3) ZNWs on (2) by hydrothermal treatment (5–10–15 h)	(1) ZAc, KOH, MeOH, FTO; (2) mesoporous ZnO film on FTO (from 1), TiO_2 paste (3) ZN, HMTA, DW, PEI, NH_4OH, HNO_3	(2) sintering: 325 °C, 5′; 375 °C, 5′; 450 °C, 30′; (3) hydrothermal treatment: 93 °C, 5, 10 or 15 h	CP: anatase, rutile, wurtzite		[104]
10 bilayers of (001) ZnO/(200) TiO_2 on (006) sapphire substrate	ALE	$ZnEt_2$, $TiCl_4$, DW	T_{dep} = 450 °C			[105]

2.9. Core–Shell Structures on Substrate

Core (ZnO)–shell (titania) nanowires (cs ZT NWs) have been deposited on a substrate by a two- or three-step route: (1) ZnO substrate seeding (facultative step), (2) ZnO nanowires (ZNWs) growth on substrate and (3) ZNWs titania coating.

cs ZT NWs were synthetized by seeding of ZNPs (4–5 nm) on a conductive glass by dip coating using an ethanol Z QDs dot dispersion, and then NWs were grown by CBD in a continuous-flow reactor, with a water solution of zinc nitrate, HMTA and PEA at 92 °C for 24 h, followed by thermal treatment at 400 °C for 30′. The TiO_2 shell was grown by atomic layer deposition using $TiCl_4$ and distilled water at T = 300 °C. The cs ZT NWs were 15 μm long and 150 nm in diameter, and the shell thickness was governed by the number of ALD cycles and was found to be amorphous TiO_2 when the thickness was less than 5 nm; otherwise, it was polycrystalline anatase. Skeletal ZnO NWs resulted in wurtzite single crystal [106].

Cs ZT NWs were grown by ZnO seeding on an FTO on glass by spin coating of a zinc acetate ethanol solution followed by ZNW growth by the hydrothermal route with a solution of similar composition to the previous one, at 88 °C for 2 h. The TiO_2 outer layer was then deposited by sol–gel with TTIP in BuOH, together with acetyl acetone. At the end, a final calcination at 350 °C for 2 h was performed. The NWs were formed by oriented (002) wurtzite and polycrystalline anatase and had a length of 1.5–2 μm and a diameter of 100–150 nm, with a shell thickness of 20–50 nm [107].

Almost vertically aligned cs ZT NWs were deposited on steel mesh by a double-step hydrothermal route: the first one, for the ZNW skeletal structure, used zinc nitrate, ammonia and distilled water and the second one, for the titania shell, used TBT, DW, and DEA. At the end, the calcination was performed at 500 °C. Wurtzite was clearly detected, and anatase was present in a small amount. Cs ZT NWs had a diameter of 150 nm and a length of 9 μm [108].

Completely aligned cs ZT NWs on a carbon-coated silicon wafer were obtained by thermal evaporation of zinc wire at 700 °C in a mixture of Ar and O_2 gases (flow rate = 0.6 $Lmin^{-1}$, deposition time = 30″) to obtain the ZNWs, followed by chemical vapor deposition of titania from TTIP and with N_2 as a carrier gas, with a furnace temperature of 450 °C, to form the outer TiO_2 coating. The shell thickness varied in the range of 5–50 nm using different times of deposition, and the final Cs ZT NWs contained (002) wurtzite and were 5 μm long and 60 nm in diameter [109].

TiO_2 coating on ZNWs obtained by hydrothermal growth was also performed by thermal evaporation of titanium. The Cs ZT NWs were 3 μm long and 30–250 nm in diameter, and were formed by (002) wurtzite; the resulting titania coating was amorphous, with a thickness in the range of 5–50 nm [110].

Similarly to the cs ZT NWs, core (ZnO) shell (titania) nanorods (cs ZT NRs) have been synthesized by a two- or three-step route. cs ZT NWs vertically oriented (within 5–10°) were grown on textured ZnO-seeded ITO by CBD, followed by titania coating. Textured ZnO-seeded ITO was obtained by dropping an ethanol solution of zinc acetate and by subsequent heating at 350 °C for 30 min in air. The ZNR growth was performed by CBD by using zinc nitrate, HMTA and PEA in water solution at 80 °C for 3 h. The TiO_2 outer coating was deposited by ALD using $TiCl_4$ and water at 300 °C. The cs ZT NRs were 150–225 nm long and 15-to-25 nm in diameter and the shell thickness was 2–30 nm, and cs ZTNRs were formed by wurtzite and anatase if the TiO_2 layer was thicker than 4 nm; otherwise, the TiO_2 was amorphous [111].

In a similar way, cs ZT NRs were grown on silicon substrate, growing the outer TiO_2 layer by spin coating, using an ethanol solution of TTIP and with a subsequential annealing at 400 °C for 1 h in air [112].

Cs ZT NRs have been obtained by ZnO seed deposition on the FTO substrate by magnetron sputtering, followed by ZNR growth, performed by hydrothermal reaction using an aqueous zinc nitrate solution in the presence of HMTA. The hydrothermal reaction was carried out at 80 °C and lasted 8 h; then, the TiO_2 coating was accomplished by magnetron sputtering, followed by annealing at 500 °C for 10′. The cs ZT NRs were made of wurtzite with the [0001] direction along the growth direction, and anatase; the cs ZT NR diameter was 80–120 nm, the length was 1.5 μm, and the shell thickness was 11 nm and resulted in NPs with a size of 5 nm [113].

Cs ZT NR arrays made of oriented (002) wurtzite and (004) anatase were obtained by spin coating of ZAc in MEA to accomplish the ZnO seeding on glass substrate, followed by a hydrothermal growth of ZNRs at 93 °C for 8 h, making use of an aqueous solution of ZAc and HMTA. The TiO_2 coating was performed by sol–gel spin coating using an ethanol solution of TBT, DEA and water. Uncoated and coated NRs had a diameter of 200 nm and 220 nm and a surface area of 16.4 and 16.7 $m^2\ g^{-1}$, respectively [114].

Cs ZT NRs with a diameter of 40–45 nm were deposited by ZnO seeding on glass substrate by thermal decomposition of zinc acetate, at 350 °C, followed by ZNR growth by CBD with an aqueous solution of zinc nitrate and ammonia; the outer TiO_2 layer was grown by multiple cycles of sol–gel/spin coating, with an ethanol solution of TTIP, AcA, DW and MeOEtOH. Wurtzite formation was evident, and anatase was detectable only for thicker TiO_2 layers [115].

Cs ZT NRs were grown by ZnO urchin-like seeding by the electrochemical method, followed by hydrothermal treatment, to grow the ZNRs and sol–gel dip coating, to obtain the outer TiO_2 coating. The ZnO urchin-like seeding on the ITO substrate was made by soaking the substrate in a zinc acetate water solution and applying a constant potential of 1.2 V versus a calomel electrode, followed by annealing at 300 °C for 1 h. The hydrothermal process was performed in autoclave at 80 °C for 2 h, with an aqueous solution of zinc nitrate and ammonia. The TiO_2 coating was performed by dipping the ZNRs in a TiO_2 sol–gel mixture, and the immersion was carried out for 6 h or by repeating the 30′ cycle 3 times, to form a rugged or continuous TiO_2 layer, respectively. The cs ZT NRs were made of (002) and (103) preferentially oriented wurtzite, and anatase was barely detectable only when the TiO_2 layer was continuous. The length of NRs was 1.3–2.2 μm and the diameter was in the range 100–300 nm; the TiO_2 coating had a thickness of 25–40 nm, and was made up of NPs with a size of 3–8 nm [116].

Cs TZ NFs were obtained by a two-step route involving the skeleton TNF synthesis and the outer ZnO coating deposition performed by electrospinning and ALD techniques, respectively. TNFs were deposited using TTIP in a solution of PVAc (polyvinyl acetate) in AcA and DMFA (dimethylformamide), onto silicon placed on an Al collector placed

20 cm away from the syringe needle. The needle had a positive voltage of 15 V, while the collector had a negative voltage of −10 V. The syringe was then operated using a pump at 0.2 mL h^{-1}. The ZnO coating was deposited by ALD, using diethyl zinc, H_2O and N_2; the temperature of the substrate was 150 °C, and the pressure was 0.3 torr. Cs TZ NFs were made up of wurtzite and anatase and had a final diameter of 250 nm [117].

Properties and synthesis conditions of cs ZTNWs, ZTNRs and TZNFs on substrate are reported in Table 10.

Table 10. cs ZTNW, cs ZTNR and cs TZNF on substrate properties and synthesis conditions. The numbering in the synthesis-method column and starting-material column indicates the succession of steps in the synthesis. The parameter r, when present, is used to express the composition, and must refer to its own line.

Shape and Particle Size	Synthesis Method	Starting Materials	Thermal Treatments	Crystal Phases (CP) and Crystallite Size (CS)	SA and E Gap	Ref.
cs ZT NWs on conductive glass PS: $\varnothing_{NWs}$ = 150 nm, length $_{NWs}$ = 15 µm, TiO_2 thickness: 5–40 nm	3-step route: (1) ZNPs seeding by dip coating; (2) ZnO NWs by CBD in a continuous flow reactor using T = 92 °C, t = 24 h; (3) TiO_2 coating by ALD using T_{dep} = 300 °C, pulse dep time = 1 s, purge time = 12 s	(1) ZNPs, EtOH, conductive glass; (2) ZN, DW, HMTA, PEA, ZnO seed on conductive glass (from 1); (3) $TiCl_4$, DW, Z NWs on glass (from 2)	(2) 400 °C, 30′	CP: anatase, (if shell thickness is more than 5 nm) amorphous TiO_2 (if shell thickness is lower than 5 nm), wurtzite (single crystal)		[106]
cs ZT NWs (vertically oriented) on FTO layer on glass. PS: $\varnothing_{NWs}$ = 100–150 nm; length$_{NWs}$ = 1.5–2 µm, TiO_2 thickness = 20–50 nm	3-step route: (1) ZnO seeding by spin coating; (2) Z NWs by hydrothermal method; (3) TiO_2 coating by sol–gel deposition	(1) ZAc, EtOH; (2) ZN, HMTA, DW, NH_4OH; ZnO seed on glass (from 1); (3) TTIP, AcA, BuOH, DW, Z NW on glass (from 2)	(1) 350 °C 20′, air; (2) hydrothermal treatment: 88 °C, 2 h; (3) annealing: 450 °C, 30′, air or N_2	CP: (002) wurtzite, anatase	E gap = 3.25 eV	[107]
cs ZT NWs (almost) vertically aligned arrays on steel mesh PS: $\varnothing_{NWs}$ = 600 nm, length$_{NWs}$ = 9 µm	2 steps: (1) ZNWs by hydrothermal method; (2) TiO_2 coating by hydrothermal method	(1) ZN, NH_4OH, DW, steel mesh; (2) TBT, DEA, EtOH, DW, ZNWs (from 1)	(1) 83 °C, 24 h; drying: 60 °C; (2) drying: 60 °C; annealing 500 °C, 1 h, air	CP: anatase, wurtzite	E gap = 3.22 eV (cs ZT NWs); 3.25 eV (ZNWs)	[108]
vertically aligned cs ZT NWs on Si. PS: $\varnothing_{NWs}$ = 60 nm; length$_{NWs}$ = 5 µm; TiO_2 thickness = 15 nm	2 steps: (1) ZNWs by thermal evaporation using f: 0.6 l min^{-1}, T_{dep}: 700 °C, t: 30 s; (2) f (N_2): 0.55 l min^{-1}, $T_{bubbler}$ = RT, T_{dep} = 450 °C, t = 30′; (3) TiO_2 coating by CVD	SM:(1) Zn wire; (2) TTIP, N_2		CP: (002) wurtzite		[109]
cs ZT NWs film on substrate PS: $\varnothing_{NWs}$ = 30–250 nm; length $_{NWs}$ = 3 µm; TiO_2 thickness: 0, 5, 10, 20, 30, 50 nm	3 steps: (1) ZnO seeding on substrate by spin coating; (2) ZNWs by hydrothermal growth; (3) TiO_2 coating by thermal evaporation using $T_{filament}$ = 1800 °C, P = 2 × 10^{-5} mbar	SM: (2) ZN, HMTA, DW (3) Ti	(2) hydrothermal growth: 95 °C, 7 h; (3) annealing: 350 °C	CP: (002) wurtzite		[110]
M: cs ZT NRs on ITO substrate PS: $\varnothing_{NRs}$ = 15–25 nm, length$_{NRs}$ = 150–225 nm	3 steps: (1) ZnO nanocrystal textured seeding by dropping with ZAc/EtOH; (2) Z NRs by chemical-bath growth; (3) TiO_2 coating by ALD. ALD performed with P = 300–500 mtorr, T = 300 °C, growth rate: 0.9 Å/cycle	Me: (1) SM: (1) ZAc, EtOH, ITO; (2) ZN, DW, HMTA, PEA, seeded ITO (from 1); (3) $TiCl_4$, DW, ZNRs (from 2)	(1) 350 °C,20′; (2) 80 °C, 30′	CP: anatase (if shell is thicker than 4 nm), (002) wurtzite		[111]
cs ZT NRs PS: $\varnothing_{NRs}$ = 30–60 nm; TiO_2 thickness: 10–20 nm	3-step route: (1) ZnO seeding by solution dropping (2) Z NRs by chemical-bath growth: (3) TiO_2 coating by spin coating	(1) ZAc, EtOH; (2) ZN, PEA, HMTA DW; (3) TTIP, EtOH	(1) annealing: 350 °C, 20′ (2) chemical-bath growth: 90 °C, 2.5 h; (3) annealing: 400 °C, 1 h			[112]

Table 10. *Cont.*

Shape and Particle Size	Synthesis Method	Starting Materials	Thermal Treatments	Crystal Phases (CP) and Crystallite Size (CS)	SA and E Gap	Ref.
cs ZT NRs (arrays) film on FTO, ZnO growth direction along [0001] direction PS: $\varnothing_{NRs}$ = 80–120 nm, length $_{NRs}$ = 1.5 µm, TiO_2 thickness = 11 nm, TiO_2 NPs = 5 nm	3-step route: (1) ZnO seeding by magnetron sputtering: f (Ar) = 20 sccm, P = 0.5 Pa, RF power = 100 W; (2) Z NRs by hydrothermal-bath deposition; (3) TiO_2 coating by magnetron sputtering: f_{Ar} = 20 sccm, P = 0.5 Pa, RF power = 100 W, T_{sub} = 450 °C, t = 9′	SM:(1) ZnO target, Ar; (2) ZN, HMTA, DW (3) TiO_2 target, Ar	(1) annealing: 350 °C, 30′; (2) hydrothermal condition: 80 °C, 8 h; (3) annealing: 500 °C, 10′	Anatase, wurtzite		[113]
cs ZT NRs arrays on glass substrate PS: $\varnothing_{NRs}$ = 200 nm (Z NRs), 220 nm (ZT NRs)	3-step route: (1) seed layer by spin coating (2) ZNRs by hydrothermal method; (3) TiO_2 layer by sol–gel spin coating method	SM: (1) ZAc, MEA, MeOEtOH; (2) ZAc, DW HMTA; (3) TBT, DEA, EtOH, DW	(1) 350 °C, 30′; (2) hydrothermal treatment: 93 °C 6 h; drying: 60 °C, 10′; (3) sintering: 550 °C, 1 h	CP: (004) anatase, (002) wurtzite, traces of Zn_2TiO_4 and $Zn_{1.7}SiO_4$	SA = 16.4 $m^2 g^{-1}$ (Z NRs), 16.7 $m^2 g^{-1}$ (ZT NRs)	[114]
cs ZT NRs on glass substrate PS: $\varnothing_{NRs}$ = 40–45 nm	3-step route: (1) seed layer by thermal decomposition at 350 °C; (2) NRs by CBD at 90 °C 1 h; (3) TiO_2 layer by sol–gel spin coating, with speed 2000 rpm. N_{cycles} = 1, 3, 5	SM: (1) ZAc; (2) ZAc, HMTA, DW; (3) TTIP, 2-MeOEtOH, AcA, DW	(3) 500 °C, 2 h	CP: anatase (n_{cycles} > 1), wurtzite		[115]
cs ZT NRs (oriented) on ITO PS: $\varnothing_{NRs}$ = 100–300 nm, length$_{NRs}$ = 1.6–2.2 µm, TiO_2 thickness = 25–40 nm (sol–gel 30′ × 3), TNPs: 3–8 nm (sol gel 6 h)	3-step route: (1) urchin-like Zn seeding by electrochemical method, V = −1.2 V (versus calomel reference electrode; (2) hydrothermal process; (3) immersion in sol–gel 6 h, or 30′ 3 times	(1) ZAc, DW, O_2; (2) ZN, DW, NH_4OH; (3) TBT, IPOH, ZNRs (from 2)	(1) 300 °C, 1 h; (2) autoclave: 80 °C, 2.5 h; drying: in air; calcination: 300 °C; (3) calcination: 450 °C	CP: A, (002), (103) preferentially oriented W	E gap: 2.86–2.93 eV (sol–gel 6 h), 2.78–2.85 eV (sol–gel 30′ × 3)	[116]
cs TZ NFs on Si wafer PS: $\varnothing_{NFs}$ = 250 nm	2 steps: (1) TNFs by electrospinning using V_{needle} = 15 kV. V_{coll} = −10 KV, distance$_{neddle/col}$ = 20 cm, feed rate: 0.2 mL h^{-1}; (2) ZnO coating by ALD using T_{dep} = 150 °C, P = 0.3 torr, alternating pulses, $ZnEt_2/N_2/DW/N_2$	SM: (1) TTIP, PVAc, DMFA, AcA; (2) $ZnEt_2$, DW, N_2	(1) calcination: 600 °C, 8 h, O_2	CP: anatase, wurtzite	E gap: 3.31 eV	[117]

2.10. Hierarchical Films on Substrate

A bottlebrush film on glass substrate consisting of TNW-coated ZNRs was grown by a three-step route. The first step was a ZnO seeding-layer deposition performed by magnetron sputtering using ZnO as target. Subsequently, ZNRs were grown by a hydrothermal synthesis with an aqueous solution of zinc nitrate, HMTA, nitric acid and ammonium hydroxide. The hydrothermal treatment was performed at 95 °C for 4 h. In the end, TNWs were grown by magnetron sputtering using TiO_2 as target to give the final bottlebrush morphology. The ZNRs had a length of 2–3 µm and were made of (002)-oriented wurtzite; the TNWs, made of rutile, were 90–100 nm long [118].

ZT NC arrays on Ti fabric were synthesized by hydrothermal treatment of TiO_2 nanotubes (TNTs) with a zinc acetate aqueous solution. TNTs, 60 µm long, with a diameter of 50 nm and a wall thickness of 10 nm, had been previously synthetized by anodic oxidation of Ti fabric using a V = 60 V for 24 h. The hydrothermal treatment was performed in autoclave at 120 °C for 2 h and the final ZT nanocomposite was made of anatase and wurtzite phases [119].

Radiolarian-like porous ZnO microspheres (RPZMs) were grown on a compact TiO_2 film on a glass substrate. TiO_2 film was deposited by spin coating with an ethanol solution

of TTIP and nitric acid followed by calcination at 450 °C for 30′. RPZMs were obtained by hydrothermal treatment of the compact TiO_2 film with an aqueous solution of zinc nitrate and MEA, performed in autoclave at 95 °C for 4 h. RPZMs were in the wurtzite phase, with a diameter of 7–9 μm; macropores of 200–500 nm were formed by ZnO sheets (500 × 100 × 50 nm) and NWs with a diameter of 20–30 nm were also present [120].

ZNRs and the flower-like microstructure in the wurtzite phase were grown by double-hydrothermal treatment on porous TiO_2 film previously screen-printed on FTO. The hydrothermal treatment was performed with an aqueous solution at pH = 11.3 of zinc nitrate and ammonium hydroxide in autoclave at 70 °C for 12 h. The hydrothermal treatment was repeated in the same conditions, except for the pH and time, which were set to 6 h and 10.8, respectively. The TiO_2 porous film was formed by spherical-like anatase particles with a diameter of 16–35 nm. The ZNRs had diameters of 60–110 nm and were 500–700 nm long; meanwhile, the flower-like microstructure had a total dimension of 5–7 μm; the petal diameter was 100–200 nm and they were 0.73–2 μm long [121].

Properties and synthesis conditions of hierarchical ZnO/TiO_2 films on substrate are reported in Table 11.

Table 11. Hierarchical ZnO/TiO_2 films on substrate: properties and synthesis conditions. The numbering in the synthesis-method column and starting-material column indicates the succession of steps in the synthesis.

Shape and Particle Size	Synthesis Method	Starting Materials	Thermal Treatments	Crystal Phases (CP) and Crystallite Size (CS)	Ref.
Bottlebrush films on glass substrate, consisting of TNWs on ZNRs. PS: $length_{ZNRs}$ = 2–3 μm; $length_{TNWs}$ = 90–100 nm	3-step route: (1) ZnO seeding by magnetron sputtering using p = 2.67 Pa, RF = 13.56 MHz, RF power = 500 W, t = 30′; (2) ZNRs by hydrothermal treatment; (3) TNWs by magnetron sputtering using T = RT, p = 10 mtorr, f = 10 sccm; carrier gas = Ar	(1) ZnO target; (2) ZN, HMTA, HNO_3, NH_4OH, DW, ZnO seeded glass (from 1); (3) TiO_2 target, ZNRs on glass (from 2)	(1) hydrothermal treatment: 95 °C, 4 h	CP: rutile, (002) wurtzite	[118]
Nanocomposite array on Ti fabric PS: TiO_2 array: Ø = 80 nm	2 steps: (1) TNTs synthesis by anodic oxidation of Ti fabric with working electrode: Ti fabric, counter electrode: Pt, V = 60 V, t = 24 (2) ZnO deposition by impregnation and hydrothermal treatment	SM: (1) Ti fabric; (2) ZAc, DW	(1) drying: 60 °C, 12 h; (2) drying: 100 °C, 1 h; autoclave: 120 °C, 2 h; drying: 70 °C, 6 h	CP: anatase, wurtzite	[119]
Radiolarian-like porous ZnO microspheres (RZMPs) PS: RZMP: 7–9 μm; macropores: 200–500 nm; ZnO nanosheets: 500 × 100 × 50 nm; NWs: Ø = 20–30 nm	2 steps: (1) compact TiO_2 film on glass by spin coating; (2) hydrothermal method	(1) TTIP, HNO_3; (2) ZN, MEA, DW, TiO_2 film on glass (from 1)	(1) 450 °C, 30′; (2): autoclave: 95 °C, 4 h	wurtzite	[120]

Table 11. *Cont.*

Shape and Particle Size	Synthesis Method	Starting Materials	Thermal Treatments	Crystal Phases (CP) and Crystallite Size (CS)	Ref.
Flower-like and NR arrays of ZnO on nanoporous TiO_2 film on FTO PS: $Ø_{TNPs}$ = 16–35 nm; ZNRs on the bottom: $Ø_{ZNRs}$: =60–110 nm, $length_{ZNRs}$ = 500–700 nm; ZnO flower-like microstructure on the top: Ø = 100–200 nm, length = 0.73–2 µm, flower-shaped total structure: 5–8 µm	3 steps: (1) TiO_2 film on FTO by screen-printing method; (2) hydrothermal synthesis on porous TiO_2 film with pH = 11.3 (3) hydrothermal treatment with pH = 10.8	SM: (1) TiO_2 paste; (2) ZN, DW. NH_4OH, TiO_2 film (from 1); (3) ZN, DW, NH_4OH, Ti/Zn film on substrate (from 2)	(2) autoclave: 70 °C, 12 h; (3) autoclave: 70 °C, 6 h	Anatase, wurtzite	[121]

2.11. Composite on TNTs on Substrate

2.11.1. ZNPs and ZNRs on TNTs

ZNPs into the TNTs (ZNPsTNTs) have been obtained by a hydrothermal treatment of TNTs in autoclave at 70 °C for 24 h with an aqueous solution of zinc nitrate and ammonia, followed by drying in air. TNTs were previously synthetized by anodic oxidation of a titanium foil in ammonium sulfate/fluoride electrolyte solution with a constant V = 20 V for 4 h, followed by calcination at 500 °C for 1 h. ZNPsTNTs were formed of anatase and wurtzite, had a diameter of 60–80 nm, and were 300 nm long [122].

ZNPs have been deposited onto TNTs also by CBD, performed by dipping TNTs in an aqueous solution of ZN and HMTA at 65 °C for 15′ several times. Increasing the number of dips increases ZNP dimension. TNTs, made of anatase, were 90 nm in diameter and 4 µm long. ZNPs were made of wurtzite; they were rice-shaped, with dimensions of 1 µm in length and 100 nm in width [123].

ZNRs embedded in highly ordered TiO_2 nanotubes (ZNRs in TNTs) were obtained by a direct cathodic electrodeposition of ZNRs on TNTs already synthetized by anodic oxidation, followed by calcination. The direct cathodic electrodeposition was performed in a three-electrode cell, and the TNT on the Ti sheet was the working electrode. The TNTs were 200–300 nm long, with a wall thickness of 10 nm and a diameter of 30–90 nm. Z NRs were formed inside the TNTs and spilled out of 100–200 nm. Crystalline anatase and wurtzite phases were present [124].

ZNRs in TNTs were synthetized also by ZnO crystal seeding on TNTs, obtained by anodic oxidation, followed by ZNR hydrothermal growth. The ZnO seeding was performed by the sol–gel method with a zinc acetate ethanol solution dropped and spun on the TNTs. The hydrothermal growth of ZNRs was performed with ZN in a water solution containing HMTA, with an autoclave treatment at 90 °, and the duration of the hydrothermal treatment was varied to control the quantity of ZNRs grafted on the TNT surface. The TNTs were made of anatase and rutile and had a diameter of 50–90 nm and a thickness of 10–15 nm. The gap between the NTs was 20 nm. The ZNRs were made of wurtzite, and had a diameter up to 50 nm and a length up to 1–2 µm, depending on the lasting time of autoclave treatment [125].

ZNRs were grown inter- and intra-tube in TNTs by crystallization from an aqueous solution of zinc nitrate and HMTA at 70 °C with ultrasonic treatment, for 10 min. TNTs were obtained by anodic oxidation of Ti foil, DEG in the electrolyte solution allowed to get larger tube diameter, 200–300 nm. An annealing post-treatment was essential to crystallize TNTs from amorphous phase to anatase, and to obtain the subsequent ZNR growth. By increasing the crystallization time from 2 to 4 h, ZNRs, in the wurtzite phase, enlarged from 10–30 nm to 30–50 nm and elongated from 100–300 nm to 300–500 nm [126].

Properties and synthesis conditions of composites on TNTs are reported in Table 12.

Table 12. Hierarchical ZnO/TiO_2 films on substrate properties and synthesis conditions. The numbering in the synthesis-method column and starting-material column indicates the succession of steps in the synthesis. The parameter r, when present, is used to express the composition, and must refer to its own line.

Shape and Particle Size	Synthesis Method	Starting Materials	Thermal Treatments	Crystal Phases (CP) and Crystallite Size (CS)	SA and E Gap	Ref.
ZNPs into the TNTs on Ti foil PS: inner $Ø_{NTs}$ = 60–80 nm, $length_{NTs}$ = 300 nm	2 steps: (1) TNTs by anodic oxidation method using working electrode: Ti foil, counter electrode: Pt, electrolyte $(NH_4)_2SO_4/NH_4F$, using V = 20 V t = 4 h; (2) ZNPs by hydrothermal synthesis on TNTs (from 1)	(1) Ti foil; (2) ZN, NH_4OH, DW	(1) calcination: 500 °C, 1 h; (2) autoclave: 70 °C, 24 h; drying: air	CP: anatase, wurtzite		[122]
ZNPs (nanorice-decorated) TNTs on Ti foil PS: $∅_{TNTs}$ = 90 nm, $length_{TNTs}$ = 4 µm; ZNPs = 1 nm × 100 nm × 1 µm	M: (1) TNTs by anodic oxidation using working electrode: Ti foil, counter electrode: Pt, V = 30 V, 3 h; (2) ZnO nanorice by 0–8 cycle of CBD at 65 °C, 15′	(1) Ti foil, EG, NH_4F, DW; (2) ZN, HMTA, DW	(1) drying: 80 °C; annealing: 450 °C, 1 h, air	CP: Anatase, wurtzite		[123]
ZNRs embedded in highly ordered TNTs on Ti sheet PS: $∅_{TNTs}$ = 30–90 nm, thickness wall = 10 nm, $length∅_{TNTs}$ = 200–300 nm; $length_{ZNRs}$ = 200 nm	2 steps: (1) TNTs by anodic oxidation using working electrode: Ti sheet, counter electrode: Pt, V = 20 V, t = 20′; (2) ZNRs by direct cathodic electrodeposition on TNTs using working electrodes: TNTs, ref. electrode; calomel, counter electrode: Pt, V = −1 V, t = 20′−60′, T = 350 K	(1) Ti sheet, HF, DW; (2) TNTs (from 1), ZN, DW	(1) annealing: 500 °C, 1 h, dry O_2	CP: anatase, wurtzite		[124]
Surface-grafted flower-like ZNRs on TNTs PS: $∅_{TNTs}$ = 50–90 nm, thickness wall = 10–15 nm, NTs gap = 20 nm; $∅_{ZNRs}$ = 50 nm, $length_{ZNRs}$ = 1–2 µm	2 steps: (1) TNTs by Ti foil anodic oxidation using V = 20 V, electrode: Ti foil, counter electrode: Pt; t = 3 h; (2) ZnO seeding by sol–gel/spin coating with speed 100 rpm, 10 s, 10 times; (3) ZNR growth by hydrothermal synthesis	(1) Ti foil; (2) TNTs (from 1) ZAc, EtOH; (3) seeded TNTs (from 2), ZN, HMTA, DW TT	(1) Annealing: 500 °C, 5 h, O_2; (2) 350 °C, 0.5 h; (3) autoclave: 90 °C, 0–12 h	CP: Anatase, rutile, wurtzite	E gap = 3.26 eV (TNTs), 3.19–3.3 eV (ZNRs on TNTs)	[125]
ZNRs intra- and inter-TNTs PS: $Ø_{TNTs}$ = 200–300 nm, wall thickness = 30 nm; $Ø_{ZNRs}$ = 10–30 nm (t = 2 h) 30–50 nm (t = 4 h), $length_{ZNRs}$ = 100–300 nm (t_{CBD} = 2 h), 300–500 (t_{CBD} = 4 h)	2 steps: (1) TNTs by Ti foil anodization using V = 60 V; (2) ZNRs by CBD at 70 °C, for 2–4 h	(1) Ti foil; (2) ZN, HMTA, DW	(1) annealing: 450 °C, 3 h, air	CP: anatase, wurtzite	SA = 0.32 $m^2\ g^{-1}$ (TNTs), 0.45 $m^2\ g^{-1}$ (ZNRs/TNTs)	[126]

2.11.2. ZnO on Lateral TNT Surface Composites

ZnO nanocrystals were deposited on the lateral surface of TNTs by the filtered cathodic vacuum-arc technique. TNTs, obtained by anodic oxidation of a Ti foil, were previously annealed at 550 °C for 3 h in air to obtain a porous crystalline anatase structure. ZnO nanocrystals, made of wurtzite, were 30 nm in diameter; the TNTs were 3.5 µm long and had a diameter of 120 nm before the ZnO deposition and 180 nm after ZnO deposition [127].

Coaxial TiO_2/ZnO NTs (TZNTs) were obtained by an electrochemical deposition of ZnO inside TNTs, which had been previously obtained by anodic oxidation of Ti foil and annealing at 450 °C for 2 h. The electrochemical deposition of ZnO was performed with an aqueous solution of ZN and EDTA with a cathodic potential V = −1 V. Coaxial TZNTs were made of anatase and wurtzite and had an inner diameter of 130 nm, a wall thickness of 15 nm and a wurtzite ZnO layer thickness of 30 nm [128].

Nanocrystals, with an average diameter of 50 nm, were grown on the framework of TNTs by dipping TNTs, with an inner diameter of 76 nm, in aqueous/ethanol solution containing ZN, followed by pyrolysis at 400 °C for 2 h. The final composite was formed by anatase and wurtzite [129].

The hydrothermal method was also used to deposit ZnO crystals on the side surface of TNTs. The hydrothermal treatment was performed with an aqueous solution of ZN, HMTA and citric acid at 70 ° for 2 h and was followed by annealing at 300 °C for 100′. The final structure contained only the anatase phase. [130].

Properties and synthesis conditions of ZnO on the lateral TNT surface composites are listed in Table 13.

Table 13. Properties and synthesis conditions of ZnO on the lateral TNT surface composites. The numbering in the synthesis-method column and starting-material column indicates the succession of steps in the synthesis. The parameter r, when present, is used to express the composition, and must refer to its own line.

Shape and Particle Size	Synthesis Method	Starting Materials	Composition	Thermal Treatments	Crystal Phases (CP) and E Gap	Ref.
ZnO crystals onto lateral surface of porous TNTs. PS: $\varnothing_{TNTs}$ = 120 nm, length $_{TNTs}$ = 3.5 µm; $\varnothing_{ZTNTs}$ = 180 nm; ZNPs = 30 nm	2 steps: (1) TNTs by anodic oxidation using working electrode: Ti foil, counter electrode: Pt, V = 20 V, t = 3–12 h (increasing time increases tube length); (2) ZnO nanocrystal by filtered cathodic vacuum-arc technique	(1) Ti foil; (2) TNTs (from 1), Zn metal, O_2		(1) annealing: 550 °C, 3 h, air	CP: anatase, wurtzite	[127]
Coaxial TZNT arrays. PS: inner $\varnothing_{TNTs}$ = 130 nm, wall thickness = 15 nm, ZnO thickness (inside TNT pore) = 30 nm	2 steps: (1) TNTs by Ti foil anodic oxidation using working electrode: Ti foil, T = RT; (2) electrochemical deposition using working electrode: TNTs, counter electrode: Pt, reference electrode: calomel, V = −1 V, t = 1 h	SM: (1) Ti foil; (2) TNTs (from 1), ZN, EDTA, DW h		(1) annealing: 450 °C, 2	CP: anatase, wurtzite E gap: ~3.2 eV	[128]
ZnO nanocrystals inside and outside well-aligned TNTs PS: $\varnothing_{innTNTs}$ = 76 nm, ZNPs = 50 nm	(1) TNTs by Ti foil anodization using working electrode: Ti foil, counter electrode: graphite sheet, V = 40 V, t = 10 h; the procedure has been repeated twice, the first time TNT formation is removed; (2) CBD followed by pyrolysis	SM: (1) Ti foil; (2) ZN, EtOH, DW; (3) TNTs (from 1), ZN, EtOH, DW	ZnO/TiO_2 (wt.% = 5, 10, 15, 20)	(1) annealing: 450 °C, 3 h, air; (2) pyrolysis: 400 °C, 2 h, air	CP: anatase, wurtzite	[129]

Table 13. *Cont.*

Shape and Particle Size	Synthesis Method	Starting Materials	Composition	Thermal Treatments	Crystal Phases (CP) and E Gap	Ref.
ZNPs (hexagonal flake) lateral decorated TNTs PS: $\varnothing_{TNTs}$ = 70 nm, length = 2 μm	(1) TNTs by Ti foil anodic oxidation using working electrode: Ti sheet, counter electrode graphite sheet, V = 30 V, t = 2 h; (2) ZNPs on/in TNTs by hydrothermal method	(1) Ti foil, EG, NH_4 F, DW; (2) TNTs (from 1), ZN, HMTA, citrA, DW	Ti/O/Zn (at. ratio) = 35/65/0, 36/62/2, 30/64/6, 26/55/19, 22/54/24	(1) annealing: 450 °C, 3 h, air; (2) hydrothermal treatment: 70 °C, 2 h; annealing: 300 °C, 100′	anatase	[130]

3. Photocatalysis

When an electromagnetic radiation of suitable energy hits a semiconductor metal oxide, some electrons of the valence band undergo excitation and pass to the conduction band. This process gives rise to the formation of electrons and holes available for chemical reactions with the surrounding species. Oxygen and water are always present in a real environment and react with electrons and holes, respectively, giving rise to the formation of reactive oxygen species (ROS).

$$H_2O + h^+ \rightarrow H^+ + HO\cdot$$

$$O_2 + e^- \rightarrow \cdot O_2^-$$

$\cdot O_2^-$ and HO·, as radical species, are extremely reactive, and can start desired (and undesired) reactions; moreover, they may diffuse into the surroundings, expanding the reaction zone compared to the catalyst place.

The photocatalytic activity of mixed titanium and zinc oxides has traditionally been tested with molecules acting as probes to determine their actual photocatalytic capabilities and factors influencing their performance; methyl orange (MO) is the most common molecule tested, in this sense. ZT photocatalytic activity has been also studied on the degradation of dyes used in the textile, biological and geological industries, with the aim to determine the effective ability of ZT to treat wastewaters. Although these catalysts have demonstrated their ability to photodegrade dyes, the toxicity has been shown to persist in water, even after their disappearance [131], probably due to the presence of fragments not completely removed [132], but studies about the exact determination of the degradation products do not yet appear in the literature. Research has focused also on exploring the potential of titanium–zinc mixed oxides for reducing environmental contaminants like Cr^{6+} [30,133], trichloroethylene (TCE) [60], antibiotics [134–136], herbicide [137], pesticides [132], landfill leachate [25], lignin [138], PCP [90] and NO [66,139]. Additionally, these oxides have been investigated for their role in energy-generation processes, including CO_2 photo-reforming to produce methane [64], hydrogen production by water splitting [108] and methanol reforming [51] reactions.

Photocatalytic activity of ZTNCs is reported in Table 14. They are more active than the respective pristine oxides, ZnO [10,25,27,31,34,37,39,40,44–46,51,54,56,60,68,72,74,80,85,99,116,127,129,136,137,140] and TiO_2 [10,25,27,31,34,37,39,40,44,45,54,56,60,65,72,74,80,85,90,93,99,127,129,136,137,140] and, sometimes, more than P25 TiO_2 [39,51,62,64,67,68,78,80,85,129], which is considered a standard reference in photocatalysis. Many factors have been involved in explaining the boosting of photocatalytic activity of ZTNCs.

ZTNCs often show a lower energy gap than ZnO and TiO_2 [45,58,67,73,116] because of the smaller particle size [89] and the creation of the energy level in the gap, due to lattice defects [116]. The smaller energy gap facilitates the photoexcitation of electrons from the valence band to the conduction band, thus contributing to increasing the reaction speed.

Table 14. ZTNC photocatalytic performances and catalyst properties.

MO Degradation			
Ref.	Catalyst Crystal phases Synthesis method	Measurement parameters	Main results
[43]	ZT/r/NPs Anatase, rutile Sol–gel method	In 250 mL beaker C_0 (cat) = 10 g L^{-1} C_0 (dye) = 0.1–1 mg L^{-1} P = 160 W Rad = UV Hg lamp	t = 5 h deg = 50–70% zinc sulfate as precursor gives more active photocatalysts than zinc chloride and nitrate
[44]	ZT/r/NPs Anatase, rutile, wurtzite Sol–gel method (with SDS or DBS surfactant)	Fixed-film batch reactor C_0 (dye) 5 mg L^{-1} P = 6 W LI = 3.0 mW cm^{-2} Rad = UV lamp	ZT/r/NPs more active than pristine oxides K = 1.81 h^{-1} (Zn/Ti at. ratio = 0.25/T_{calc} = 600 °, DBS) DBS allows higher K than SDS
[39]	ZT/r/NPs Anatase, wurtzite Hydrothermal method	Quartz-glass reactor C_0 (cat) = 2.5 g L^{-1} C_0 (dye) = 0.02 g L^{-1} P = 125 W d = 20 cm Rad = UV Hg lamp	t ~20′ deg ~80% ZT/r/NPs more active than TNPs ZT/r/NPs more active ZNPs ZT/r/NPs a little more active than P25 ZT/r/NPs more resistant than P25
[34]	ZT/r/NPs A W Precipitation method	C_0 (cat) = 0.2 g L^{-1} C_0 (dye) = 0.01 M P = 4 × 8 W LI = 1.4 W m^{-2} Rad = UVA Phillips TL	t = 140′ deg = 100% K = 1.86 × 10^{-2} min^{-1} ZT/r/NPs more active than TNPs, K = 0.1 × 10^{-2} min^{-1} ZT/r/NPs more active ZNPs, K = 1.23 × 10^{-2} min^{-1}
[24]	ZT/r/NPs A, W Mechanical mixing	Photoreactor with 250 mL beaker C_0 (cat) = 0.5 g L^{-1} C_0 (dye) = 40 ppm P = 375 W Rad = UV Hg lamp	t = 20′ deg = 45–50% with increasing ZnO content degradation decreases, increases, and decreases Maximum deg.: ZnO wt.% = 95% minimum deg.: ZnO wt.% = 5%
[48]	ZT/r/NPs A, W, Am Sol–and precipitation, (different composition) methods	100 mL beaker C_0 (cat) = 0.5 g L^{-1} C_0 (dye) 10^{-5} M P = 40 W LI = 413 W cm^{-2} Rad = UV VL 340 lamp	t = 5 h deg = 100% $\chi_{Zn} \leq 0.67$: precipitate catalysts more active than sol–gel catalyst $\chi Zn \geq 0.67$: precipitate catalysts less active than sol–gel catalyst, amorphization and high E gap decreases MO photodegradation
[62]	hollow spheres anatase Solvothermal method	C_0 (dye) = 10 mg L^{-1} Rad = UV light	t = 9′ deg = 100% ZT hollow spheres much more active than TiO_2 hollow spheres ZT hollow spheres a little more active than P25 ZT hollow spheres more resistant than P25
[112]	Cs ZT NRs on Si substrate Hydrothermal/spin coating	C_0 (dye) = 0.25 mg L^{-1}. P = 66.2 W cm^{-2}, 16.7 W cm^{-2}. Rad = black-ray UV light and oriel solar simulator	Cs ZTNRs less active than ZNRs
[80]	UTZs (urchin-like TiO_2/ZnO) Anatase, wurtzite Hydrothermal method	C_0 (cat) = 0.5 g L^{-1} C_0 (dye) = 10 mg L^{-1} P = 300 W Rad = UV Xenon lamp d = 15 cm	t = 25′ deg = 100% UTZs more active than ZNPs UTZs more active than P25 UTZs more active than TiO_2 urchin-like

Table 14. *Cont.*

MO Degradation			
Ref.	Catalyst Crystal phases Synthesis method	Measurement parameters	Main results
[56]	TNPsZNRs Anatase, wurtzite PLAL	C_0 (cat) = 0.5 g L^{-1} P = 500 W Rad = Xenon lamp (UV)	TNPsZNRs with ZnO/TiO_2 (wt. ratio) = 9/1 the most active t = 35′ deg = 100% K = 0.1142 min^{-1} more active than other composition more active than pristine ZNRs (K = 0.04062 min^{-1}) s more active than TNPs (K = 0186 min^{-1})
[124]	ZNRs embedded in TNTs on Ti sheet Anatase, wurtzite TNTs by anodic oxidation method; ZNRs by direct cathodic electrodeposition on TNTs	Photo-electrocatalytic measurements WE: ZNRs/TNTs WE area = 1.0 cm^2 CE: Pt RE: SCE C_0 (dye) = 5×10^{-5} M P = 11 W LI = 10 mW cm^{-2}. Rad = UV lamp	t = 90′ deg = 100% ZNRs embedded in TNTs slightly more active than TNTs
[126]	ZNRs/TNTs (intra- and extra-tube) Anatase, wurtzite TNTs by Ti foil anodization; ZnO NRs by CBD	C_0 (dye) = 5×10^{-5} M P = 400 W LI = 23 mW cm^{-2} Rad = Hg lamp d = 12 cm	t = 105′ deg = 75–80% ZNRs/TNTs more active than TNTs 2nd cycle t = 105′ deg. = 20–25%
[119]	ZT NCs arrays on Ti fabric Anatase, wurtzite Anodic oxidation followed by hydrothermal treatment	C_0 (cat) = 1×1 cm^2/100 mL C_0 (dye) = 20 mg L^{-1} P = 300 W Rad = UV Xenon lamp	t = 60′ deg = 100% ZT NCs more active than TNPs (at pH 7) pH = 10 more active than other pH Reusable
[92]	ZT film on glass anatase, ($\chi_{Ti} \geq 75\%$), wurtzite ($\chi_{T\,i} \leq 50\%$.), amorphous (χ_{Ti} = 25 and 50%) Sol–gel/dip coating	In small beaker C_0 (dye) = 2.5×10^{-5} M P = 20 W Rad = UV lamp	t = 3 h deg = 90–95% The higher the titanium content, the higher the MO photodegradation Films with poorest crystallization show lowest photocatalytic degradation
[93]	ZT macroporous film anatase (ZnO/TiO_2 = 0, 10, 20%), amorphous (ZnO/TiO_2 = 30, 40%) Sol–gel/spin coating	Water-cooled reactor C_0 (cat) = 1 g L^{-1}. C_0 (dye) = 10.3 mg L^{-1} P = 100 mWcm^{-2} Rad = solar simulator with an AM1.5 filter	ZT macroporous film with ZnO/TiO_2 (molar ratio) = 10% the most active t = 280′ deg = 70–80 more active than TNPs more active than other compositions (ZnO/TiO_2 = 20, 30 and 40%) less active then P25
[85]	self-standing ZT photonic crystal with IOS Anatase, wurtzite Self-standing TiO_2 by impregnation of PS sphere between 2 slides and Zn impregnation	C_0 (cat) = 3 cm × 2 cm/10 mL C_0 (dye) = 5 mg L^{-1} P = 500 W Rad = Xe arc lamp/IR cut-off solar-light simulator	t = 120′ deg = 90–100% self-standing ZT more active than ZNPs self-standing ZT more active than TNPs self-standing ZT more active than ZTNPs self-standing ZT more active than TPC self-standing ZT more active than P25
MB degradation			
Ref.	Catalyst Crystal phases Synthesis method	Measurement parameters	Main results
[78]	ZNRs TNPs Anatase, wurtzite Hydrothermal method	3 mL quartz-glass vessel photoreactor C_0 (dye) = 1×10^{-5} M P = 100 W LI = 35 mW cm^{-2} Rad = UV vis Hg lamp light d = 12 cm	ZNRs TNPs with Z/Ti (at. ratio) = 2/1 the most active t = 180′ deg = 90% k = 1.37×10^{-2} min^{-1} more active than other composition more active than ZNPs and TNPs more active than P25

Table 14. *Cont.*

MB degradation			
Ref.	Catalyst Crystal phases Synthesis method	Measurement parameters	Main results
[128]	Coaxial TZNTs arrays film Anatase, wurtzite TNTs by Ti foil anodic oxidation; ZnO nanocrystal by filtered cathodic vacuum-arc technique.	C_0 (dye) = 5 mg L^{-1}	t = 150′ deg = 80% Coaxial TZNT-array film more active than TNTs
[33]	ZT/r/NPs Anatase, wurtzite MW precipitation method	C_0 (cat) = 14.3 g L^{-1} C_0 (dye) = 5 × 10^{-6} M P = 18 W Rad = UV lamp	t = 150′ deg = 95%
[116]	cs ZT NRs (oriented) on ITO anatase, (002) and (103) preferentially oriented wurtzite Urchin-like Zn seeding by electrochemical method; ZNRs by hydrothermal process; TiO_2 shell by sol–gel	C_0 (cat) = in a quartz cuvette C_0 (dye) = 10 mM Rad = LED LI = 140 mW cm^{-2} d = 2 cm International standard procedure	cs ZT NRs with a non-uniform layer (nul) of TiO_2, the most active t = 180′ deg = 80–85% k = 1.2 × 10^{-2} min^{-1} cs ZT NRs on ITO (nul) more active than ZNRs on ITO cs ZT NRs on ITO (nul) more active than pristine ZnO, k= 0.2 × 10^{-2} min^{-1} cs ZT NRs on ITO (nul) more active than uniform layer (of TiO_2) on NRs on ITO, k= 0.7 × 10^{-2} min^{-1}
[45]	ZT/r/NPs Anatase, rutile, wurtzite Sol–gel method	Batch reactor C_0 (cat) = 0.5 g L^{-1} LI = 42 (UV) 121 (vis) Wm^{-2} Rad = UV and visible light	t = 30′ deg = 90% K = 0.07 (UV), 0.008 (vis) min^{-1} ZT/r/NPs more active than ZNPs ZT/r/NPs more active than TNPs In UV and vis light
[73]	ZT cs NPs anatase, (W before TiO_2 precipitation) double-step precipitation	C_0 (cat) = 0.16 g L^{-1} C_0 (dye) = 10 ppm pH = 8 P = 2 × 18 W LI = 115 mW cm^{-2} Rad = Philips UV lamp	ZT cs NPs with ZnO/TiO_2 (wt. ratio) = 1/25 the most active t = 120′ deg = 59.56% more active than ZNPs
[37]	ZT/r/NPs Wurtzite (ZnO/TiO_2 vol. ratio > 0), anatase, rutile (ZnO/TiO_2 vol. ratio = 0), $ZnTiO_3$ (traces). Sol–gel method	50 mL borosilicate glass C_0 (cat) = 5 mg L^{-1} C_0 (dye) = 10 mM LI = 862 W cm^{-2} Rad = solar light	ZT/r/NPs with ZnO/TiO_2 (mol ratio) = 4/6 the most active t = 75′ deg = 90% more active than TNPs (deg. = 77%) more active than ZNPs (deg. = 74%)
[87]	TNPs/ZNFls Anatase, wurtzite Hydrothermal method	C_0 (cat) = 1 g L^{-1} C_0 (dye) = 10 mg L^{-1} pH = 7 P = 100 W Rad = vis W bulb	Catalyst with Zn/Ti (volume ratio) = 4 the most active t = 6′ deg = 100% more active than ZNFls more active than catalyst with Zn/Ti (volume ratio) = 2
[10]	ZT/r/NPs Anatase (Z/Ti mol ratio = 0/1), rutile (Z/Ti = 0/1, 1/3), wurtzite (Z/Ti > 0/1), $ZnTiO_3$ (traces Z/Ti = 1/1, 2/1) Sol–gel method	Glass beaker C_0 (cat) = 0.5 g L^{-1} C_0 (dye) = 20 mM P = 413 $mWcm^{-2}$ LI = 413 mW cm^{-2} Rad = UV d = 12 cm	ZT/r/NPs with Zn/Ti mol ratio = 1 the most active t = 6 h deg = 100% K = 9.5 × 10^{-3} min^{-1} (Zn/Ti mol ratio = 1) more active than TNPs, deg. = 60%, K = 3.06 × 10^{-3} min^{-1} (TiO_2) more active than ZNPs, deg = 65%, K = 2.64 × 10^{-3} min^{-1} (ZnO)

Table 14. *Cont.*

MB degradation			
Ref.	Catalyst Crystal phases Synthesis method	Measurement parameters	Main results
[25]	ZT/r/NP Anatase, wurtzite SSR (TiO_2 and ZnO by Hydrothermal synthesis)	Tot. volume 250 mL C_0 (cat) = 0.8 g L^{-1} C_0 (dye) = 2 mg L^{-1} P = 300 W Rad = UV Xe lamp	ZT/r/NPs with Ti/Zn wt. ratio = 1 the most active t = 150′ deg = 91.6% K = 1.412 × 10^{-2} min^{-1} more active than other composition more active than ZNPs, K = 0.424 × 10^{-2} min^{-1} more active than TNPs, K = 1.041 × 10^{-2} min^{-1}
[140]	ZnO-decorated TiO_2, NPs Anatase, wurtzite Sol–gel method + reflux	50 mL quartz glass C_0 (cat) = 2.5 g L^{-1} C_0 (dye) = 2.9 mg L^{-1} t = 30′ deg = 70% Rad = UVA light	K = 5.86 × 10^{-2} min^{-1} ZnO-decorated TNPs more active than ZNPs, K = 3.67 × 10^{-2} min^{-1} ZnO-decorated TNPs more active than TNPs, K = 2.09 × 10^{-2} min^{-1}
RhB degradation			
Ref.	Catalyst Crystal phases Synthesis method	Measurement parameters	Main results
[65]	TZNFs Anatase, rutile, wurtzite Electrospinning	C_0 (cat) = 0.5 g L^{-1} C_0 (dye) = 20 ppm P = 12 W Rad = UV lamp Philips 365 D = 10 cm	ZNFs with ZnO (wt.%) = 15.8% the most active t = 25′ deg = 100% K = 0.7467 mg L^{-1} h^{-1} more active than T NFs, K = 0.5733 mg L^{-1} h^{-1}
[129]	ZTNTs Anatase, wurtzite Anodic oxidation and pyrolysis approach	SA (cat) = 3 × 1 cm^2 C_0 (dye) = 5 mg L^{-1} pH = 7 P = 300 W Rad = UV Xe lamp D = 15 cm	t = 150′ deg = 70–80% ZTNTs more active than TNTs ZTNTs more active than P25 film ZTNTs more active than ZnO film
[67]	TZNFs Anatase (T_{calc} = 550–750 °C), rutile ($T_{calc} \geq$ 650 °C) wurtzite. Electrospinning	In Luzchem CCP-4 photo-chemical reactor C_0 (cat) = 1 g L^{-1} C_0 (dye) = 10^{-6} M P = 8 × low P UV Hg lamps	t = 75′ deg = 100% TZ NFs more active than P25 TZ NFs calcinated at 650 °C more active than TZ NFs calcinated at 550, 750 and 850 °C
[86]	IOS Z QDs TiO_2 anatase Impregnation on self-assembled PSs on filter paper	C_0 (cat) = 400 mg L^{-1} C_0 (dye) = 10^{-3} M P = 6 × 18 W LI = 6 ×1250 lm Rad = UV lamp	t = 25 ‘ deg = 100% more active than P25, deg = 40–45%
[123]	ZNRsTNTs film on Titanium Anatase, wurtzite TNTs by anodic oxidation; ZnO nanorice by CBD	3 mL quartz cuvette in Luzchem photoreactor C_0 (dye) = 5 mg L^{-1} Rad = UVC, UVB, UVA and visible region lamps	ZNRsTNTs with 2 ZnO CBD cycles the most active t = 240′ deg = 90–95% (UVA) K = 0.011 min^{-1} more active than TNTs more active than catalyst with 4, 6, 8 CBD cycles
[82]	ZTNTs Anatase, wurtzite Double step hydrothermal route	C_0 (dye) = 10^{-5} M Rad = visible light	ZTNTs more active than TNTs, ZnO, P25 t = 180′ deg = 89% (ZTNTs); 77% (TNTs), 61% (P25), 31% (ZnO) K = 0.011 (ZTNTs). 0.085 (TNTs), 0.0059 (P25), 0.0023 (ZnO)
[54]	ZT/r/NPs Anatase, wurtzite Green synthesis	In 250 mL Pyrex glass photochemical reactor C_0 (cat) = 1 g L^{-1} C_0 (dye) 0.3 mM Rad = halogen light lamp	t = 3 h deg = 59% ZT/r/NPs more active than ZNPs, deg = 39% ZT/r/NPs more active than TNPs, deg = 45%

Table 14. *Cont.*

Other dye degradation			
Ref.	Catalyst Crystal phases Synthesis	Measurement parameters	Main results
[31]	ZT/r/NPs Anatase: except Ti/Zn (at. ratio) = 0/1, wurtzite: Ti/Zn $\leq$ 3/1 Us precipitation method	CI basic blue 41 degradation C_0 (cat) = 10 g L^{-1} C_0 (dye) = 20 mg L^{-1} pH = 6.21 Rad = solar light	ZT/r/NPs with Ti/Zn (at. ratio) = 1/1 the most active t = 1 h deg = 99% K = 0.08256 min^{-1} more active than TNPs more active than ZNPs more active than all other compositions
[38]	ZT/r/NPs Anatase, wurtzite Precipitation method	Procyon red MX oxidation in Teflon-sealed borosilicate vials C_0 (cat) = 0.5 g L^{-1} C_0 (dye) = 15 mg L^{-1} pH = 6.8 P = 4 × 8 W Rad = UV D = 7.6 cm	Catalysts with composition close to pristine oxides the most active
[68]	TZ NFs (flower like) Anatase, wurtzite Electrospinning	Degradation of ARS (alizarin red S) C_0 (cat) = 20 mg L^{-1} C_0 (dye) = 20 mg L^{-1} Rad = UV lamp D = 15 cm	t = 70′ deg = 100% TZ NFs more active than P25 TZ NFs more active than ZNPs
[46]	ZT/r/NPs Anatase, wurtzite Sol–gel method	Congo-red degradation in 50 mL opened Pyrex vessel C_0 (cat) = 0.5 g L^{-1} C_0 (dye) = 5 ppm P = 30 W Rad = UVC lamp D = 15 cm	t = 5′ and 10′ deg = 80% and 98% ZT/r/NPs more active than ZNPs with T_{calc} = 420 °C higher performance than T_{calc} = 220 °C or 800 °C (Zn_2TiO_4 formation)
[36]	ZT/r/NPs Anatase Homogeneous hydrolysis method	OII degradation in aqueous slurry C_0 (dye) = 0.02 M P = 8 W Rad = florescent lamp (λ = 254 and 365 nm)	λ = 254 nm ZT/r/NPs with Ti/Zn (at. ratio) = 1.55/54.97 the most active t = 25′ deg = 100% K = 0.1235 min^{-1} more active than P25 λ = 365 nm ZT/r/NPs less active than P25
[23]	ZT/r/NPs Anatase, wurtzite SSR	Acid-red degradation in 50 mL tot. volume C_0 (cat) = 1 mg L^{-1} C_0 (dye) = 10 mg L^{-1} pH = 7 US: t = 100 min	t = 100′ deg = 75% (TNPs) deg = 35–40% (ZNPs) degradation decreases with increase in ZnO content
[71]	cs ZT NPs Anatase(at highest TiO_2 loading), wurtzite ZnO mw impregnation method	Orange G degradation P = 5 × 15 W Rad = UV light	t = 90′ deg = 100% Increasing amorphous titanium dioxide-layer thickness, decreasing photocatalytic degradation
[32]	ZT/r/NPs Anatase, rutile, wurtzite Modified ammonia evaporation-induced synthetic method	Cyanides MB SY RB C_0 (cat) = 0.8 g L^{-1} C_0 (dye) = 50 ppm P = UV: 150 W; vis: 8 W Rad = UV: W halogen lamp; vis: Hg lamp	Cyanides t = 150 min deg = 25% ZT/r/NPs more active than P25 MB, SY, RB ZT/r/NPs less active than P25
[27]	ZT/r/NPs Anatase, wurtzite mixing and SSR	BGY in 50 mL borosilicate glass/batch reactor C_0 (cat) = 6 g L^{-1} C_0 (dye) = 20 mg L^{-1} Rad = solar light	ZT/r/NPs with Zn/Ti (mol ratio) = 1/1 and 3/1 the most active t = 2 h deg = 100% more active than ZNPs more active than TNPs

Table 14. *Cont.*

Other dye degradation			
Ref.	Catalyst Crystal phases Synthesis	Measurement parameters	Main results
[72]	Cs ZT NPs Anatase (detectable only with thicker shell), wurtzite ZnO by precipitation, TiO_2 by chemical growth from TiO_2 gel.	Acridine orange (AO) in homemade photo-reaction apparatus C_0 (cat) = 1 g L^{-1} C_0 (dye) = 0.03 mM Rad = solar light irradiation	t = 120 ‘ deg = 100% Cs ZT NPs with the thickest TiO_2 (anatase) layer the most active more active than ZNPs (deg = 87%) more active than TNPs (deg = 80%)
Phenol degradation			
Ref.	Catalyst Crystal phases Synthesis	Measurement parameters	Main results
[90]	ZT compact film on Ti plate Anatase Sol–gel/dip coating	PCP degradation 600 mL photoreactor WE: ZT film on Ti CE stainless steel RE: SCE C_0 (dye) = 5 mg L^{-1} P = 300 W Rad = Hg lamp	K = 0.0144 min^{-1} (ZT film photocatalysis) K = 0.0309 min^{-1} (ZT film electrophotocatalysis) K = 0.0249 min^{-1} (TiO_2 electrophotocatalysis) More active than TNPs
[75]	TZ cs tetrapods Anatase, wurtzite Z tetrapods by thermal evaporation; TiO_2 layer by VHM	Phenol photooxidation in 400 mL Pyrex photoreactor C_0 (cat) = 0.36 g L^{-1} C_0 (dye) = 100 mg L^{-1} pH = 6.56 O_2 = 100 mL min^{-1} Rad = UV light with and without filter glass (λ < 340 nm).	Without cut-off t = 90′ deg = 100% Slightly more active than P25 More active than Z tetrapods With cut-off (λ < 340 nm). t = 300′ deg = 100% More active than P25 More active than Z tetrapods
[125]	Flower-like ZNRs on TNTs Anatase, rutile, wurtzite TNTs by Ti foil anodic oxidation, ZNRs by sol–gel/dipping and hydrothermal method	PEC oxidation of Bis Phenol A in 100 mL quartz electrolytic cell WE: ZNRs on TNTs SA (cat) = 4.5 cm^2 CE platinum RE: calomel C_0 (dye) = 25 mg L^{-1} P = 300 W UV lamp LI = 3 mW cm^{-2} Rad = UV lamp	t = 180′ deg = 90% Flower-like ZNRs on TNTs more active than TNTs
[74]	Cs ZT NPs Anatase, wurtzite ZNRs by thermal decomposition; TiO_2 shell by chemical growth from TiO_2 gel.	4 Cl phenol degradation in 250 mL glass photoreactor C_0 (cat) = 0.4 g L^{-1} C_0 (dye) = 40 ppm LI = 2.0 mW cm^{-2} Rad = UV Hg lamp	t = 1 h deg = 90.6% Cs ZT NPs with ZnO (mol.%) = 6%, the most active more active than ZNPs, deg. = 54.2% more active than TNPs, deg = 32.3% more active than other compositions
[80]	Urchin-like hierarchical ZT architectures Anatase, wurtzite Hydrothermal method	nitrophenol in aqueous solution C_0 (cat) = 0.5 g L^{-1} C_0 (dye) = 10 mg L^{-1} P = 300 W Rad = Xenon lamp D = 15 cm	t = 25′ deg = 100% Urchin-like ZT more active then ZNPs Urchin-like ZT more active than TiO_2 urchin-like structure Urchin-like ZT $_2$ more active than P25
[65]	TZ NFs Anatase, rutile, wurtzite Electrospinning	phenol degradation in aqueous solution C_0 (cat) = 0.5 g L^{-1} C_0 (dye) = 20 ppm P = 12 W Rad = UV lamp Phillips 365 D = 10 cm	t = 30′ deg = 75–80% K = 1.833 mg L^{-1} h^{-1} TZ NFs more active than pure TNFs, K = 0.5733 mg L^{-1} h^{-1}

Table 14. *Cont.*

Other pollutant degradation			
Ref.	Catalyst Crystal phases Synthesis	Measurement parameters	Main results
[138]	Mixing ZT/r/NPs	Lignin degradation P = 5 × 30 W(UV), 35 W m^2 (solar light) Rad = UV and solar light	less active than ZnO in UV and solar light
[127]	ZnO crystals onto TNTs Anatase, wurtzite TNTs by anodic oxidation; ZnO nanocrystal by filtered cathodic vacuum-arc technique	humic acid degradation C_0 cat = 2.5 × 1 cm^2 in 10 mL bottle C_0 (dye) 50 mg L^{-1} P = 8 W Rad = UV light (λ = 254 nm) D = 5 cm	t =65′ deg = 100% K = 0.015 min^{-1} More active than ZNRs, deg = 80% More active than TNTs, deg = 55% Catalyst stability: photocatalytic activity decreases 10% after 20 catalytic cycles, recovery with 10 min of darkness
[30]	ZT/r/NPs Anatase, rutile Wetness impregnation method	Cr^{6+} reduction in 200 mL Pyrex photoreactor C_0 (cat) = 1 g L^{-1} C_0 (Cr^{6+}) = 20 mg L^{-1} pH = 5.5 P = 10 W Rad = UV Hg lamp (λ = 365 nm)	ZT/r/NPs with ZnO (mol.%) = 2% more active than other compositions (ZnO (mol,%) = 0, 1, 4, 10) K = 1.2 × 10^{-2} min^{-1}
[60]	Hollow sphere (or almost) Anatase, rutile, wurtzite Spray pyrolysis method	TCE degradation C_0 (TCE) = 58.56 ppm Rad = UV lamp (λ = 300–420 nm)	Hollow sphere with ZnO (mol,%) = 5%, the most active more active than ZNPs more active than P25 more active than Hollow sphere with ZnO (mol,%) = 0, 16,33,66,100
[136]	ZT/r/NPs Anatase, wurtzite Precipitation method	Flumequine (antibiotic) degradation C_0 (cat) = 4 g L^{-1} C_0 (Fl) = 10 mg L^{-1} P = 2 mW cm^{-2} Rad = UV lamp (λ = 260 nm)	t = 240′ deg = 67% more active than TNPs, deg = 23% more active than ZNPs deg, = 11% still more active if supported on sepiolite, deg = 85%
[26]	ZT/r/NPs Anatase, wurtzite mixing and SSR	Quinoline degradation in 250 mL borosilicate beaker batch reactor C_0 (cat) = 2.5 g L^{-1} C_0 (dye) = 100 mg L^{-1} Rad = UV Hg bulb (l = 365 nm) Distance = 10 cm pH = 8	ZT/r/NPs Ti/Zn (molar ratio) = 1 more active than other compositions (Ti/Zn = 1/2, 1/3, 3/1 or 2/1) t = 240′ deg = 82%
[134]	Layered TiO_2/ZnO/ITO Anatase, wurtzite Magnetron sputtering	Ciprofloxacin removal C_0 (cat) = 1 × 1 cm^2/50 mL C_0 (dye) = 10 mg L^{-1} P = 300 W LI = 208.5 mW cm^{-2} Rad = Hg lamp Distance = 10 cm pH = 7	t = 120′ deg = 100% more active than ZnO film more active than TiO_2 film on ITO
[137]	ZT/r/NPs Anatase, wurtzite Deposition–precipitation method	Bentazon (herbicide) degradation C_0 (cat) = 0.5 g L^{-1} C_0 (B) = 5 mg L^{-1} Rad = UV lamp	t = 60′ deg = 100% K = 0.0649 min^{-1} more active than TNPs more active than ZNPs
[25]	ZT/r/NPs Anatase, wurtzite SSR	Landfill leachate (from Yiyang city) degradation, diluted 1/100 Cat.: 200 mg in diluted landfill leachate Rad = Xenon lamp	ZT/r/NPs with TiO_2/ZnO (wt. ratio) =1 t = 40′ deg = 90% K = 2.84 × 10^{-2} min^{-1} more active than TNPs: K = 2.19 × 10^{-2} min^{-1} more active than ZNPs: K = 0.95 × 10^{-2} min^{-1}
[67]	TZ NFs Anatase (T_{calc} = 550–750 °C), rutile (T_{calc} ≥ 650 °C) W Electrospinning	NO oxidation in continuous flow reactor dish 150 × 25 mm [NO] = 1000 ppb Total flow = 3 l min^{-1} P = 300 W Rad = solar-light simulator (W halogen lamp)	t = 30′ deg = 34% catalyst calcinated at 650 °C more active than catalyst calcinated at T = 550 °C (deg = 23%), 750 °C (deg = 24%), 850 °C (deg = 19%) More active than P25, deg. = 18%)

Table 14. *Cont.*

Other pollutant degradation			
Ref.	Catalyst Crystal phases Synthesis	Measurement parameters	Main results
[139]	ZT/r/NPs Anatase, rutile, wurtzite Mixing by ball milling	NO oxidation to NO_3 in in continuous-flow reactor [NO] = 1 ppm Total flow = 3 l min^{-1} P = 1 mW cm^{2} Rad = UV Philips lamp (λ = 365 nm), vis Philips lamp	ZT/r/NPs more active than P25
fuel production reaction			
Ref.	Catalyst Crystal phases Synthesis	Measurement parameters	Main results
[64]	Mesoporous French fries Anatase, rutile FAPO (furfural alcohol derived polymerization-oxidation) reaction	CO_2 photo-reforming to CH_4 cat = 0.1 g/8.1 cm^2 total volume = 390 mL H_2O (liquid) volume = 0.8 mL Reactants: CO_2 + H_2O P = 300 W LI = 60 mWm^2 Rad = Xe lamp	CH_4 yield = 55 μmol g^{-1} h^{-1} More active than P25 (9.3 μmol g^{-1} h^{-1}) More active than ZT NCs by SSR (5 μmol g^{-1} h^{-1})
[51]	ZT/r/NPs Anatase (%TiO_2 > 0), wurtzite (%ZnO 50–100) Sol–gel method	H_2 generation in aqueous methanol solution in 5 mL quartz semi-batch reactor cat = 2 mg H_2O = 1.6 mL CH_3OH = 0.4 mL P = 300 W Rad = UV Xe lamp (240 < λ < 400 nm)	ZT/r/NPs with ZnO (wt.%) = 30% the most active t = 10 h H_2 yield = 17.3 mL g^{-1} more active than P25, H_2 yield = 8.01 mL g^{-1} More active than ZNPs, H_2 yield = 0 mL g^{-1}
[40]	ZT/r/NPs Anatase, amorphous Hydrothermal method	H_2 evolution in Labsolar II photocatalytic water-splitting testing system cat = 10 mg H_2O = 90 mL CH_3OH = 10 mL P = 300 W Rad = UV Xe lamp nm	ZT/r/NPs with Ti/Zn (at. ratio = 3) more active than other compositions (Ti/Zn at. ratio = 1, 2, 5, 7) H_2 yield = 865 μmol g^{-1} h^{-1}
[108]	Cs ZT NWs (vertically aligned on steel mesh) Anatase, wurtzite 2-step hydrothermal route	H_2 evolution in Perfect Light Labsolar IIIAG photocatalytic reaction system (piezo-photocatalytic Perfectlight labsolar-IIIAG) cat = 220 mg (5 × 9 cm^2) H_2O = 120 mL CH_3OH = 30 mL P = 50 W Rad = Xe lamp (200 < λ < 2500) Ultrasound: 50 A 50 W	H_2 yield = 3.05 μmol g^{-1} h^{-1} Piezo-photo reaction more active than photo reaction (1.98 μmol g^{-1} h^{-1}) Cs ZT NWs more active than piezo-photo Z NWs (1.86 μmol g^{-1} $h^{-(1)}$ Cs ZT NWs less active than P25 (11 μmol g^{-1} h^{-1})
[79]	ZnO-decorated TNWs anatase, TiO_2 (B), wurtzite TNWs by P25 hydrothermal treatment; ZnO by reflux method	Water splitting in the presence of sacrificial methanol in jacketed British purple-glass reactor cat = 50 mg H_2O = 72 mL CH_3OH = 8 mL P = 300 W Rad = Xe lamp	ZnO-decorated TNWs with ZnO (wt.%) = 20% the most active H_2 yield = 193 μmol g^{-1} h^{-1} more active than TNWs, H_2 yield = 145 μmol g^{-1} h^{-1} more active than other compositions

The greater photocatalytic activity of the ZT nanocomposite compared to the pure oxides has often been attributed to the coupling of two oxides, which causes an interface creation with a transfer of electrons and which prevents electron–hole recombination [78,106,127]. ZnO and TiO_2 have similar band gap energy; ZnO and TiO_2 are n-type semiconductors, direct and indirect [141], respectively. The energy levels of conduction and the valence band of zinc oxide are slightly higher than those of titanium dioxide. When

the ZT nanocomposite is passed through by UV–vis radiation, a stronger excitation occurs, mainly by ZnO, as a direct semiconductor, rather than by TiO_2. Due to the presence of the interface, the excited electrons can migrate from the conduction band of ZnO to the conduction band of TiO_2 and the holes from the valence band of TiO_2 to the valence band of ZnO. TiO_2, as an indirect semiconductor, offers a reduced electron–hole recombination compared to ZnO, and the overall mechanism enables a more efficient photocatalytic pathway. The electrons and the holes created can start the desired reaction or can be useful to create active oxygen species, $\cdot O_2^-$ and HO·, which can generate the desired reaction, making use of an aqueous medium. Efforts have been made to understand which species effectively start the reaction, using scavenger molecules [85]. For example, it was proved that HO· plays an important role in methylene blue (MB) degradation using isopropanol [10] or methanol [116] scavengers with ZT/r/NPs and cs ZT NRs, respectively.

It was found that an excess of zinc oxide can inhibit such a mechanism towards Rhodamine B (RhB) degradation by ZT NFs, because it hinders the contact between the TiO_2 surface and reacting species, and this favors the electron–hole recombination [65].

This mechanism has been proposed for the ZTNCs with TiO_2 in the anatase phase. Nonetheless, it was found that rutile co-presence in ZT/r/NPs could further improve photocatalytic activity towards MO degradation [43]. Again, it was shown that the rutile phase, together with anatase in ZTNFs, played a crucial role in enhancing photocatalytic activity in NO degradation, because rutile has a lower energy gap than anatase, with the conduction band at a lower energy and the valence band at a higher energy. The rutile phase can therefore enter in the electronic exchange by collecting electrons in the conduction band and providing holes from the valence band towards the anatase phase. In contrast, an excess of rutile phase decreased photocatalytic activity, since it became a center of electron–hole recombination [67].

The TiO_2(B) in TNWs (anatase and TiO_2(B))/ZNPs also played a role in the electronic change in the water-splitting photocatalytic reaction with the anatase phase. Since TiO_2(B) has the conduction and valence-band levels located between those of zinc oxide and anatase, it was supposed that it could give electrons to the anatase phase and holes to zinc oxide, increasing the lifetime of charge carriers, and thus contributing favorably to the photocatalytic activity [79].

ZT/r/NPs synthesized by wet impregnation showed lower photoluminescence than pure TNPs, because the coupling between two oxides hinders electron–hole recombination. The magnitude of this decrease was relevant at lower ZnO concentrations and decreased at higher ZnO content, as recombination was enabled by the excess of ZNPs. The decrease in photoluminescence in ZTNCs was associated with an increase in photocatalytic activity towards the reduction of Cr^{6+} [30]. A reduction in photoluminescence associated with higher photocatalytic activity of ZTNCs compared to pristine oxides was also found for ZTNF behaviors calcinated at different temperature in the range 550–850 °C towards NO removal [67].

As is obvious, crystallinity plays a crucial role in determining photocatalytic activity. It has been demonstrated that titanium–zinc oxide composite films with a poor crystallization show lower photocatalytic activity, and that the photocatalytic activity is enhanced by a longer-lasting calcination treatment, which improves crystallinity [92]. On the other hand, small crystallite sizes are required to achieve good photocatalytic activity [45]. Increasing the thickness of titanium dioxide in cs ZT NPs increased the photocatalytic activity if the outer shell of TiO_2 was in the crystalline anatase phase [73]; it was also shown, coherently, that the photocatalytic activity decreased if the outer shell of TiO_2 was an amorphous phase [71]. On the other hand, it was highlighted that the presence of amorphous TiO_2, together with the anatase phase, could increase the photocatalytic activity in ZT/r/NPs synthetized by the hydrothermal method, because it helped to obtain higher surface areas [40].

The higher surface area and pore volume [40,51] can contribute to enhance photocatalytic activity, because it allows higher light harvesting. When the surface area decreased

because of increasing calcination temperature, a clear decrease in photoactivity was observed [30]. On the other hand, when the difference in surface area was due to different values of catalyst composition, other factors could play a role in determining the final photocatalytic activity, and the catalyst with largest surface area may not be the most active one [78].

The zero-point charge can influence the photocatalytic activity, especially if the reacting species have an anionic structure. If the surface of the catalyst is charged, it can generate electrostatic repulsions towards the reacting species and block the reaction. This point was highlighted by comparing the use of ZT/r/NPs with various compositions obtained by calcination and hydrothermal treatment in the photodegradation reaction of Procion Red MX-5B. It was observed that catalysts with a composition close to pristine oxides, which had a less negative value of zero-point charge, had a greater photocatalytic efficiency [38].

The acidity of the catalyst surface influences its photoactivity. It was shown that MO degradation by ZT/r/NPs obtained by the sol–gel method was enhanced if zinc sulphate was used during the synthesis instead of zinc chloride or nitrate. Moreover, the photocatalytic activity was enhanced by a sulphating treatment. The enhanced photocatalytic activity was related to the measured higher-acidity behavior of the surface [43].

The creation of oxygen vacancy in the interface ZnO/TiO_2 is a factor enhancing photocatalytic activity. The oxygen-vacancy presence has been estimated by a PL study in MO degradation by TNPs/ZNRs composites, which were obtained by integrating TNPs and ZNRs by PLAL. It was argued that oxygen vacancies could create donor levels which could improve electron–hole separation [56]. Oxygen vacancies were specially created in a ZT powder mixture by applying a high-pressure torsion, and subsequently, their presence was effectively detected by ESR. In this way, it was established that oxygen vacancy in ZT/r/NPs can increase photocatalytic H_2 production in a water-splitting reaction [142].

The photocatalytic activity may be enhanced or decreased by changing photocatalytic working parameters, such as catalyst loading, solution pH, and dye concentration. The effect of catalyst loading on the photodegradation of CI basic blue 41 by ZT/r/NPs was studied [31]. Increasing the catalyst loading increased photodegradation, but at higher catalyst loading a saturation effect prevailed, due to the loss of transparency of the solution, which decreased the effective intensity of the light. A similar effect had been observed for photodegradation of BGY [27] and quinoline [26] by ZT/r/NPs.

The pH can influence the photodegradation of the dye: the photodegradation of CI basic blue 41 by ZT/r/NPs resulted as optimized at 6.21 [31]. It was the result of various factors: the zero-point charge of the catalyst, which influenced its ability to adsorb the cationic dye, the stability of the dye, and the stability of ZnO, which could undergo photo corrosion at pH lower than 6. BGY [27] and bentazon (a herbicide) [137] photodegradation on ZT/r/NPs had their optimal pH at 7.0. No pH effect was found on photodegradation of quinoline [26].

The initial dye concentration has effects on its degradation because it influences the transparency of the solution and the pH of the same. So, it was proved that higher initial dye concentrations decreased degradation of CI basic blue [31], BGY [27], quinoline [26] and by ZT/r/NPs [137].

ZTNC photocatalytic performances, together with catalyst properties, are reported in Table 14.

4. Bioactivity

Zinc oxide and titanium oxide are bioactive materials; zinc oxide is an antimicrobial, thanks to the ability to give electrostatic interactions, to produce ROS, and the release of Zn^{2+} ions [143]. Titanium oxide is antibacterial, thanks to the ability to produce ROS [144]. They are both biocompatible, and zinc oxide is a disinfectant. Both ZnO and TiO_2 are known as non-toxic compounds [4,145], so they have been widely used in sunscreens and cosmetic products; due to their photoprotective properties, they are also used for wastewater treatment. Since they are not transparent, they were subsequently replaced by

the respective NPs, which have a better aesthetic appearance. When they are used in the form of nanoparticles, the risk related to the possibility that they break cell membranes causing damage to living systems must be considered. Furthermore, their bioactivity as a composite system can change, compared to the behaviour of the individual oxides. In this part of the work, the topic of the antimicrobial activity of the composite ZTNPs is addressed and compared to the activity of the individual oxides, as well as the repercussions of their use and release on human and environmental health. It should be noted that studies on bioactivity began later than those on photocatalysis, and that, therefore, their treatment in the literature is less conspicuous. Therefore, it is not possible to carry out a capillary analysis comparable to the previous one relating to photocatalysis. However, this section provides some interesting common lines found.

Antimicrobial activity of ZTNCs has been tested on Gram-positive and Gram-negative bacteria and on fungi, also comparing behaviors in the dark and in UV light [66,102,146].

Antimicrobial activity of ZnO and TiO_2 NPs is due to electrostatic attraction between NPs and the cell wall and to the action of the produced ROS; moreover, ZNPs can release Zn^{2+} ions. All these species can contribute to interacting and damaging the cell wall and to successively attacking and disrupting the vital internal part of the cell [102]. It has been seen that the antimicrobial activity of ZTNFs increases in the presence of UV radiation, because it increases the production of ROS [66].

ZTNPs show higher antimicrobial activity than the respective pristine oxides [50,59,66,102,147–150]. The increased activity was ascribed to the increased ROS production, which was due to the reduced electron–hole recombination at the ZnO-TiO_2 interface [66]. The increased surface area value and decreased crystallite size value of ZTNPs compared to pristine oxides contributed to increased ROS production [50]. Equally, ZT bi-layered films exhibited higher antimicrobial activity than pristine oxides, because of the smaller crystallite size [102]. Also, it had been pointed out that the increased antimicrobial activity of ZTNPs, with respect to pristine oxides, could be due to the lower zeta-potential value, which promoted the electrostatic interaction with the cell [150], and to the smaller particle size, which promoted an easier penetration of the ZTNPs into the cell [59].

Comparing antimicrobial activity of ZTNPs against Gram-positive (S. aureus) and Gram-negative (*E. coli*), it was found that efficiency was higher towards Gram-negative bacteria, due to the difference of the cell wall in terms of thickness, strength and composition [55,59,150]. Anyway, different results were also found, and sometimes the antimicrobial activity of ZTNPs resulted in being higher towards Gram-positive bacteria; in this case, the higher activity was associated with an active transport of the species through the cell wall, more than with a diffusion mechanism [151].

Antimicrobial activity of ZTNPs towards *E. coli* could be activated also by visible light, and was higher than the antimicrobial activity of P25 TiO_2 [32].

The effect of ultrasound irradiation on antimicrobial activity of ZTNPs, ZNPs and TNPs towards S. mutans has been explored, and has shown a synergistic effect of ultrasound irradiation and NPs. Also, in this case, the increased activity was ascribed to the higher ROS production [152].

The antimicrobial properties of ZTNCs make these materials candidates for bio-implant coatings. However, it is necessary to consider what activity these materials may exert on the human cells with which they come into contact. In the case of Z-decorated TNTs, the antimicrobial activity increased with the increased quantity of ZNPs. However, only the higher doses of ZNPs caused the non-proliferation of stem cells, resulting, thus, in being cytotoxic, while medium or lower ZNP quantities did not inhibit the stem cell proliferation. In this way, the maximum usable amount was determined as the highest amount of ZNP that allowed stem cell proliferation [130].

Cell viability on human osteoblast treated with ZT/r/NPs for three days was 92%, which was even higher than the value found treating human osteoblast with Z NPs (81%) [55].

Cell viability was tested also for the ZT multi-shell hollow sphere, and compared with cell viability of ZNPs and TNPs. In this case, a higher cell viability was found for the composite system, 97%, compared to those of pristine oxides, which was 82% and 83% for ZNPs and TNPs [153].

Zinc and titanium oxide nanoparticles are used in multiple fields, which include cosmetic products and sun creams, photocatalytic materials to purify water and air, and pigments in paints, such as pesticides and, fertilizers. This can cause cytotoxic effects on human health, due to direct use [154,155], and, potentially, also on the environment, because of the inevitable dispersion associated with the use. ZNPs and TNPs are often co-present in sunscreens; due to their small size, they penetrate the skin. Adverse-effect studies have shown that ZNPs decrease skin cell viability, causing changes in morphology, mitochondrial activity and cell cycle distribution. The dose limiting is 15 mg L^{-1} and 10 mg L^{-1} in the short-term and long-term, respectively. TNPs do not cause these effects [156], even if TNPs can penetrate more deeply [157]. Again, it was shown that ZNPs damage DNA and prevent cell proliferation. ZnO damage is caused by the Zn^{2+} release and by the non-aggregated ZNPs. However, co-exposure of ZNPs with TNPs reduces ZNPs damage because the released Zn^{2+} ions and non-aggregated ZNPs can aggregate on the TNP surface [158].

When inhaled, ZNPs have greater long-term toxicity than TNPs on lung epithelial cells, in terms of cell viability, proliferation and membrane integrity [159]. TNPs induce oxidative stress in a time- and dose-dependent manner [159]. Acute airway inflammation in mice by ZNPs is much higher than by TNPs [160]. ZNP toxicity is mainly caused by its dissolution and consequent Zn^{2+} release [161,162]. ZNP toxicity of for the nanorod-like shape is higher than that of the spherical ones, and TNP toxicity depends on crystalline structure, in the order rutile < anatase < amorphous [163]. ZNP toxicity on lung epithelial cells was decreased by depositing an outer layer of amorphous TiO_2 [164].

The continuous use of ZNPs and TNPs in cosmetic, pharmaceutical and industrial products inevitably causes their presence in aquatic and terrestrial environments. Both have been shown to have toxic effects on zebrafish. Also, in this case, ZNPs are more toxic than TNPs, and ZnO and ZNPs are equally toxic. TNP toxicity is due to the generation of hydroxyl radicals, without entering the cell membrane. ZNPs can release Zn+ ions, but this is not the only toxicity element [145,165]. TNPs reduce ZNPs and Zn^{2+} concentration in the water medium, because they can adsorb both on the surface [166]. As a result, ZNPs toxicity in water is reduced in the presence of TNPs [167]. On the other hand, Zn-doped TNPs have greater toxicity on zebrafish compared to TNPs, and in a greater extent if TiO_2 is in the rutile phase compared to the anatase phase [168].

So, in this last section, it has been shown that ZTNCs may have higher antimicrobial activity and lower toxicity compared to the pristine oxides ZNPs and TNPs.

5. Conclusions

This review reports the syntheses of ZTNCs, and their photocatalytic activity for the degradation of dyes, pollutants and for reactions to produce fuels, as well as their bioactivity. It has been shown that, in most cases, ZTNCs have greater photocatalytic and antimicrobial activity than pure oxides. The greater photocatalytic activity is attributable to various factors, such as the lower energy gap due to the formation of smaller particles, the lower electron–hole recombination due to the creation of the interface between the two semiconductors, the increase in surface area, the creation of oxygen vacancies, and the zero-point charge value. The antimicrobial activity of ZTNCs is also increased compared to that of pure oxides, because of the increased ROS production. Furthermore, ZTNCs present lower toxicity towards the environment and towards humans, when compared to ZnO nanoparticles and ZnO itself. The reduced toxicity is due to the action of the TNPs, which can aggregate Zn^{2+} and ZNPs on its surface; Zn^{2+} and ZNPs are responsible for the strong toxicity of ZnO. To conclude, ZTNCs have superior properties to those of single oxides, and can be used for the same applications which are valid for single oxides, such

as wastewater treatment, decontamination of pollutants, filters in sunscreen, protective coating for various materials in the field of cultural heritage [169], and prothesis [170].

Funding: This research received no external funding.

Conflicts of Interest: The author declares no conflict of interest.

Lists of Abbreviations

List of dye abbreviations	
MB	Methylene blue
MO	Methyl orange
PCP	Pentachlorophenol,
RhB	Rhodamine B
TCE	trichloroethylene
List of molecule abbreviations	
AcA	acetic acid
Acacetone	acetylacetone,
BuOH	butyl alcohol
CA	cellulose acetate
CitrA	citric acid
DBS	sodium dodecyl benzene sulfonate
DEA	diethanolamine
DMAA	N,N-dimethyl acetamide
DMFA	N,N-dimethylformamide
DW	distilled water
EG	ethylene glycol
EtOH	ethyl alcohol
FA	Furfural alcohol
HMTA	hexamethylenetetramine
IPOH	isopropyl alcohol
KTO	Potassium titanium oxide oxalate
MEA	monoethanolamine
MeOH	methyl alcohol
MeOEtOH	2 methoxy ethanol
OxA	oxalic acid
PCP	penta-chlorophenol
PEG	poly(ethylene glycol)
PEI	polyethanolimine
PEO	poly(ethylene oxide)
PG	polyglycol
PMMA	poly(methyl methacrylate)
PVA	polyvinyl alcohol
PVAc	polyvinyl acetate
PVP	polyvinyl pyrrolidone
PS	polystyrene
SDS	sodium dodecyl sulfonate
TAA	thioacetamide
TBT	tetrabutyl titanate
TCE	trichloroethylene
TEA	triethanolamine
TEOS	tetraethylorthosilicate
TEA	triethylamine
$Ti(Oi\ Pr)_2(dpm)_2$	Oi Pr: iso-propoxy; dpm: 2,2,6,6-tetramethyl3,5-heptanedionate
TOSO	titanium oxosulphate
TS	titanium sulphate
TTIP	titanium tetraisopropoxide

ZAc	zinc acetate
ZAcAc	zinc acetylacetonate
ZN	zinc nitrate
$Zn(hfa)_2$,TMEDA	hfa: 1,1,1,5,5,5-hexafluoro-2,4-pentanedionate; and TMEDA: N,N,N′,N′-tetramethylethylenediamine
ZS	zinc sulphate
List of synthesis method abbreviations	
ALD	Atomic layer deposition
ALE	Atomic layer epitaxy
CVD	Chemical vapor deposition
DC	Direct current
CBD	Chemical Bath deposition
FAPO	Furfural alcohol-derived polymerization–oxidation
LbL	Layer-by-layer
MW	Microwave
PLAL	Pulsed laser ablation in liquid
PLD	Pulsed laser deposition
RF	Radio Frequency
RT	Room temperature
SSR	Solid-state reaction
List of structure abbreviations	
ZT	ZnO-TiO_2
Cs TZ	Core (TiO_2)–shell (ZnO)
Cs ZT	Core (ZnO)–shell (TiO_2)
IOS	Inverse opal structure
NFls	Nanoflakes
NFs	Nanofibers
NPs	Nanoparticles
NRs	Nanorods
NTs	Nanotubes
NWs	Nanowires
T	TiO_2
TNFs	TiO_2 nanofibers
TNPs	TiO_2 nanoparticles
TNTs	TiO_2 nanotubes
TNWs	TiO_2 nanowires
UTZs	Urchin-like TiO_2/ZnO
Z	ZnO
ZTNCs	ZnO-TiO_2 nanocomposites
ZNFls	ZnO nanoflakes
ZNPs	ZnO nanoparticles
ZNRs	ZnO nanorods
ZNWs	ZnO nanowires
Z QDs	ZnO quantum dots
ZTNFs	ZnO-TiO2 NFs
ZNFls	ZnO nanoflakes
ZTNTs	ZnO-TiO_2 nanotubes
ZT/r/NPs	ZnO-TiO_2 random nanoparticles

References

1. Özgür, Ü.; Alivov, Y.I.; Liu, C.; Teke, A.; Reshchikov, M.A.; Doğan, S.; Avrutin, V.; Cho, S.-J.; Morkoçd, H. A Comprehensive Review of ZnO Materials and Devices. *J. Appl. Phys.* **2005**, *98*, 041301. [CrossRef]
2. Carp, O.; Huisman, C.L.; Reller, A. Photoinduced Reactivity of Titanium Dioxide. *Prog. Solid State Chem.* **2004**, *32*, 33–177. [CrossRef]
3. Wang, Y.; He, Y.; Lai, Q.; Fan, M. Review of the Progress in Preparing Nano TiO_2: An Important Environmental Engineering Material. *J. Environ. Sci.* **2014**, *26*, 2139–2177. [CrossRef] [PubMed]
4. Ong, C.B.; Ng, L.Y.; Mohammad, A.W. A Review of ZnO Nanoparticles as Solar Photocatalysts: Synthesis, Mechanisms and Applications. *Renew. Sustain. Energy Rev.* **2018**, *81*, 536–551. [CrossRef]

5. Wang, R.; Hashimoto, K.; Fujishima, A.; Chikuni, M.; Kojima, E.; Kitamura, A.; Shimohigoshi, M.; Watanabe, T. Light-Induced Amphiphilic Surfaces. *Nature* **1997**, *388*, 431–432. [CrossRef]
6. Dulin, F.H.; Rase, D.E. Phase Equilibria in the System ZnO-TiO_2. *J. Am. Ceram. Soc.* **1960**, *43*, 125–131. [CrossRef]
7. Bartram, S.F.; Slepetys, R.A. Compound Formation and Crystal Structure in the System ZnO-TiO_2. *J. Am. Ceram. Soc.* **1961**, *44*, 493–499. [CrossRef]
8. Yamaguchi, O.; Morimi, M.; Kawabata, H.; Shimizu, K. Formation and Transformation of $ZnTiO_3$. *J. Am. Ceram. Soc.* **1987**, *70*, C97–C98. [CrossRef]
9. Surendar, T.; Kumar, S.; Shanker, V. Influence of La Doping on Phase Transformation and Photocatalytic Properties of $ZnTiO_3$ Nanoparticles Synthesized via Modified Sol-gel Method. *Phys. Chem. Chem. Phys.* **2014**, *16*, 728. [CrossRef]
10. Munguti, L.; Dejene, F. Effects of Zn:Ti Molar Ratios on the Morphological, Optical and Photocatalytic Properties of ZnO-TiO_2 Nanocomposites for Application in Dye Removal. *Mater. Sci. Semicond. Process.* **2021**, *128*, 105786. [CrossRef]
11. Kolen'ko, Y.V.; Kovnir, K.A.; Gavrilov, A.I.; Garshev, A.V.; Meskin, P.E.; Churagulov, B.R.; Bouchard, M.; Colbeau-Justin, C.; Lebedev, O.I.; Van Tendeloo, G.; et al. Structural, Textural, and Electronic Properties of a Nanosized Mesoporous $ZnxTi_{1-x}O_{2-x}$ Solid Solution Prepared by a Supercritical Drying Route. *J. Phys. Chem. B* **2005**, *109*, 20303–20309. [CrossRef]
12. Bouchet, R.; Weibel, A.; Knauth, P.; Mountjoy, G.; Chadwick, A.V. EXAFS Study of Dopant Segregation (Zn, Nb) in Nanocrystalline Anatase (TiO_2). *Chem. Mater.* **2003**, *15*, 4996–5002. [CrossRef]
13. Zhang, Y.; Wang, L.; Liu, B.; Zhai, J.; Fan, H.; Wang, D.; Lin, Y.; Xie, T. Synthesis of Zn-Doped TiO_2 Microspheres with Enhanced Photovoltaic Performance and Application for Dye-Sensitized Solar Cells. *Electrochim. Acta* **2011**, *56*, 6517–6523. [CrossRef]
14. Zhu, F.; Zhang, P.; Wu, X.; Fu, L.; Zhang, J.; Xu, D. The Origin of Higher Open-Circuit Voltage in Zn-Doped TiO_2 Nanoparticles-Based Dye Sensitized Solar Cells. *Chem. Phys. Chem.* **2012**, *13*, 3731–3737. [CrossRef] [PubMed]
15. Huang, F.; Li, Q.; Thorogood, G.J.; Cheng, Y.-B.; Caruso, R.A. Zn-Doped TiO_2 Electrodes in Dye Sensitized Solar Cells Enhanced Photocurrent. *J. Mater. Chem.* **2012**, *22*, 17128. [CrossRef]
16. Su, C.-Y.; Wang, C.-C.; Hsueh, Y.-C.; Gurylev, V.; Kei, C.-C.; Perng, T.-P. Enabling High Solubility of ZnO in TiO_2 by Nanolamination of Atomic Layer Deposition. *Nanoscale* **2015**, *7*, 19222–19230. [CrossRef]
17. Gandelman, H.; da Silvia, A.L.; Batista Caliman, L.; Gouvêa, D. Surface and Grain Boundary Excess of ZnO-Doped TiO_2 Anatase Nanopowders. *Ceram. Int.* **2018**, *44*, 11390–11396. [CrossRef]
18. Mazabuel-Collazos, A.; Daza Gómez, C.; Rodríguez-Páez, J.E. ZnO-TiO_2 Nanocomposites Synthetized by Wet Chemical Route: Study of Their Structural and Optical Properties. *Mater. Chem. Phys.* **2019**, *222*, 230–245. [CrossRef]
19. Lin, S.-S.; Huang, J.-L.; Šajgalik, P. The Properties of Ti-Doped ZnO Films Deposited by Simultaneous RF and DC Magnetron Sputtering. *Surf. Coat. Technol.* **2005**, *191*, 286–292. [CrossRef]
20. Chung, J.-L.; Chen, J.-C.; Tseng, C.-J. Electrical and Optical Properties of TiO_2-Doped ZnO Films Prepared by Radio-Frequency Magnetron Sputtering. *J. Phys. Chem. Solids* **2008**, *69*, 535–539. [CrossRef]
21. Ye, Z.-Y.; Lu, H.-L.; Geng, Y.; Gu, Y.-Z.; Xie, Z.-Y.; Zhang, Y.; Sun, Q.-Q.; Ding, S.-J.; Zhang, D.W. Structural, Electrical, and Optical Properties of Ti-Doped ZnO Films Fabricated by Atomic Layer Deposition. *Nanoscale Res. Lett.* **2013**, *8*, 108. [CrossRef] [PubMed]
22. Zheng, K.; Gu, L.; Sun, D.; Mo, X.L.; Chen, G. The Properties of Ethanol Gas Sensor Based on Ti Doped ZnO Nanotetrapods. *Mater. Sci. Eng. B* **2010**, *166*, 104–107. [CrossRef]
23. Wang, J.; Jiang, Z.; Zhang, L.; Kang, P.; Xie, Y.; Lv, Y.; Xu, R.; Zhang, X. Sonocatalytic Degradation of Some Dyestuffs and Comparison of Catalytic Activities of Nano-Sized TiO_2, Nanosized ZnO and Composite TiO_2/ZnO Powders under Ultrasonic Irradiation. *Ultrason. Sonochem.* **2009**, *16*, 225–231. [CrossRef] [PubMed]
24. Sun, W.; Meng, S.; Zhang, S.; Zheng, X.; Ye, X.; Fu, X.; Chen, S. Insight into the Transfer Mechanisms of Photogenerated Carriers for Heterojunction Photocatalysts with the Analogous Position of Valence Band and Conduction Band: A Case Study of ZnO/TiO_2. *J. Phys. Chem. C* **2018**, *122*, 15409–15420. [CrossRef]
25. Li, B.; Yuan, D.; Gao, C.; Zhang, H.; Li, Z. Synthesis and Characterization of TiO_2/ZnO Heterostructural Composite for Ultraviolet Photocatalytic Degrading DOM in Landfill Leachate. *Environ. Sci. Pollut. Res.* **2022**, *29*, 85510–85524. [CrossRef] [PubMed]
26. Gupta, D.; Chauhan, R.; Kumar, N.; Singh, V.; Srivastava, V.C.; Mohanty, P.; Mandal, T.K. Enhancing Photocatalytic Degradation of Quinoline by ZnO:TiO_2 Mixed Oxide: Optimization of Operating Parameters and Mechanistic Study. *J. Environ. Manag.* **2020**, *258*, 110032. [CrossRef]
27. Habib, M.A.; Shahadat, M.T.; Bahadur, N.M.; Ismail, I.M.I.; Mahmood, A.J. Synthesis and Characterization of ZnO-TiO_2 Nanocomposites and Their Application as Photocatalysts. *Int. Nano Lett.* **2013**, *3*, 5. [CrossRef]
28. Marcì, G.; Augugliaro, V.; López-Muñoz, M.J.; Martín, C.; Palmisano, L.; Rives, V.; Schiavello, M.; Tilley, R.J.D.; Venezia, A.M. Preparation Characterization and Photocatalytic Activity of Polycrystalline ZnO/TiO_2 Systems. 1. Surface and Bulk Characterization. *J. Phys. Chem. B* **2001**, *105*, 1026–1032. [CrossRef]
29. Ahmad, W.; Mehmood, U.; Al-Ahmed, A.; Al-Sulaiman, F.A.; Aslam, M.Z.; Kamal, M.S.; Shawabkeh, R.A. Synthesis of Zinc Oxide/Titanium Dioxide (ZnO/TiO_2) Nanocomposites by Wetness Impregnation Method and Preparation of ZnO/TiO_2 Paste Using Poly(vinylpyrrolidone) for Efficient Dye-Sensitized Solar Cells. *Elecrochim. Acta* **2016**, *222*, 473–480. [CrossRef]
30. Ku, Y.; Huang, Y.-H.; Chou, Y.-C. Preparation and Characterization of ZnO/TiO_2 for the Photocatalytic Reduction of Cr (VI) in Aqueous Solution. *J. Mol. Catal. A Chem.* **2011**, *342–343*, 18–22. [CrossRef]
31. Jiang, Y.; Sun, Y.; Liu, H.; Zhu, F.; Yin, H. Solar Photocatalytic Decolorization of CI Basic Blue 41 in an Aqueous Suspension of TiO_2-ZnO. *Dyes Pigm.* **2008**, *78*, 77–83. [CrossRef]

32. Karunakaran, C.; Abiramasundari, G.; Gomathisankar, P.; Manikandan, G.; Anandi, V. Preparation and Characterization of ZnO-TiO_2 Nanocomposite for Photocatalytic Disinfection of Bacteria and Detoxification of Cyanide under Visible Light. *Mater. Res. Bull.* **2011**, *46*, 1586–1592. [CrossRef]
33. Arin, J.; Thongtem, S.; Thongtem, T. Single-Step Synthesis of ZnO/TiO_2 Nanocomposites by Microwave Radiation and Their Photocatalytic Activities. *Mater. Lett.* **2013**, *96*, 78–81. [CrossRef]
34. Lachom, V.; Poolcharuansin, P.; Laokul, P. Preparation, Characterizations and Photocatalytic Activity of a ZnO/TiO_2 Nanocomposite. *Mater. Res. Express* **2017**, *4*, 035006. [CrossRef]
35. She, M.; Li, X.; Xiong, P.; Tian, Y.; Song, S.; Ding, T.; Li, X. Assembly of Hydrolysis, Activation and Reforming Sites Boosting Steam Reforming of DME over ZnO/TiO_2 catalysts. *Mater. Today Chem.* **2023**, *33*, 101688. [CrossRef]
36. Houšková, V.; Štengl, V.; Bakardjieva, S.; Murafa, N. Photoactive Materials Prepared by Homogeneous Hydrolysis with Thioacetamide: Part 2—TiO_2/ZnO Nanocomposites. *J. Phys. Chem. Solids* **2008**, *69*, 1623–1631. [CrossRef]
37. Upadhyay, G.K.; Rajput, J.K.; Pathaka, T.K.; Kumara, V.; Purohit, L.P. Synthesis of ZnO:TiO_2 Nanocomposites for Photocatalyst Application in Visible Light. *Vacuum* **2019**, *160*, 154–163. [CrossRef]
38. Kostedt, W.L.; Ismail, A.A.; Mazyck, D.W. Impact of Heat Treatment and Composition of ZnO-TiO_2 Nanoparticles for Photocatalytic Oxidation of an Azo Dye. *Ind. Eng. Chem. Res.* **2008**, *47*, 1483–1487. [CrossRef]
39. Zhang, M.; An, T.; Liu, X.; Hu, X.; Sheng, G.; Fu, J. Preparation of a High-Activity ZnO/TiO_2 Photocatalyst via Homogeneous Hydrolysis Method with Low Temperature Crystallization. *Mater. Lett.* **2010**, *64*, 1883–1886. [CrossRef]
40. Guo, S.-y.; Han, S.; Chi, B.; Pu, J.; Li, J. A Facile Low Temperature Approach to Designing Controlled Amorphous Based Titania Composite Photocatalysts with Excellent Noble-Metal-Free Photocatalytic Hydrogen Production. *ACS Appl. Mater. Interfaces* **2014**, *6*, 4743–4751. [CrossRef]
41. Siwińska-Stefańska, K.; Kubiak, A.; Piasecki, A.; Dobrowolska, A.; Czaczyk, K.; Motylenko, M.; Rafaja, D.; Ehrlich, H.; Jesionowski, T. Hydrothermal Synthesis of Multifunctional TiO_2-ZnO Oxide Systems with Desired Antibacterial and Photocatalytic Properties. *Appl. Surf. Sci.* **2019**, *463*, 791–801. [CrossRef]
42. Pan, L.; Shen, G.-Q.; Zhang, J.-W.; Wei, X.-C.; Wang, L.; Zou, J.-J.; Zhang, X. TiO_2−ZnO Composite Sphere Decorated with ZnO Clusters for Effective Charge Isolation in Photocatalysis. *Ind. Eng. Chem. Res.* **2015**, *54*, 7226–7232. [CrossRef]
43. Liao, S.; Donggen, H.; Yu, D.; Su, Y.; Yuan, G. Preparation and Characterization of ZnO/TiO_2, SO_4^{2-}/ZnO/TiO_2 Photocatalyst and their Photocatalysis. *J. Photochem. Photobiol. A Chem.* **2004**, *168*, 7–13. [CrossRef]
44. Liao, D.L.; Badour, C.A.; Liao, B.Q. Preparation of Nanosized TiO_2/ZnO Composite Catalyst and its Photocatalytic Activity for Degradation of Methyl Orange. *J. Photochem. Photobiol. A Chem.* **2008**, *194*, 11–19. [CrossRef]
45. Rajbongshi, B.M.; Samdarshi, S.K.; Boro, B. Multiphasic Bi-Component TiO_2-ZnO Nanocomposite: Synthesis, Characterization and Investigation of Photocatalytic Activity under Different Wavelengths of Light Irradiaion. *J. Mater. Sci. Mater. Electron.* **2015**, *26*, 377–384. [CrossRef]
46. Janitabar-Darzi, S.; Mahjoub, A.R. Investigation of Phase Transformations and Photocatalytic Properties of Sol-Gel Prepared Nanostructured ZnO/TiO_2 Composites. *J. Alloys Compd.* **2009**, *486*, 805–808. [CrossRef]
47. Sridevi, K.P.; Guru Prasad, L.; Sangeetha, B.; Sivakumar, S. Structural and Optical Study of ZnO-TiO_2 Nanocomposites. *J. Ovonic Res.* **2022**, *18*, 453–464. [CrossRef]
48. El Mragui, A.; Daou, I.; Zegaoui, O. Influence of the Preparation Method and ZnO/(ZnO+TiOP) Weight Ratio on the Physicochemical and Photocatalytic Properties of ZnO-TiO_2. *Catal. Today* **2019**, *321–322*, 41–51. [CrossRef]
49. Suo, H.; Peng, C.; Jing, F.; Yu, S.; Cui, S.; Shen, X. Facile Preparation of TiO_2/ZnO Composite Aerogel with Excellent Antibacterial Activities. *Mater. Lett.* **2019**, *234*, 253–256. [CrossRef]
50. Ilkhechi, N.N.; Mozammel, M.; Khosroushahi, A.Y. Antifungal Effects of ZnO, TiO_2 and ZnO-TiO_2 nanostructures on Aspergillus flavus. *Pestic. Biochem. Phys.* **2021**, *176*, 104869. [CrossRef]
51. Hussein, A.M.; Mahoney, L.; Peng, R.; Kibombo, H.; Wu, C.-M.; Koodali, R.T.; Shende, R. Mesoporous Coupled ZnO/TiO_2 Photocatalyst Nanocomposites for Hydrogen Generation. *J. Renew. Sustain. Energy* **2013**, *5*, 033118. [CrossRef]
52. Rusman, E.; Heryanto, H.; Fahri, A.N.; Rahmat, R.; Mutmainna, I.; Tahir, D. Green Synthesis ZnO/TiO_2 for High Recyclability Rapid Sunlight Photodegradation Wastewater. *MRS Adv.* **2022**, *7*, 444–449. [CrossRef]
53. Roy, D.; Yadav, A.K. Green TiO_2-ZnO Nanocomposite Stimulator for the Growth of Solanum Lycopersicum in Aquaculture. *Appl. Nanosci.* **2022**, *12*, 1403–1423. [CrossRef]
54. Umar, K.; Adnan, R. Biomass Mediated Green Synthesis of ZnO/TiO_2 Nanocomposite and Enhanced Photocatalytic Activity for the Decolorization of Rhodamine B under Visible Light. *KEM* **2022**, *920*, 36–42. [CrossRef]
55. Menazea, A.A.; Awwad, N.S. Antibacterial Activity of TiO_2 Doped ZnO Composite Synthesized via Laser Ablation Route for Antimicrobial Application. *J. Mater. Res. Technol.* **2020**, *9*, 9434–9441. [CrossRef]
56. Gondal, M.A.; Ilyas, A.M.; Baig, U. Pulsed Laser Ablation in Liquid Synthesis of ZnO/TiO_2 Nanocomposite Catalyst with Enhanced Photovoltaic and Photocatalytic Performance. *Ceram. Int.* **2016**, *42*, 13151–13160. [CrossRef]
57. Madhuvilakku, R.; Piraman, S. Biodiesel Synthesis by TiO_2-ZnO Mixed Oxide Nanocatalyst Catalyzed Palm Oil Transesterification Process. *Bioresour. Technol.* **2013**, *150*, 55–59. [CrossRef]
58. Mousa, H.M.; Fares Alenezi, J.; Mohamed, I.M.A.; Yasin, A.S.; Hashem, A.-F.M.; Abdal-hay, A. Synthesis of TiO_2@ZnO Heterojunction for Dye Photodegradation and Wastewater Treatment. *J. Alloys Compd.* **2021**, *886*, 161169. [CrossRef]

59. Sirotkin, N.; Khlyustova, A.; Costerin, D.; Naumova, I.; Titov, V.; Agafonov, A. Applications of Plasma Synthesized ZnO, TiO_2, and Zn/TiO_x Nanoparticles for Making Antimicrobial Wound-Healing Viscose Patches. *Plasma Process Polym.* **2022**, *19*, e2100093. [CrossRef]
60. Lee, J.H.; Jung, K.Y.; Park, S.B. Modification of Titania Particles by Ultrasonic Spray Pyrolysis of Colloid. *J. Mater. Sci.* **1999**, *34*, 4089–4093. [CrossRef]
61. Ohshima, K.; Tsuto, K.; Okuyama, K.; Tohge, N. Preparation of ZnO-TiO_2 Composite Fine Particles Using the Ultrasonic Spray Pyrolysis Method and Their Characteristics on Ultraviolet Cutoff. *Aerosol Sci. Technol.* **1993**, *19*, 468–477. [CrossRef]
62. Lü, X.; Huang, F.; Mou, X.; Wang, Y.; Xu, F. A General Preparation Strategy for Hybrid TiO_2 Hierarchical Spheres and Their Enhanced Solar Energy Utilization Efficiency. *Adv. Mater.* **2010**, *22*, 3719–3722. [CrossRef] [PubMed]
63. Huo, S.; Ding, S.; Zhao, C.; Wang, C.; Yu, F.; Fang, J.; Yang, Y. Growth and Photocatalytic Activities of Porous ZnO/TiO_2 Composite Microspheres with Crystalline–Amorphous Phase Boundary. *Catal. Lett.* **2021**, *151*, 1937–1947. [CrossRef]
64. Xi, G.; Ouyang, S.; Ye, J. General Synthesis of Hybrid TiO_2 Mesoporous "French Fries" Toward Improved Photocatalytic Conversion of CO_2 into Hydrocarbon Fuel: A Case of TiO_2/ZnO. *Chem. Eur. J.* **2011**, *17*, 9057–9061. [CrossRef] [PubMed]
65. Liu, R.; Ye, H.; Xiong, X.; Liu, H. Fabrication of TiO_2/ZnO Nanofibers by Electrospinning and Their Photocatalytic Property. *Mater. Chem. Phys.* **2010**, *121*, 432–439. [CrossRef]
66. Hwang, S.H.; Song, J.; Jung, Y.; Kweon, O.Y.; Song, H.; Jang, J. Electrospun ZnO/TiO_2 composite Nanofibers as a Bactericidal Agent. *Chem. Commun.* **2011**, *47*, 9164–9166. [CrossRef]
67. Pei, C.C.; Leung, W.W.-F. Enhanced Photocatalytic Activity of Electrospun TiO_2/ZnO Nanofibers with Optimal Anatase/Rutile Ratio. *Catal. Commun.* **2013**, *37*, 100–104. [CrossRef]
68. Murugan, R.; Babu, V.J.; Khin, M.M.; Nair, A.S.; Ramakrishna, S. Synthesis and Photocatalytic Applications of Flower Shaped Electrospun ZnO–TiO_2 Mesostructures. *Mater. Lett.* **2013**, *97*, 47–51. [CrossRef]
69. Kim, S.-S.; Yum, J.-H.; Sung, Y.-E. Flexible Dye-Sensitized Solar Cells Using ZnO Coated TiO_2 Nanoparticles. *J. Photochem. Photobiol. A Chem.* **2005**, *171*, 269–273. [CrossRef]
70. Byun, K.-T.; Seo, K.W.; Shim, I.-W.; Kwak, H.-Y. Synthesis of ZnO and ZnO-Coated TiO_2 Nanoparticles in Various Alcohol Solutions at Multibubble Sonoluminescence (MBLS) Condition. *Chem. Eng. J.* **2008**, *135*, 168–173. [CrossRef]
71. Bahadur, N.M.; Furusawa, T.; Sato, M.; Kurayama, F.; Suzuki, N. Rapid Synthesis, Characterization and Optical Propertis of TiO_2 Coated ZnO Nanocomposite Particles by a Novel Microwave Irradiation Method. *Mater. Res. Bull.* **2010**, *45*, 1383–1388. [CrossRef]
72. Ajay Rakkesh, R.; Balakumar, S. Facile Synthesis of ZnO/TiO_2 Core–Shell Nanostructures and Their Photocatalytic Activities. *JNN* **2013**, *13*, 370–376. [CrossRef]
73. Haghighatzadeh, A.; Hosseini, M.; Mazinani, B.; Shokouhimehr, M. Improved Photocatalytic Activity of ZnO-TiO_2 Nanocomposite Catalysts by Modulating TiO_2 thickness. *Mater. Res. Express* **2019**, *6*, 115060. [CrossRef]
74. Ramírez-Ortega, D.; Meléndez, A.M.; Acevedo-Peña, P.; González, I.; Arroyo, R. Semiconducting Properties of ZnO/TiO_2 Composites by Electrochemical Measurements and Their Relationship with Photocatalytic Activity. *Electrochim. Acta* **2014**, *140*, 541–554. [CrossRef]
75. Zhang, Q.; Fan, W.; Gao, L. Anatase TiO_2 Nanoparticles Immobilized on ZnO tetrapods as a Highly Efficient and Easily Recyclable Photocatalyst. *Appl. Catal. B* **2007**, *76*, 168–173. [CrossRef]
76. Xu, Y.; Zheng, L.; Yang, C.; Zheng, W.; Liu, X.; Zhang, J. Chemiresistive Sensors Based on Core-Shell ZnO@TiO_2 Nanorods Designed by Atomic Layer Deposition for n-Butanol Detection. *Sens. Actuators B Chem.* **2020**, *310*, 127846. [CrossRef]
77. Zhou, M.; Wu, B.; Zhang, X.; Cao, S.; Ma, P.; Wang, K.; Fan, Z.; Su, M. Preparation and UV Photoelectric Properties of Aligned ZnO-TiO_2 and TiO_2-ZnO Core-Shell Structured Heterojunction Nanotubes. *ACS Appl. Mater. Interfaces* **2020**, *12*, 38490–38498. [CrossRef]
78. Chen, D.; Zhang, H.; Hu, S.; Li, J. Preparation and Enhanced Photoelectrochemical Performances of Coupled Bicomponent ZnO-TiO_2 Nanocomposites. *J. Phys. Chem.* **2008**, *112*, 117–122. [CrossRef]
79. Sun, C.; Xu, Q.; Xie, Y.; Ling, Y.; Hou, Y. Designed Synthesis of Anatase–TiO_2 (B) Biphase Nanowire/ZnO Nanoparticle Heterojunction for Enhanced Photocatalysis. *J. Mater. Chem. A* **2018**, *6*, 8289–8298. [CrossRef]
80. Cheng, P.; Wang, Y.; Xu, L.; Sun, P.; Su, Z.; Jin, F.; Liu, F.; Sun, Y.; Lu, G. High Specific Surface Area Urchin-like Hierarchical ZnO-TiO_2 Architectures: Hydrothermal Synthesis and Photocatalytic Properties. *Mater. Lett.* **2016**, *175*, 52–55. [CrossRef]
81. Yang, H.G.; Zeng, H.C. Synthetic architectures of $TiO_2/H_2T_5O_{11}$*H_2O, $ZnO/H_2T_5O_{11}$*H_2O, $ZnO/TiO_2/H_2T_5$ O_{11}*H_2O and ZnO/TiO_2 nanocomposites. *J. Am. Chem. Soc.* **2005**, *127*, 270–278. [CrossRef] [PubMed]
82. Qin, R.; Meng, F.; Khan, M.W.; Yu, B.; Li, H.; Fan, Z.; Gong, J. Fabrication and Enhanced Potocatalytic Property of TiO_2-ZnO Composite Photocatalysts. *Mater. Lett.* **2019**, *240*, 84–87. [CrossRef]
83. Athauda, T.J.; Neff, J.G.; Sutherlin, L.; Butt, U.; Ozer, R.R. Systematic Study of the Structure-Property Relationships of Branched Hierarchical TiO_2/ZnO Nanostructures. *ACS Appl. Mater. Interfaces* **2012**, *4*, 6917–6926. [CrossRef]
84. Deng, J.; Yu, B.; Lou, Z.; Wang, L.; Wang, R.; Zhang, T. Facile Synthesis and Enhanced Ethanol Sensing Properties of the Brush-like ZnO–TiO_2 Heterojunctions Nanofibers. *Sens. Actuators B Chem.* **2013**, *184*, 21–26. [CrossRef]
85. Zheng, X.; Li, D.; Li, X.; Chen, J.; Cao, C.; Fang, J.; Wang, J.; He, Y.; Zheng, Y. Construction of ZnO/TiO_2 Photonic Crystal Heterostructures for Enhanced Photocatalytic Properties. *Appl. Catal. B Environ.* **2015**, *168–169*, 408–415. [CrossRef]

86. Zalfani, M.; van der Schueren, B.; Mahdouani, M.; Bourguiga, R.; Yu, W.-B.; Wu, M.; Deparis, O.; Li, Y.; Su, B.-L. ZnO Quantum Dots Decorated 3DOM TiO_2 Nanocomposites: Symbiose of Quantum Size Effects and Photonic Structure for Highly Enhanced Photocatalytic Degradation of Organic Pollutants. *Appl. Catal. B* **2016**, *199*, 187–198. [CrossRef]
87. Singh, J.; Kumar, S.; Rishikesh; Manna, A.K.; Soni, R.K. Fabrication of ZnO–TiO_2 Nanohybrids for Rapid Sunlight Driven Photodegradation of Textile Dyes and Antibiotic Residue Molecules. *Opt. Mater.* **2020**, *107*, 110138. [CrossRef]
88. Chen, M.; Kang, Z.; Wu, J.; Qin, N.; Bao, D. Significantly Enhanced Piezo-Photocatalytic Properties of Recyclable Nanocomposite Films by Growing ZnO Nanorods on Inverse Opal Structured TiO_2 framework. *J. Alloys Compd.* **2024**, *985*, 174032. [CrossRef]
89. Yuan, Z.-H.; Tang, C.-C.; Fan, S.-S. Optical Absorption of Sol-Gel Derived ZnO-TiO_2 Nanocomposite Films. *Chin. Phys. Lett.* **2001**, *18*, 1520–1522. [CrossRef]
90. Shaogui, Y.; Xie, Q.; Xinyong, L.; Yazi, L.; Shuo, C.; Guohua, C. Preparation, Characterization and Photoelectrocatalytic Properties of Nanocrystalline Fe_2O_3/TiO_2, ZnO/TiO_2 and $Fe_2O_3/ZnO/TiO_2$ Composite Film Electrodes Towards Pentachlorophenol Degradation. *Phys. Chem. Chem. Phys.* **2004**, *6*, 659–664. [CrossRef]
91. Vaezi, M.R. Two-Steps Solochemical Synthesis of ZnO/TiO_2 Nano-Composite Materials. *J. Mater. Process. Technol.* **2008**, *205*, 332–337. [CrossRef]
92. Tian, J.; Chen, L.; Yin, Y.; Wang, X.; Dai, J.; Zhu, Z.; Liu, X.; Wu, P. Photocatalyst of TiO_2/ZnO Nano Composite Film: Preparation, Characterization and Photodegradation Activity of Methyl Orange. *Surf. Coat. Technol.* **2009**, *204*, 205–214. [CrossRef]
93. Chen, Y.; Zhang, C.; Huang, W.; Yang, C.; Huang, T.; Situ, Y.; Huang, H. Synthesis of Porous ZnO/TiO_2 Thin Films with Superhydrophilicity and Photocatalytic Activity via a Template-Free Sol-Gel Method. *Surf. Coat. Technol.* **2014**, *258*, 531–538. [CrossRef]
94. Firdaus, C.M.; Shah Rizam, M.S.B.; Rusop, M.; Rahmatul Hidayah, S. Characterization of ZnO and ZnO: TiO_2 Thin Films Prepared by Sol-Gel Spray-Spin Coating Technique. *Procedia Eng.* **2012**, *41*, 1367–1373. [CrossRef]
95. Barreca, D.; Comini, E.; Ferrucci, A.P.; Gasparotto, A.; Maccato, C.; Maragno, C.; Sberveglieri, G.; Tondello, E. First Example of ZnO-TiO_2 Nanocomposites by Chemical Vapor Deposition: Structure, Morphology, Composition, and Gas Sensing Performances. *Chem. Mater.* **2007**, *19*, 5642–5649. [CrossRef]
96. Mane, R.S.; Lee, W.J.; Pathan, H.M.; Han, S.-H. Nanocrystalline TiO_2/ZnO Thin Films: Fabrication and Application to Dye-Sensitized Solar Cells. *J. Phys. Chem. B* **2005**, *109*, 24254–24259. [CrossRef]
97. Roh, S.-J.; Mane, R.S.; Min, S.-K.; Lee, W.-J.; Lokhande, C.D.; Han, S.-H. Achievement of 4.51% Conversion Efficiency using ZnO Recombination Barrier Layer in TiO_2 Based Dye-Sensitized Solar Cells. *Appl. Phys. Lett.* **2006**, *89*, 253512. [CrossRef]
98. Kim, K.E.; Jang, S.-R.; Park, J.; Vittal, R.; Kim, K.-J. Enhancement in the Performance of Dye-Sensitized Solar Cells Containing ZnO-Covered TiO_2 Electrodes Prepared by Thermal Chemical Vapor Deposition. *Sol. Energy Mater. Sol. Cells* **2007**, *91*, 366–370. [CrossRef]
99. Zhang, Z.; Yuan, Y.; Fang, Y.; Liang, L.; Ding, H.; Jin, L. Preparation of Photocatalytic Nano-ZnO/TiO_2 Film and Application for Determination of Chemical Oxygen Demand. *Talanta* **2007**, *73*, 523–528. [CrossRef]
100. Shi, L.; Shen, H.; Jiang, L.; Li, X. Co-Emission of UV, Violet and Green Photoluminescence of ZnO/TiO_2 Thin Film. *Mater. Lett.* **2007**, *64*, 4735–4737. [CrossRef]
101. Choi, W.S.; Kim, E.J.; Seong, S.G.; Kim, Y.S.; Park, C.; Hahn, S.H. Optical and Structural Properties of ZnO/TiO_2/ZnO Multilayers Prepared via Electron Beam Evaporation. *Vacuum* **2009**, *83*, 878–882. [CrossRef]
102. Widyastuti, E.; Chiu, C.-T.; Hsu, J.-L.; Lee, Y.C. Photocatalytic Antimicrobial and Photostability Studies of TiO_2/ZnO Thin Films. *Arab. J. Chem.* **2023**, *16*, 105010. [CrossRef]
103. Yang, G.; Wang, Q.; Miao, C.; Bu, Z.; Guo, W. Enhanced Photovoltaic Performance of Dye-Sensitized Solar Cells Based on ZnO Microrod Aray/TiO_2 Nanoparticle Hybrid Films. *J. Mater. Chem. A* **2013**, *1*, 3112. [CrossRef]
104. Deng, J.; Wang, M.; Zhang, P.; Ye, W. Preparing ZnO Nanowires in Mesoporous TiO_2 Photoanode by an in-Situ Hydrothermal Growth for Enhanced Light-Trapping in Quantum Dots-Sensitized Solar Cells. *Electrochim. Acta* **2016**, *200*, 12–20. [CrossRef]
105. Kumagai, H.; Tanaka, Y.; Murata, M.; Masuda, Y.; Shinagawa, T. Novel TiO_2/ZnO Multilayer Mirrors at 'Water-Window' Wavelengths Fabricated by Atomic Layer Epitaxy. *J. Phys. Condens. Matter* **2010**, *22*, 474008. [CrossRef]
106. Law, M.; Greene, L.E.; Radenovic, A.; Kuykendall, T.; Liphardt, J.; Yang, P. ZnO-Al_2O_3 and ZnO-TiO_2 Core-Shell Nanowire Dye Sensitized Solar Cells. *J. Phys. Chem. B* **2006**, *110*, 22652–22663. [CrossRef]
107. Hernández, S.; Cauda, V.; Chiodoni, A.; Dallorto, S.; Sacco, A.; Hidalgo, D.; Celasco, E.; Pirri, C.F. Optimization of 1D ZnO@TiO_2 Core−Shell Nanostructures for Enhanced Photoelectrochemical Water Splitting under Solar Light Illumination. *ACS Appl. Mater. Interfaces* **2014**, *6*, 12153–12167. [CrossRef]
108. Wang, Z.; Hu, T.; He, H.; Fu, Y.; Zhang, X.; Sun, J.; Xing, L.; Liu, B.; Zhang, Y.; Xue, X. Enhanced H_2 Production of TiO_2/ZnO Nanowires co-Using Solar and Mechanical Energy through Piezo-Photocatalytic Effect. *ACS Sustain. Chem. Eng.* **2018**, *6*, 10162–10172. [CrossRef]
109. Jeong, K.; Deshmukh, P.R.; Park, J.; Sohn, Y.; Shin, W.G. ZnO-TiO_2 Core−Shell Nanowires: A Sustainable Photoanode for Enhanced Photoelectrochemical Water Splitting. *ACS Sustain. Chem. Eng.* **2018**, *6*, 6518–6526. [CrossRef]
110. Ramgir, N.; Bhusari, R.; Rawat, N.S.; Patil, S.J.; Debnath, A.K.; Gadkari, S.C.; Muthe, K.P. TiO_2/ZnO Heterostrucure Nanowire Based NO_2 Sensor. *Mater. Sci. Semicond. Process.* **2020**, *106*, 104770. [CrossRef]
111. Greene, L.E.; Law, M.; Yuhas, B.D.; Yang, P. ZnO-TiO_2 Core-Shell Nanorod/P3HT Solar Cells. *J. Phys. Chem. C* **2007**, *111*, 18451–18456. [CrossRef]

112. Guo, M.Y.; Fung, M.K.; Fang, F.; Chen, X.Y.; Ng, A.M.C.; Djurišić, A.B.; Chan, W.K. ZnO and TiO_2 1D Nanostructures for Photocatalytic Applications. *J. Alloys Compd.* **2011**, *509*, 1328–1332. [CrossRef]
113. Wang, M.; Huang, C.; Cao, Y.; Yu, Q.; Deng, Z.; Liu, Y.; Huang, Z.; Huang, J.; Huang, Q.; Guo, W.; et al. Dye-Sensitized Solar Cells Based on Nanoparticle-Decorated ZnO/TiO_2 Core/Shell Nanorod Arrays. *J. Phys. D Appl. Phys.* **2009**, *42*, 155104. [CrossRef]
114. Gu, L.; Zheng, K.; Zhou, Y.; Li, J.; Mo, X.; Patzke, G.R.; Chen, G. Humidity Sensors Based on ZnO/TiO_2 Core/Shell Nanorod Arrays with Enhanced Sensitivity. *Sens. Actuators B Chem.* **2011**, *159*, 1–7. [CrossRef]
115. Panigrahi, S.; Basak, D. Core–Shell TiO_2@ZnO Nanorods for Efficient Ultraviolet Photodetection. *Nanoscale* **2011**, *3*, 2336–2341. [CrossRef]
116. Kwiatkowski, M.; Bezverkhyy, I.; Skompska, M. ZnO Nanorods Covered with a TiO_2 layer: Simple Sol–Gel Preparation, and Optical, Photocatalytic and Photoelectrochemical Properties. *J. Mater. Chem. A* **2015**, *3*, 12748. [CrossRef]
117. Park, J.Y.; Choi, S.-W.; Lee, J.-W.; Lee, C.; Kim, S.S. Synthesis and Gas Sensing Properties of TiO_2-ZnO Core-Shell Nanofibers. *J. Am. Ceram. Soc.* **2009**, *92*, 2551–2554. [CrossRef]
118. Zou, C.W.; Yan, X.D.; Han, J.; Chen, R.Q.; Bian, J.M.; Haemmerle, E.; Gao, W. Preparation and Enhanced Photoluminescence Property or Ordered ZnO/TiO_2 Bottlebrush Nanostructures. *Chem. Phys. Lett.* **2009**, *476*, 47684–47688. [CrossRef]
119. Li, X.; Wang, C.; Xia, N.; Jiang, M.; Liu, R.; Huang, J.; Li, Q.; Luo, Z.; Liu, L.; Xu, W.; et al. Novel ZnO-TiO_2 Nanocomposite Arrays on Ti Fabric for Enhanced Photocatalytic Application. *J. Mol. Struct.* **2017**, *1148*, 347–355. [CrossRef]
120. Shi, L.; Sun, X.; Li, H.; Weng, D. Hydrothermal Growth of Novel Radiolarian-like Porous ZnO Microspheres on Compact TiO_2 Substrate. *Mater. Lett.* **2006**, *60*, 210–213. [CrossRef]
121. Jiang, Y.; Wu, M.; Wu, X.; Sun, Y.; Yin, H. Low-Temperature Hydrothermal Synthesis of Flower-like ZnO Microstructure and Nanorod Array on Nanoporous TiO_2 Film. *Mater. Lett.* **2009**, *63*, 275–278. [CrossRef]
122. Wang, N.; Li, X.; Wang, Y.; Hou, Y.; Zou, X.; Chen, G. Synthesis of ZnO/TiO_2 Nanotube Composite Film by a Two-Step Route. *Mater. Lett.* **2008**, *62*, 3691–3693. [CrossRef]
123. Çırak, B.B.; Caglar, B.; Kılınç, T.; Karadeniz, S.M.; Erdoğan, Y.; Kılıç, S.; Kahveci, E.; Ekinci, A.E.; Çırak, Ç. Synthesis and Characterization of ZnO Nanorice Decorated TiO_2 Nanotubes for Enhanced Photocatalytic Activity. *Mater. Res. Bull.* **2019**, *109*, 160–167. [CrossRef]
124. Zhang, Z.; Yuan, Y.; Liang, L.; Cheng, Y.; Shi, G.; Jin, L. Preparation and Photoelectrocatalytic Activity of ZnO Nanorods Embedded in Highly Ordered TiO_2 Nanotube Arrays Electrode for Azo Dye Degradation. *J. Hazard. Mater.* **2008**, *158*, 517–522. [CrossRef]
125. Lei, Y.; Zhao, G.; Liu, M.; Zhang, Z.; Tong, X.; Cao, T. Fabrication, Characterization and Photoelectrocatalytic Application of ZnO Nanorods Grafted on Vertically Aligned TiO_2 Nanotubes. *J. Phys. Chem. C* **2009**, *113*, 19067–19076. [CrossRef]
126. Huang, Y.-C.; Chang, S.-Y.; Lin, C.-F.; Tseng, W.J. Synthesis of ZnO Nanorod Grafted TiO_2 Nanotube 3-D Arrayed Heterostructure as Supporting Platform for Nanoparticle Deposition. *J. Mater. Chem.* **2011**, *21*, 14056. [CrossRef]
127. Yang, H.Y.; Yu, S.F.; Lau, S.P.; Zhang, X.; Sun, D.D.; Jun, G. Direct Growth of ZnO Nanocrystals onto the Surface of Porous TiO_2 Nanotube Arays for Highly Efficient and Recyclable Photocatalysts. *Small* **2009**, *5*, 2260–2264. [CrossRef]
128. Xie, Y.-L.; Li, Z.-X.; Xu, Z.-G.; Zhang, H.-L. Preparation of Coaxial TiO_2/ZnO Nanotube Arrays for High Efficiency Photo-Energy Conversion Application. *Electrochem. Commun.* **2011**, *13*, 788–791. [CrossRef]
129. Xiao, F.-X. Construction of Highly Ordered ZnO−TiO_2 Nanotube Arrays (ZnO/TNTs) Heterostructure for Photocatalytic Application. *ACS Appl. Mater. Interfaces* **2012**, *4*, 7055–7063. [CrossRef]
130. Liu, W.; Su, P.; Chen, S.; Wang, N.; Ma, Y.; Liu, Y.; Wang, J.; Zhang, Z.; Li, H.; Webster, T.J. Synthesis of TiO_2 Nanotubes with ZnO Nanoparticles to Achieve Antibacterial Properties and Stem Cell Compatibility. *Nanoscale* **2014**, *6*, 9050–9062. [CrossRef]
131. Gouvêa, C.A.K.; Wypych, F.; Moraes, S.G.; Durán, N.; Nagata, N.; Peralta-Zamora, P. Semiconductor-Assisted Photocatalytic Degradation of Reactive Dyes in Aqueous Solution. *Chemosphere* **2000**, *40*, 433–440. [CrossRef] [PubMed]
132. Cifre-Herrando, M.; Roselló-Márquez, G.; Navarro-Gázquez, P.J.; Muñoz-Portero, M.J.; Blasco-Tamarit, E.; García-Antón, J. Characterization and Comparison of WO_3/WO_3-MoO_3 and TiO_2/TiO_2-ZnO Nanostructures for Photoelectrocatalytic Degradation of the Pesticide Imazalil. *Nanomaterials* **2023**, *13*, 2584. [CrossRef] [PubMed]
133. Naimi-Joubani, M.; Shirzad-Siboni, M.; Yang, J.-K.; Gholami, M.; Farzadki, M. Photocatalytic Reduction of Hexavalent Chromium with Illuminated ZnO/TiO_2 composite. *J. Ind. Eng. Chem.* **2015**, *22*, 317–323. [CrossRef]
134. Li, M.; Zhang, R.; Zou, Z.; Zhang, L.; Ma, H. Optimizing Physico-Chemical Properties of Hierarchical ZnO/TiO_2 Nano-Film by the Novel Heating Method for Photocatalytic Degradation of Antibiotics and Dye. *Chemosphere* **2024**, *346*, 140392. [CrossRef]
135. Mancuso, A.; Mottola, S.; Sacco, O.; Vaiano, V.; De Marco, I. Photocatalytic Degradation of Ceftriaxone Using TiO_2 Coupled with ZnO Micronized by Supercritical Antisolvent Route. *Nanomaterials* **2023**, *13*, 3130. [CrossRef]
136. Vaizoğullar, A.İ. TiO_2/ZnO Supported on Sepiolite Preparation, Structural Characterization and Photocatalytic Degradation of Flumequine Antibiotic in Aqueous Solution. *Chem. Eng. Commun.* **2017**, *204*, 695–703. [CrossRef]
137. Gholami, M.; Shirzad-Siboni, M.; Farzadkia, M.; Yang, J.-K. Synthesis, Characterization, and Application of ZnO/TiO_2 Nanocomposite for Photocatalysis of a Herbicide (Bentazon). *Desalin. Water. Treat.* **2015**, *57*, 13632–13644. [CrossRef]
138. Kansal, S.K.; Singh, M.; Sud, D. Studies on TiO_2/ZnO Photocatalysed Degradation of Lignin. *J. Hazard. Mater.* **2008**, *153*, 412–417. [CrossRef]
139. Muzikova, B.; Martiniakova, I.; Mikyskova, E.; Mergl, M.; Kalbac, M.; Zouzelka, R.; Rathousky, J. Composite TiO_2-Based Photocatalyst with Enhanced Performance. *Photochem. Photobiol. Sci.* **2023**, *22*, 73–86. [CrossRef]

140. Ramadhika, L.N.; Suryaningsih, S.; Aprilia, A. Photocactivity Enhancement of TiO_2 Nanoparticle-Decorated ZnO as a Photocatalyst in Methylene Blue Degradation. *J. Phys. Conf. Ser.* **2022**, *2376*, 012003. [CrossRef]
141. Kim, D.W.; Lee, S.; Jung, H.S.; Kim, J.Y.; Shin, H.; Hong, K.S. Effects of Heterojunction on Photoelectrocatalytic Properties of ZnO–TiO_2 films. *Int. J. Hydrogen Energy* **2007**, *32*, 3137. [CrossRef]
142. Hidalgo-Jimenez, J.; Wang, Q.; Edalati, K.; Cubero-Sesin, J.M.; Razavi-Khosroshahi, H.; Ikoma, Y.; Gutiérrez-Fallas, D.; Dittel-Meza, F.A.; Rodríguez-Rufino, J.C.; Fuji, M.; et al. Phase Transformations, Vacancy Formation and Variations of Optical and Photocatalytic Properties in TiO_2-ZnO Composites by High-Pressure Torsion. *Int. J. Plast.* **2020**, *124*, 170–175. [CrossRef]
143. Sirelkhatim, A.; Mahmud, S.; Seeni, A.; Kaus, N.H.M.; Ann, L.C.; Bakhori, S.K.M.; Hasan, H.; Mohamad, D. Review on Zinc Oxide Nanoparticles: Antibacterial Activity and Toxicity Mechanism. *Nano-Micro Lett.* **2015**, *7*, 219–242. [CrossRef] [PubMed]
144. Ahmad, R.; Mohsin, M.; Ahmad, T.; Sardar, M. Alpha Amylase Assisted Synthesis of TiO_2 Nanoparticles: Structural Characterization and Application as Antibacterial Agents. *J. Hazard. Mater.* **2015**, *283*, 171–177. [CrossRef]
145. Xiong, D.; Fang, T.; Yu, L.; Sima, X.; Zhu, W. Effects of Nano-Scale TiO_2, ZnO and Their Bulk Counterparts on Zebrfish: Acute Toxicity, Oxidative Stress and Oxidative Damage. *Sci. Total. Environ.* **2011**, *409*, 1444–1452. [CrossRef]
146. Stoyanova, A.; Hitkova, H.; Bachvarova-Nedelcheva, A. Synthesis and Antibacterial Activity of TiO_2/ZnO Nanocomposites Prepared via Nonhydrolytic Route. *J. Chem. Technol. Metall.* **2013**, *48*, 154–161.
147. Chakra, C.H.S.; Rajendar, V.; Rao, K.V.; Kumar, M. Enhanced Antimicrobial and Anticancer Properties of ZnO and TiO_2 Nanocomposites. *3 Biotech* **2017**, *7*, 89. [CrossRef]
148. Ren, D.; Li, J.; Bao, Y.; Wu, Z.; He, S.; Wang, A.; Guo, F.; Chen, Y. Low-Temperature Synthesis of Flower-Like ZnO Microstructure Supported on TiO_2 Thin Films as Efficient Antifungal Coatings for Bamboo Protection under Dark Conditions. *Colloids Surf. A Physicochem. Eng. Asp.* **2018**, *555*, 381–388. [CrossRef]
149. Soria, R.B.; Zhu, J.; Gonza, I.; Van der Bruggen, B.; Luis, P. Effect of (TiO_2: ZnO) Ratio on the Anti-fouling Properties of Bio-inspired Nanofiltration Membranes. *Sep. Purif. Technol.* **2020**, *251*, 1117280. [CrossRef]
150. Halfadji, A.; Bennabi, L.; Giannakis, S.; Marrani, A.G.; Bellucci, S. Sono-synthesis and Characterization of Next-generation Antimicrobial ZnO/TiO_2 Fe_3O_4/TiO_2 bi-nanocomposites, for Antibacterial and Antifungal Applications. *Ceram. Int.* **2024**, *50*, 39097–39108. [CrossRef]
151. Wang, C.; Abidin, S.Z.; Toyong, N.M.P.; Zhu, W.; Zhang, Y. Mildew Resistance and Antibacterial Activity of Plywood Decorated with ZnO/TiO_2 Nanoparticle. *J. Saudi Chem. Soc.* **2024**, *28*, 101877. [CrossRef]
152. Pourhajibaghera, M.; Bahador, A. Synergistic Biocidal Effects of Metal Oxide Nanoparticles-assisted Ultrasound Irradiation: Antimicrobial Sonodynamic Therapy against Streptococcus Mutans Biofilms. *Photodiagn. Photodyn.* **2021**, *35*, 102432. [CrossRef] [PubMed]
153. Parvin, N.; Nallapureddy, R.R.; Mandal, T.K.; Joo, S.W. Construction of Bimetallic Hybrid Multishell Hollow Spheres via Sequential Template Approach for Less Cytotoxic Antimicrobial Effect. *IEEE Trans. Nanobiosci.* **2023**, *22*, 447. [CrossRef] [PubMed]
154. Shi, H.; Magaye, R.; Castranova, V.; Zhao, J. Titanium Dioxide Nanoparticles: A Review of Current Toxicological Data. *Part. Fibre Toxicol.* **2013**, *10*, 15. [CrossRef] [PubMed]
155. Vandebriel, R.J.; De Jong, W.H. A review of Mammalian Toxicity of ZnO Nanoparticles. *Nanotechnol. Sci. Appl.* **2012**, *5*, 61–71. [CrossRef] [PubMed]
156. Kocbek, P.; Teskač, K.; Kreft, M.E.; Kristl, J. Toxicological Aspects of Long-Term Treatment of Keratinocytes with ZnO and TiO_2 Nanoparticles. *Small* **2010**, *6*, 1908. [CrossRef] [PubMed]
157. Monteiro-Riviere, N.A.; Wiench, K.; Landsiedel, R.; Schulte, S.; Inman, A.O.; Riviere, J.E. Safety Evaluation of Sunscreen Formulations Containing Titanium Dioxide and Zinc Oxide Nanoparticles in UVB Sunburned Skin: An In Vitro and In Vivo Study. *Toxicol. Sci.* **2011**, *123*, 264–280. [CrossRef]
158. Liang, Y.; Simaiti, A.; Xu, M.; Lv, S.; Jiang, H.; He, X.; Fan, Y.; Zhu, S.; Du, B.; Yang, W.; et al. Antagonistic Skin Toxicity of Co-Exposure to Physical Sunscreen Ingredients Zinc Oxide and Titanium Dioxide Nanoparticles. *Nanomaterials* **2022**, *12*, 2769. [CrossRef]
159. Kim, I.-S.; Baek, M.; Choi, S.-J. Comparative Cytotoxicity of Al_2O_3, CeO_2, TiO_2 and ZnO Nanoparticles to Human Lung Cells. *J. Nanosci. Nanotechnol.* **2010**, *10*, 3453–3458. [CrossRef]
160. Larsen, S.T.; Jackson, P.; Poulsen, S.S.; Levin, M.; Jensen, K.A.; Wallin, H.; Nielsen, G.D.; Koponen, I.K. Airway Irritation, Inflammation, and Toxicity in Mice Following Inhalation of Metal Oxide Nanoparticles. *Nanotoxicology* **2016**, *10*, 1254–1262. [CrossRef]
161. Simón-Vázquez, R.; Lozano-Fernández, T.; Dávila-Grana, A.; González-Fernández, Á. Analysis of the Activation Routes Induced by Different Metal Oxide Nanoparticles on Human Lung Epithelial Cells. *Future Sci. OA* **2016**, *2*, FSO118. [CrossRef] [PubMed]
162. Remzova, M.; Zouzelka, R.; Brzicova, T.; Vrbova, K.; Pinkas, D.; Rőssner, P.; Topinka, J.; Rathousky, J. Toxicity of TiO_2, ZnO, and SiO_2 Nanoparticles in Human Lung Cells: Safe-by-Design Development of Construction Materials. *Nanomaterials* **2019**, *9*, 968. [CrossRef] [PubMed]
163. Hsiao, I.-L.; Huang, Y.-J. Effects of Various Physicochemical Characteristics on the Toxicities of ZnO and TiO_2 Nanoparticles Toward Human Lung Epithelial Cells. *Sci. Total Environ.* **2011**, *409*, 1219. [CrossRef] [PubMed]
164. Hsiao, I.-L.; Huang, Y.-J. Titanium Oxide Shell Coatings Decrease the Cytotoxicity of ZnO Nanoparticles. *Chem. Res. Toxicol.* **2011**, *24*, 303–313. [CrossRef]

165. Wang, J.; Wang, W.-X. Significance of Physicochemical and Uptake Kinetics in Controlling the Toxicity of Metallic Nanomaterials to Aquatic Organisms. *J. Zhejiang Univ.-Sci. A (Appl. Phys. Eng.)* **2014**, *15*, 573–592. [CrossRef]
166. Tong, T.; Fang, K.; Thomas, S.A.; Kelly, J.J.; Gray, K.A.; Gaillard, J.-F. Chemical Interactions between Nano-ZnO and Nano-TiO_2 in a Natural Aqueous Medium, Environ. *Sci. Technol.* **2014**, *48*, 7924–7932. [CrossRef]
167. Hua, J.; Peijnenburg, W.J.G.M.; Vijver, M.-G. TiO_2 Nanoparticles Reduce the Effects of ZnO Nanoparticles and Zn Ions on Zebrafish Embryos (*Danio rerio*). *NanoImpact* **2016**, *2*, 45–53. [CrossRef]
168. Sezer, S.; Yücel, A.; Turhan, D.Ö.; Emre, F.B.; Sarikaya, M. Comparison of ZnO Doped Different Phases TiO_2 Nanoparticles in Terms of Toxicity Using Zebrafish (*Danio rerio*). *Chemosphere* **2023**, *325*, 138342. [CrossRef]
169. Speziale, A.; González-Sánchez, J.F.; Taşcı, B.; Pastor, A.; Sánchez, L.; Fernández-Acevedo, C.; Oroz-Mateo, T.; Salazar, C.; Navarro-Blasco, I.; Fernández, J.M.; et al. Development of Multifunctional Coatings for Protecting Stones and Lime Mortars of the Architectural Heritage. *Int. J. Archit. Herit.* **2020**, *14*, 1008–1029. [CrossRef]
170. Zhang, R.; Liu, X.; Xiong, Z.; Huang, Q.; Yang, X.; Yan, H.; Ma, J.; Feng, Q.; Shen, Z. Novel Micro/Nanostructured TiO_2/ZnO Coating with Antibacterial Capacity and Cytocompatibility. *Ceram. Int.* **2018**, *44*, 9711–9719. [CrossRef]